EUROPEAN ORGANIZATION FOR NUCLEAR RESEARCH

CERN-PPE/92-62
April 21, 1992

Properties of Hadronic Z Decays and Test of QCD Generators

The ALEPH Collaboration[1]

Abstract

Distributions are presented of event shape variables, jet production rates and charged particle momenta obtained from 53000 hadronic Z decays. They are compared to the predictions of the QCD + hadronization models JETSET, ARIADNE and HERWIG, and are used to optimize several model parameters. The JETSET and ARIADNE coherent parton shower (PS) models with running α_s and string fragmentation yield the best description of the data. The HERWIG parton shower model with cluster fragmentation fits the data less well. The data are in better agreement with JETSET PS than with JETSET $O(\alpha_s^2)$ matrix elements (ME) even when the renormalization scale is optimized.

(Submitted to Zeitschrift für Physik C)

[1] See the following pages for the list of authors.

The ALEPH Collaboration

D. Buskulic, D. Decamp, C. Goy, J.-P. Lees, M.-N. Minard, B. Mours

Laboratoire de Physique des Particules (LAPP), IN^{2}P^3-CNRS, 74019 Annecy-le-Vieux Cedex, France

R. Alemany, F. Ariztizabal, P. Comas, J.M. Crespo, M. Delfino, E. Fernandez, V. Gaitan, Ll. Garrido, Ll.M. Mir, A. Pacheco, A. Pascual

Institut de Fisica d'Altes Energies, Universitat Autonoma de Barcelona, 08193 Bellaterra (Barcelona), Spain[8]

D. Creanza, M. de Palma, A. Farilla, G. Iaselli, G. Maggi, M. Maggi, S. Natali, S. Nuzzo, M. Quattromini, A. Ranieri, G. Raso, F. Romano, F. Ruggieri, G. Selvaggi, L. Silvestris, P. Tempesta, G. Zito

INFN Sezione di Bari e Dipartimento di Fisica dell' Università, 70126 Bari, Italy

Y. Gao, H. Hu,[21] D. Huang, X. Huang, J. Lin, J. Lou, C. Qiao,[21] T. Wang, Y. Xie, D. Xu, R. Xu, J. Zhang, W. Zhao

Institute of High-Energy Physics, Academia Sinica, Beijing, The People's Republic of China[9]

W.B. Atwood,[2] L.A.T. Bauerdick,[26] E. Blucher, G. Bonvicini, F. Bossi, J. Boudreau, T.H. Burnett,[3] H. Drevermann, R.W. Forty, R. Hagelberg, J. Harvey, S. Haywood, J. Hilgart, R. Jacobsen, B. Jost, J. Knobloch, E. Lançon, I. Lehraus, T. Lohse, A. Lusiani, M. Martinez, P. Mato, T. Mattison, H. Meinhard, S. Menary,[27] T. Meyer, A. Minten, A. Miotto, R. Miquel, H.-G. Moser, J. Nash, P. Palazzi, J.A. Perlas, F. Ranjard, G. Redlinger, L. Rolandi,[28] A. Roth,[30] J. Rothberg,[3] T. Ruan,[21,33] M. Saich, D. Schlatter, M. Schmelling, F. Sefkow, W. Tejessy, H. Wachsmuth, W. Wiedenmann, T. Wildish, W. Witzeling, J. Wotschack

European Laboratory for Particle Physics (CERN), 1211 Geneva 23, Switzerland

Z. Ajaltouni, F. Badaud, M. Bardadin-Otwinowska, A.M. Bencheikh, R. El Fellous, A. Falvard, P. Gay, C. Guicheney, P. Henrard, J. Jousset, B. Michel, J-C. Montret, D. Pallin, P. Perret, B. Pietrzyk, J. Proriol, F. Prulhière, G. Stimpfl

Laboratoire de Physique Corpusculaire, Université Blaise Pascal, IN^{2}P^3-CNRS, Clermont-Ferrand, 63177 Aubière, France

T. Fearnley, J.D. Hansen, J.R. Hansen, P.H. Hansen, R. Møllerud, B.S. Nilsson

Niels Bohr Institute, 2100 Copenhagen, Denmark[10]

I. Efthymiopoulos, A. Kyriakis, E. Simopoulou, A. Vayaki,[1] K. Zachariadou

Nuclear Research Center Demokritos (NRCD), Athens, Greece

J. Badier, A. Blondel, G. Bonneaud, J.C. Brient, G. Fouque, A. Gamess, S. Orteu, A. Rosowsky, A. Rougé, M. Rumpf, R. Tanaka, H. Videau

Laboratoire de Physique Nucléaire et des Hautes Energies, Ecole Polytechnique, IN^{2}P^3-CNRS, 91128 Palaiseau Cedex, France

D.J. Candlin, M.I. Parsons, E. Veitch

Department of Physics, University of Edinburgh, Edinburgh EH9 3JZ, United Kingdom[11]

L. Moneta, G. Parrini

Dipartimento di Fisica, Università di Firenze, INFN Sezione di Firenze, 50125 Firenze, Italy

M. Corden, C. Georgiopoulos, M. Ikeda, J. Lannutti, D. Levinthal,[16] M. Mermikides[†], L. Sawyer, S. Wasserbaech

Supercomputer Computations Research Institute and Dept. of Physics, Florida State University, Tallahassee, FL 32306, USA [13,14,15]

A. Antonelli, R. Baldini, G. Bencivenni, G. Bologna,[5] P. Campana, G. Capon, F. Cerutti, V. Chiarella, B. D'Ettorre-Piazzoli,[32] G. Felici, P. Laurelli, G. Mannocchi,[6] F. Murtas, G.P. Murtas, L. Passalacqua, M. Pepe-Altarelli, P. Picchi[5]

Laboratori Nazionali dell'INFN (LNF-INFN), 00044 Frascati, Italy

B. Altoon, O. Boyle, P. Colrain, I. ten Have, J.G. Lynch, W. Maitland, W.T. Morton, C. Raine, J.M. Scarr, K. Smith, A.S. Thompson, R.M. Turnbull

Department of Physics and Astronomy, University of Glasgow, Glasgow G12 8QQ,United Kingdom[11]

B. Brandl, O. Braun, R. Geiges, C. Geweniger, P. Hanke, V. Hepp, E.E. Kluge, Y. Maumary, A. Putzer, B. Rensch, A. Stahl, K. Tittel, M. Wunsch

Institut für Hochenergiephysik, Universität Heidelberg, 6900 Heidelberg, Fed. Rep. of Germany[17]

A.T. Belk, R. Beuselinck, D.M. Binnie, W. Cameron, M. Cattaneo, D.J. Colling, P.J. Dornan,[1] S. Dugeay, A.M. Greene, J.F. Hassard, N.M. Lieske, S.J. Patton, D.G. Payne, M.J. Phillips, J.K. Sedgbeer, I.R. Tomalin, A.G. Wright

Department of Physics, Imperial College, London SW7 2BZ, United Kingdom[11]

E. Kneringer, D. Kuhn, G. Rudolph

Institut für Experimentalphysik, Universität Innsbruck, 6020 Innsbruck, Austria[19]

C.K. Bowdery, T.J. Brodbeck, A.J. Finch, F. Foster, G. Hughes, D. Jackson, N.R. Keemer, M. Nuttall, A. Patel, T. Sloan, S.W. Snow, E.P. Whelan

Department of Physics, University of Lancaster, Lancaster LA1 4YB, United Kingdom[11]

T. Barczewski, K. Kleinknecht, J. Raab, B. Renk, S. Roehn, H.-G. Sander, H. Schmidt, F. Steeg, S.M. Walther, B. Wolf

Institut für Physik, Universität Mainz, 6500 Mainz, Fed. Rep. of Germany[17]

J-J. Aubert, C. Benchouk, V. Bernard, A. Bonissent, J. Carr, P. Coyle, J. Drinkard, F. Etienne, S. Papalexiou, P. Payre, Z. Qian, D. Rousseau, P. Schwemling, M. Talby

Centre de Physique des Particules, Faculté des Sciences de Luminy, IN^{2}P^3-CNRS, 13288 Marseille, France

S. Adlung, H. Becker, W. Blum,[1] D. Brown, P. Cattaneo,[29] G. Cowan, B. Dehning, H. Dietl, F. Dydak,[25] M. Fernandez-Bosman, M. Frank, A.W. Halley, T. Hansl-Kozanecka,[2,22] J. Lauber, G. Lütjens, G. Lutz, W. Männer, Y. Pan, R. Richter, H. Rotscheidt, J. Schröder, A.S. Schwarz, R. Settles, U. Stierlin, U. Stiegler, R. St. Denis, M. Takashima,[4] J. Thomas,[4] G. Wolf

Max-Planck-Institut für Physik und Astrophysik, Werner-Heisenberg-Institut für Physik, 8000 München, Fed. Rep. of Germany[17]

V. Bertin, J. Boucrot, O. Callot, X. Chen, A. Cordier, M. Davier, J.-F. Grivaz, Ph. Heusse, P. Janot, D.W. Kim,[20] F. Le Diberder, J. Lefrançois,[1] A.-M. Lutz, M.-H. Schune, J.-J. Veillet, I. Videau, Z. Zhang, F. Zomer

Laboratoire de l'Accélérateur Linéaire, Université de Paris-Sud, IN^{2}P^3-CNRS, 91405 Orsay Cedex, France

D. Abbaneo, S.R. Amendolia, G. Bagliesi, G. Batignani, L. Bosisio, U. Bottigli, C. Bradaschia, M. Carpinelli, M.A. Ciocci, R. Dell'Orso, I. Ferrante, F. Fidecaro,[1] L. Foà, E. Focardi, F. Forti, A. Giassi, M.A. Giorgi, F. Ligabue, E.B. Mannelli, P.S. Marrocchesi, A. Messineo, F. Palla, G. Rizzo, G. Sanguinetti, J. Steinberger, R. Tenchini, G. Tonelli, G. Triggiani, C. Vannini, A. Venturi, P.G. Verdini, J. Walsh

Dipartimento di Fisica dell'Università, INFN Sezione di Pisa, e Scuola Normale Superiore, 56010 Pisa, Italy

J.M. Carter, M.G. Green, P.V. March, T. Medcalf, I.S. Quazi, J.A. Strong, L.R. West

Department of Physics, Royal Holloway & Bedford New College, University of London, Surrey TW20 OEX, United Kingdom[11]

D.R. Botterill, R.W. Clifft, T.R. Edgecock, M. Edwards, S.M. Fisher, T.J. Jones, P.R. Norton, D.P. Salmon, J.C. Thompson

Particle Physics Dept., Rutherford Appleton Laboratory, Chilton, Didcot, Oxon OX11 OQX, United Kingdom[11]

B. Bloch-Devaux, P. Colas, W. Kozanecki,[2] M.C. Lemaire, E. Locci, S. Loucatos, E. Monnier, P. Perez, F. Perrier, J. Rander, J.-F. Renardy, A. Roussarie, J.-P. Schuller, J. Schwindling, D. Si Mohand, B. Vallage

Service de Physique des Particules, DAPNIA, CE-Saclay, 91191 Gif-sur-Yvette Cedex, France[18]

R.P. Johnson, A.M. Litke, G. Taylor, J. Wear

Institute for Particle Physics, University of California at Santa Cruz, Santa Cruz, CA 95064, USA[36]

J.G. Ashman, W. Babbage, C.N. Booth, C. Buttar, R.E. Carney, S. Cartwright, F. Combley, F. Hatfield, P. Reeves, L.F. Thompson

Department of Physics, University of Sheffield, Sheffield S3 7RH, United Kingdom[11]

E. Barberio, S. Brandt, C. Grupen, L. Mirabito,[31] U. Schäfer, H. Seywerd

Fachbereich Physik, Universität Siegen, 5900 Siegen, Fed. Rep. of Germany[17]

G. Ganis,[35] G. Giannini, B. Gobbo, F. Ragusa[24]

Dipartimento di Fisica, Università di Trieste e INFN Sezione di Trieste, 34127 Trieste, Italy

L. Bellantoni, D. Cinabro,[34] J.S. Conway, D.F. Cowen,[23] Z. Feng, D.P.S. Ferguson, Y.S. Gao, J. Grahl, J.L. Harton, R.C. Jared,[7] B.W. LeClaire, C. Lishka, Y.B. Pan, J.R. Pater, Y. Saadi, V. Sharma, M. Schmitt, Z.H. Shi, Y.H. Tang, A.M. Walsh, F.V. Weber, M.H. Whitney, Sau Lan Wu, X. Wu, G. Zobernig

Department of Physics, University of Wisconsin, Madison, WI 53706, USA[12]

[†] Deceased.

[1] Now at CERN, PPE Division, 1211 Geneva 23, Switzerland.

[2] Permanent adddress: SLAC, Stanford, CA 94309, USA.

[3] Permanent address: University of Washington, Seattle, WA 98195, USA.

[4] Now at SSCL, Dallas, TX, U.S.A.

[5] Also Istituto di Fisica Generale, Università di Torino, Torino, Italy.

[6] Also Istituto di Cosmo-Geofisica del C.N.R., Torino, Italy.

[7] Permanent address: LBL, Berkeley, CA 94720, USA.

[8] Supported by CICYT, Spain.

[9] Supported by the National Science Foundation of China.

[10] Supported by the Danish Natural Science Research Council.

[11] Supported by the UK Science and Engineering Research Council.

[12] Supported by the US Department of Energy, contract DE-AC02-76ER00881.

[13] Supported by the US Department of Energy, contract DE-FG05-87ER40319.

[14] Supported by the NSF, contract PHY-8451274.

[15] Supported by the US Department of Energy, contract DE-FC0S-85ER250000.

[16] Supported by SLOAN fellowship, contract BR 2703.

[17] Supported by the Bundesministerium für Forschung und Technologie, Fed. Rep. of Germany.

[18] Supported by the Direction des Sciences de la Matière, C.E.A.

[19] Supported by Fonds zur Förderung der wissenschaftlichen Forschung, Austria.

[20] Supported by the Korean Science and Engineering Foundation and Ministry of Education.

[21] Supported by the World Laboratory.

[22] On leave of absence from MIT, Cambridge, MA 02139, USA.

[23] Now at California Institute of Technology, Pasadena, CA 91125, USA.

[24] Now at Dipartimento di Fisica, Università di Milano, Milano, Italy.

[25] Also at CERN, PPE Division, 1211 Geneva 23, Switzerland.

[26] Now at DESY, Hamburg, Germany.

[27] Now at University of California at Santa Barbara, Santa Barbara, CA 93106, USA.

[28] Also at Dipartimento di Fisica, Università di Trieste, Trieste, Italy.

[29] Now at INFN, Pavia, Italy.

[30] Now at Lufthansa, Hamburg, Germany.

[31] Now at Institut de Physique Nucléaire de Lyon, 69622 Villeurbanne, France.

[32] Also at Università di Napoli, Dipartimento di Scienze Fisiche, Napoli, Italy.

[33] On leave of absence from IHEP, Beijing, The People's Republic of China.

[34] Now at Harvard University, Cambridge, MA 02138, U.S.A.

[35] Supported by the Consorzio per lo Sviluppo dell'Area di Ricerca, Trieste, Italy.

[36] Supported by the US Department of Eenrgy, grant DE-FG03-92ER40689.

1 Introduction

The jet structure of multi-hadronic events from e^+e^- annihilation at high energies can be explained as the result of electroweak production of a $q\bar{q}$ pair followed by multiple gluon radiation, the soft hadronization of the quarks and gluons and, finally, the decay of unstable particles. While the perturbative QCD part is rather well tested, the hadronization process can only be described by phenomenological models. In order to compare with data, Monte Carlo programs have been developed which generate complete final states. A comprehensive overview can be found in [1]. Recent versions of the generators JETSET [2], ARIADNE [3] and HERWIG [4] are investigated.

The present paper which extends the work of ref.[5], presents corrected distributions from hadronic Z decays which are used to optimize the main parameters of the models and to investigate the agreement between the tuned models and the data. The global characteristics of hadronic Z decays are described in terms of event shape variables, n-jet production rates and inclusive charged particle momenta. Using the optimized parameters at 91 GeV the energy dependence of the model predictions is compared with published data at lower energies.

2 Event Selection

A description of the ALEPH detector and the trigger conditions can be found in [6]. The analysis presented here is based on charged particle tracks measured with the time projection chamber (TPC) and the inner tracking chamber (ITC). At the magnetic field of 1.5 T, a combined momentum resolution of dp/p = 0.0008 p (GeV) is achieved [7]. The track selection criteria require at least four space coordinates from the TPC, a polar angle of more than 20 degrees and a transverse momentum component of more than 0.20 GeV with respect to the beam direction. Furthermore, the tracks are required to originate from the interaction point within 5 cm along the beam direction and within 2 cm in the transverse plane. Hadronic events are required to have at least 5 accepted charged tracks, a total charged energy in excess of 15 GeV and, in addition, the polar angle of the sphericity axis above 35 degrees. The cuts described result in a data sample of 52700 events taken with the ALEPH detector at LEP in 1989 and 1990 at center-of-mass energies close to the Z peak, $91.0 < E_{c.m.} < 91.5$ GeV. The average energy is 91.25 GeV. The largest background arises from $\tau^+\tau^-$ events and is estimated to be 0.2 % . Its effect is taken into account in the systematic error estimate.

3 Corrected Distributions

3.1 Variables used

The following standard event shape and single particle variables are computed from the charged particle momenta (see the appendix or [8, 9, 5] for definitions) :

1) sphericity, S
2) aplanarity, A
3) planarity, P = 2(S–2A)/3
4) C - parameter
5) thrust, T
6) major, M
7) minor, m

8) oblateness, O = M – m

9) heavy jet mass, M_h^2/s

10) light jet mass, M_l^2/s

11) jet mass difference, $M_d^2/s = (M_h^2 - M_l^2)/s$

12) the jet resolution parameter y_3, which marks the transition from 3 to 2 jets for a given event. The jets are reconstructed with the JADE+E0 cluster algorithm [12]

13) the rate of n-jet events, calculated with the JADE+E cluster algorithm [27] for various values of the jet resolution parameter y_{cut}

14) x_p, the charged particle momentum divided by the beam momentum

15) y_T, the rapidity of charged particles with respect to the thrust axis

16) y_S, the rapidity of charged particles with respect to the sphericity axis

17) p_t^{out}, the charged particle momentum component perpendicular to the event plane defined by the sphericity tensor

18) p_t^{in}, the charged particle momentum component transverse to the sphericity axis and projected into the event plane

The raw data distributions are normalized to the number of observed events. For bin i

$$D_{i,raw}(X) = \frac{1}{N_{events}}(\frac{dN}{dX})_i,$$

where X is any quantity listed above.

3.2 Corrections

The distributions were corrected, using standard Monte Carlo methods, for the effects of geometrical acceptance, detector efficiency and resolution, decays, secondary interactions and initial state photon radiation. For this, hadronic events were generated using the JETSET PS generator, version 6.3 [2] including initial state radiation, and the events were then passed through the detector simulation program. The simulated raw data were then processed through the same reconstruction and analysis chain as the real data, yielding distributions $D_{i,sim}$. Hadronic events were also generated using the same generator, with neither detector simulation nor initial state radiation and with the requirement that all particles with mean lifetimes $> 10^{-9} sec$ are stable, yielding distributions $D_{i,gen}$. The correction factors C_i are the bin-by-bin ratios of the two normalized Monte Carlo distributions. Corrected data distributions are then obtained from

$$D_{i,corr}(X) = C_i(X) D_{i,raw}(X) = \frac{D_{i,gen}(X)}{D_{i,sim}(X)} D_{i,raw}(X).$$

The parameter values used in JETSET were obtained from a fit to an earlier data set [10]. The raw data distributions are well represented by the full simulation. This is a necessary prerequisite for the correction method to be reliable. In contrast to the full matrix deconvolution, the simple factor method applied here is stable, however slightly model dependent.

Two types of correction factors were computed giving two sets of corrected distributions. For the first set only charged particles are used. For the second set all charged and neutral stable particles (including ν's) are used in the Monte Carlo calculation of $D_{i,gen}$. This second set allows comparison with other experiments. The inclusive charged particle variables y_T, y_S, p_t^{out} and p_t^{in} of the second set are corrected such that they refer to axes calculated with all charged plus neutral

particles.

The binning of the distributions of the first set was chosen such that the experimental resolution is equal or smaller than the binsize. The resolution is determined from the Monte Carlo and is defined as the 1σ deviation of a variable before and after detector simulation. With the chosen binning the 2-jet peaks of the shape variables are resolved. The same binning is used for the distributions of the second set, although the resolution is often somewhat larger than the binsize. As a consequence, systematic errors are larger.

The distributions corrected for charged particles only are shown in figures 1 to 18. They are used to perform the QCD model fits since the corrections are smaller in this case. Tables 1 to 18 contain the numerical values of both sets of corrected distributions, together with the average values. A comparison of the two columns shows that the event shape distributions computed with charged particles and with charged+neutral particles are very similar except for narrow regions close to the phase space boundaries.

Figure 19a-d shows the correction factors of the first set for two inclusive and two shape variables, as examples. It is seen that the corrections are not larger than 10 % in most of the bins. The corrections vary rapidly and become large near the phase space boundaries of the shape variables. These regions are : $0.985 < T < 1.000$, $0.0 < m < 0.04$, and $0.0 < C < 0.08$, $0.02 < M < 0.05$, $0.0 < M_d^2/s < 0.005$, $0.0 < y_3 < 0.005$ for the variables not shown in fig.19. For the jet masses M_h^2/s and M_l^2/s the corrections are large everywhere. The corrections are also large in the region of low particle momenta where the geometrical acceptance and the track selection cuts are important : $0.005 < x_p < 0.010$, $p_t^{in,out} < 0.3$ GeV and $y < 1.5$. At large rapidities, $y > 4$, the correction grows due to mass effects.

3.3 Systematic uncertainties

Systematic uncertainties in the corrections may arise from
(1) possible discrepancies between the actual and simulated detector performance, and from
(2) the choice of a QCD generator to calculate the corrections for detector effects.

To estimate the uncertainties of the first kind, all the track and event selection cuts described in section 2 were varied and the corresponding changes in the corrected distributions were observed. In each bin, the maximum change with respect to the standard set of cuts is taken as the systematic error. This error exceeds the statistical error only in the low momentum region, $0.005 < x_p < 0.015$ (systematic error = 0.9 %), and in the above mentioned boundary regions of the shape variables T, M, m, C and y_3, where the corrections are already large. In these latter regions the dominant contribution to the error arises from residual tau pair events which have an extremely 2-jet like topology and which are removed from the data if the cut on N_{tracks} is changed from 5 to 7.

After momentum calibration using the reaction $e^+e^- \to \mu^+\mu^-$ no important systematic shifts in the measurement of charged particle momenta are observed [7] .

To estimate uncertainties of the second type, the correction procedure should in principle be repeated using different QCD generators. Since this requires excessive computing time, a simplified method [11] has been applied. Correction factors have been computed using 500 K events with each of the following tuned QCD models (see next section) :

1) JETSET 7.2 coherent PS + $O(\alpha_s)$ (=reference model)

2) JETSET 7.2 incoherent PS + $O(\alpha_s)$

3) JETSET 7.2 ME optimized scale

4) JETSET 7.2 ME optimized scale, $W_{min,0} = 1.9$ GeV

5) HERWIG 4.3 PS

by simply applying the selection cuts described in section 2 to the charged particles generated. Results from models 1),3) and 5) are drawn as lines in fig.19. This demonstrates that the bulk of the correction is due to the geometrical acceptance and the selection cuts. The maximum relative change of the correction factor with respect to that of the reference model is conservatively taken as the systematic error from this source in every bin. This error is found to be smaller than or equal to the statistical error for the majority of the bins. Exceptions are the critical regions of the shape variables C, T, M, m, and y_3 mentioned above, the full rapidity distribution and the low momentum regions $0.005 < x_p < 0.030$ and $p_t^{out,in} < 0.15$ GeV.

The systematic errors given in tables 1 to 18 and included in figures 1 to 18 are the quadratic sum of errors of type (1) and (2). Inspection of the tables shows that the estimated systematic uncertainties are already of the same size or, in some regions, even larger than the statistical errors; they are even larger if the data are corrected for the unmeasured neutrals. The errors quoted for the mean values are calculated in the same way as for the individual bins. The systematic nature of these errors leads to correlations between adjacent bins which are found to be present in all distributions. Their effect on the QCD model fits is discussed in section 5.2.1.

Some of the event shape distributions, corrected for charged and neutral particles, have been used previously by ALEPH for a measurement of the strong coupling constant α_s [12]. The distributions, corrected for charged and neutral particles, can be compared to results from other LEP experiments. Within errors, good agreement is found for the event shape distributions published by OPAL [13] and DELPHI [14]. This is also true for the n-jet rates versus y_{cut} reported by the OPAL [15], DELPHI [16] and L3 [17] collaborations.

4 QCD and Hadronization Models

In this section, some information is given about the event generators considered and those parameters are listed which are varied in this work. All other parameters, in particular those which control the production of specific particle types or flavours, are left at their default values. It is clear that, as more detailed information is collected on exclusive particle production, these other parameters may have to be revised. This will probably change the results of the fits presented below.

4.1 JETSET version 7.2 Parton Shower (PS)

The program JETSET [2] has a number of options available for the generation of quarks and gluons and for the subsequent hadronization. In the default version the primary quark and antiquark develop quark-gluon cascades based on the leading-logarithm approximation (LLA) of perturbative QCD. The cascade is controlled by the scale parameter Λ_{LLA}, which enters a first order expression in α_s, and by the infrared cut-off M_{min}. Here α_s is not a constant since its argument is related to the virtual mass at each branching. Two improvements of the branching probabilities are provided. Soft gluon coherence is included by ordering the emission angles, as pioneered by Marchesini and Webber [18]. Secondly, the probability of the first branching is matched to the $O(\alpha_s)$ matrix element, resulting in a reduction of the rate of hard large-angle gluon radiation at the same value

of Λ_{LLA}. This program version is referred to as JETSET coherent PS + $O(\alpha_s)$. It has been checked that final state photon radiation has negligible effects on the results presented in this paper.

The hadronization of the multi-parton final state is modelled by a colour string which stretches from the quark to the antiquark via the gluons, often called the "Lund fragmentation model" [19]. Gluons act as transverse excitations on the string. The model has the desirable property of infrared stability, i.e. situations with soft or colinear gluons are dealed with in a continuous manner. The Lund symmetric fragmentation function is of the form $((1-z)^A/z)\, exp(-Bm_t^2/z)$ where z is the fraction of $(E+p_l)$ taken by a hadron of transverse mass m_t. The parameter A is left at the default value (0.5) because of the strong correlation with B. Since the Lund symmetric fragmentation function, with flavour-independent values for A and B, is known [1] to give too hard an energy spectrum for bottom hadrons, the fragmentation of the heavy c and b hadrons is parametrized by the function due to Peterson et al. [20]. For the fits the ϵ parameters characterizing this function are fixed using PETRA/PEP data [21, 22, 23] giving $\epsilon_c = 0.020$ and $\epsilon_b = 0.015$ within JETSET PS. The values $\epsilon_c = 0.050$ and $\epsilon_b = 0.006$ as derived from ALEPH data [24, 25] have also been examined.

The following four model parameters will be considered as free parameters (the default values in the program stem from MARK II [26]) :

- Λ_{LLA} , the QCD scale parameter
- M_{min} , the mass parameter used to terminate the parton shower, constrained to $M_{min} > 2\Lambda_{LLA}$
- σ , the Gaussian p_t width of primary hadrons
- B , fragmentation parameter for light hadrons.

4.2 ARIADNE version 3.1

A complementary way to formulate the QCD parton cascade is in terms of colour dipoles [3]. This model differs from the JETSET PS model only in the sub-leading terms. The $O(\alpha_s)$ matrix element for $e^+e^- \to q\bar{q}g$ as well as the ordering of the emission angles are taken into account by construction. The hadronization of the partonic state is performed with JETSET 7.2. The adjustable parameters are the same as in the previous section, except that the cut-off parameter M_{min} is replaced by the invariant p_t^{min}. The Peterson et al. parameters used are $\epsilon_c = 0.050$ and $\epsilon_b = 0.006$.

4.3 HERWIG versions 4.3 and 5.0

HERWIG [4] is a general simulation program for hard processes involving hadrons. Its predecessor, BIGWIG, was the first parton shower generator to include the effects of soft gluon coherence in leading order. In comparison with JETSET, the formulation of the kinematics is different, and there is no matching to the $O(\alpha_s)$ matrix element at the first branching. In the recent version 5.0 the QCD scale parameter Λ_{LLA} has been re-defined such that it equals $\Lambda_{\overline{MS}}$ in the limit $x \to 1$.

A simple scheme is applied to describe hadronization : first, all gluons are split non-perturbatively into $q\bar{q}$ pairs (the Wolfram Ansatz), adjacent quarks and antiquarks are combined into colourless clusters and, finally, each cluster usually decays into two hadrons according to phase space and spin factors. Special treatment is provided for very light or very heavy clusters. This concept has the advantage that it possesses no explicit fragmentation functions. In particular, there are no adjustable parameters for heavy quark fragmentation. The differences in physics content between

the earlier program versions 3.4 and 4.1, which have also been studied, and version 4.3 are small.

The three main model parameters are considered as variables (the default values in the program stem from OPAL [13, 36]) :

- Λ_{LLA} , the QCD scale parameter
- M_g , the minimum virtual gluon mass used to terminate the shower, constrained to $M_g > 2\Lambda_{LLA}$ in version 4.3
- M_{cl} , the maximum allowed cluster mass (in addition to quark masses). If this mass is exceeded, the cluster is split into 2 clusters of lower mass.

4.4 JETSET version 7.2, $O(\alpha_s^2)$ matrix elements (ME)

Before the advent of parton shower models, matrix elements up to $O(\alpha_s^2)$ have been used at PETRA/PEP energies. At LEP energies the missing higher orders are expected to become increasingly important. A way to partly simulate these higher orders is to choose a small renormalization mass μ. Studies of multi-jet production at PETRA/PEP [27, 28] and at LEP [29, 16] reveal that the jet rates at small values of the jet resolution parameter $y_{cut} < 0.04$, where 4 jets are resolved, can only be reproduced by $O(\alpha_s^2)$ QCD if $f = \mu^2/E_{cm}^2 \approx 0.002$. This procedure is commonly called "experimental optimization".

The default option in JETSET is the Zhu implementation of the $O(\alpha_s^2)$ corrections to three jets. For technical reasons, however, the infrared cut-off y_{min} cannot be varied continuously. The smallest available value $y_{min} = 0.01$ is used, corresponding to an invariant mass of 9 GeV.

The same string hadronization scheme is used as in the PS case. The fragmentation parameter A is kept at the default value of 1.0. The Peterson et al. functions for c and b fragmentation are used with $\epsilon_c = 0.055$ and $\epsilon_b = 0.012$ as derived from PETRA/PEP data.

Four parameters are adjusted to fit the ME model to the data :

- Λ_{eff} , the QCD scale parameter
- $f = \mu^2/E_{cm}^2$, where μ is the renormalization mass
- σ and
- B as in the PS case.

5 Fit of QCD Generators to Corrected Distributions at 91 GeV

5.1 Fit Procedure

The adjustment of the QCD generators is done by varying the parameters listed in section 4 until a minimum of χ^2 between data and Monte Carlo distributions is obtained. A multi-dimensional fitting method (similar to [30]) has been developed in order to take the correlations between the parameters into account. The Monte Carlo generators are run at various points in parameter space and the event shape and inclusive distributions are calculated at each point (without detector simulation). The variation of the content of each bin of each distribution is approximated by a second order Taylor polynomial. Each polynomial has $N_{coeff} = 1 + n + n(n+1)/2$ coefficients to be determined from the Monte Carlo calculation, where n denotes the dimension of the parameter space.

The points in parameter space are arranged on the surface of an n-dimensional hypersphere with unit radius. Previous methods [30] have used a cubic lattice. $N_{coeff} - 1$ points are chosen by random methods such that their mutual distances are as large as possible. The centre of the hypersphere is taken as the remaining point. The coordinates of the points are then linearly mapped on to the actually chosen parameter regions. The advantage of choosing the smallest possible number of points ($=N_{coeff}$) for a given total of Monte Carlo statistics is that enough entries are available in the sparsely populated tails of some distributions. For comparison, the number of points of a cubic lattice grows exponentially with n. The hypersphere method can therefore be more easily extended to higher dimensions (say 5 or more).

For each QCD model, 200000 Monte Carlo events were generated per point, and twice this number at the central point. There are 10 (15) points in case of 3 (4) dimensions. This sample size is sufficiently large that the Monte Carlo statistical errors can be neglected relative to those of the data, for parameter values inside the hypersphere.

The best fit parameter values are found by minimizing the sum of χ^2 between the data distributions and the parameterized Monte Carlo distributions using MINUIT . Only the statistical errors on the data are included. If the solution lies outside the hypersphere, the whole procedure is repeated with a better choice of the parameter region. The regions given in table 19 are those of the last iteration. Although, in principle, local χ^2 minima may exist (χ^2 is of 4th order in the parameters) none has actually been found when fitting data. This is due to the fact that the linear terms in the parametrization dominate.

The choice of the set of distributions to perform the fit is arbitrary to a large extent. It is found that each distribution is sensitive to each model parameter and that the inclusive momentum distributions are more sensitive than the event shapes. Therefore it is not possible to assign a given distribution to a given parameter. In principle a single distribution would be sufficient to determine all parameters. In practice, however, results are unstable because of the small but systematic deviations of the QCD models from the data. In order to ensure a good overall description of the data, a combination of single particle and event shape variables is chosen as the standard set :

$$x_p,\ p_t^{out},\ p_t^{in},\ S,\ A,\ T,\ m.$$

These contain information on both the longitudinal and transverse momentum distribution with respect to the jet axis of the events. The integral of the p_t^{out} or p_t^{in} distributions which is equal to the mean charged multiplicity (data value = 20.85) strongly constrains the parameter space. Sphericity and aplanarity are quadratic in the momenta while thrust and minor are linear and thus emphasize different regions of phase space. The possible statistical correlations between the quantities of this set have not been taken into account.

5.2 Fit Results and Discussion

The best fit parameter values for the QCD models listed in section 4 are given in table 19. Statistical correlation coefficients based on an analysis of the χ^2 function are given in table 20. The χ^2 values for each distribution of the standard set are given in table 21 for each QCD model. The predictions of three of the tuned generators are superimposed on the data distributions in figures 1 to 18, together with the differences between predictions and data in units of the total error.

5.2.1 Systematic effects

Three types of systematic errors of the fit parameters are considered. For each type, the largest change with respect to the best fit results as given in table 19 is conservatively taken as the error.

No systematic error is assigned for possible changes of the model parameters that have been kept fixed in the fits.

First, the effect of varying the experimental cuts (errors of type (1) in section 3) is studied by performing separate fits to data sets for which each cut has been changed at a time.

Second, the QCD model dependence of the correction factors (errors of type (2) in section 3) influences the fitted parameter values and the corresponding χ^2 values in a systematic way. Fits are performed to data sets modified according to

$$D'_{i,corr} = D_{i,corr} * C_i(\text{model j})/C_i(\text{reference model})$$

where the C_i were computed for models j=2,3,4,5 among the list given in section 3.3. Table 22 shows how the total χ^2 value depends on the model used to correct the data. Evidence for model bias is seen since the χ^2 for a given model is smallest if the data were corrected with the same model. The effect is most pronounced for JETSET PS and HERWIG. However, this kind of model bias (which has been first described by OPAL [13] for the example of thrust) is limited to only a few bins. For the distributions being fitted these are : the first bin of p_t^{out} and p_t^{in}, the very high thrust $0.99 < T < 1.00$ and the low minor $0.0 < m < 0.02$ regions. In contrast there are a few other regions where the opposite happens : the χ^2 for a given model grows if the data are corrected with that model. The important thing to note from table 22 is that the hierarchy of χ^2 values is preserved, i.e. JETSET PS still fits better than HERWIG even if the data were corrected with HERWIG.

Third, the fit results may depend on the choice of distributions. The systematic error from this source is estimated by performing fits to the following four sub-sets :

- x_p, p_t^{out}, p_t^{in}, S, A
- x_p, p_t^{out}, p_t^{in}, T, m
- x_p, $< N_{ch} >$, S, A, T, m
- p_t^{out}, p_t^{in}, S, A, T, m

where in each case one or two quantities were removed from the standard set. The measured mean charged multiplicity, $< N_{ch} >= 20.85 \pm 0.02(stat.) \pm 0.24(syst.)$, from a previous ALEPH analysis [31] is added to the 3rd set because the x_p distribution does not cover the full range. (As with the distributions from this analysis, only the statistical error is used in the fit.) For the total systematic error estimates in table 19 the three types of error are added in quadrature.

5.2.2 JETSET 7.2 PS

Of all QCD generators considered, JETSET coherent PS + $O(\alpha_s)$ as well as ARIADNE (see next section) yields the best overall agreement with the data. This also holds when systematic errors are included. The sum of χ^2 of the four shape variables used in the global fit is 89 for 74 bins considering only statistical errors. The shape variables not used in the fit are also well described, see the figures. The model is able to reproduce remarkably well the n-jet production rates over a wide range of jet resolutions, see fig.13.

In the single-particle distributions, though reasonably well described, small but systematic discrepancies are observed. Although the mean multiplicities agree between data and PS model, the model prediction of the x_p distribution is low by up to 5 % in the region $0.1 < x_p < 0.2$, see fig 14. This discrepancy also shows up in the mean scaled momentum sum [32] which is related to the momentum spectrum by $2 < \sum p > /E_{cm} =< N_{ch} >< x_p >$. Another discrepancy can be seen in the tail of the p_t^{out} distribution where the model prediction is low by 7 to 30 % for $p_t^{out} > 0.8$ GeV.

The fitted value of the QCD scale parameter, $\Lambda_{LLA} = 0.318 \pm 0.025$ GeV, lies between the values reported at lower energies by MARK II (0.40 GeV) [26] and TASSO (0.26 GeV) [30], but agrees within errors with the value obtained at Z energy by OPAL ($0.29^{+0.02}_{-0.01}$ GeV) [13] and L3 (0.30 ± 0.03 GeV) [33]. The best fit value for the shower cut-off mass, M_{min}, is around 1.5 GeV which is in the domain where non-perturbative effects are already important. The mean number of partons in the shower depends critically on the M_{min} value and amounts to 2.3 quarks (including antiquarks) and 5.0 gluons using the best fit parameters.

Strong correlations are observed among the pairs of parameters (Λ_{LLA}, σ), (Λ_{LLA}, B) and (σ, B), see table 20a. This indicates that there is no clear-cut discrimination between perturbative and non-perturbative descriptions.

The fits have been done with charm and bottom fragmentation parameters fixed at $\epsilon_c = 0.020$ and $\epsilon_b = 0.015$. These values result in average scaled energies $< x_E >_{D*} = 0.54$ for D^* mesons fragmented from primary c-quarks and $< x_E >_B = 0.66$ for bottom hadrons (x_E is defined as $2E_{hadron}/E_{c.m.}$). Simultaneously changing the ϵ parameters to $\epsilon_c = 0.050$ and $\epsilon_b = 0.006$ and keeping the other parameters fixed, yields $< x_E >_{D*} = 0.50$ and $< x_E >_B = 0.70$, but hardly changes the overall χ^2 value.

Three further variants of the parton shower within the JETSET program have been optimized, see tables 19b and 21. The first variant was to switch off the $O(\alpha_s)$ modification at the first branching. The result is a substantial reduction of Λ_{LLA} from 0.32 to 0.19 GeV. The fit quality gets slightly worse.

The second variant was incoherent branching (discussed in ref.[34]), i.e. no ordering of emission angles due to soft gluon coherence. At the same time the argument of α_s was changed from $z(1-z)m^2$ to $m^2/4$ where m is the virtual parton mass and z is the splitting variable. This variant gives a much worse overall χ^2 than the coherent option, which manifests itself mainly in the shape of the p_t^{in} distribution : the predicted rate of particles in the range $1.5 < p_t^{in} < 5.0$ GeV is about 10 % below the data. The parameters Λ_{LLA} and B are rather unstable and therefore have large errors. The average number of partons, 11.0, is much higher in this case. It seems that the differences between coherent and incoherent parton showers cannot be completely compensated by merely changing parameters.

The third variant was a parton shower with constant α_s. This is in contrast to the default mode where α_s is assumed to run with the virtual mass at each branching. A rather high value of α_s is required. In addition, σ and B change in order to match the average charged multiplicity. The fit quality of the x_p, p_t^{out}, S and T distributions is worse than in the default mode. The higher order contributions in the perturbative prediction which are included through the running of α_s in the parton cascade, are thus found to improve the description of the data.

5.2.3 ARIADNE 3.1 PS

The models ARIADNE and JETSET coherent PS + $O(\alpha_s)$ are found to give equally good overall fits with only small differences in detail, see table 21. Since the fragmentation models are the same in the two cases, the colour dipole and the leading-log implementations of the QCD shower are equivalent descriptions of these data, although with different values of Λ. The shower cut-off p_t^{min} is in the vicinity of 1 GeV.

5.2.4 HERWIG 4.3 and 5.0

The HERWIG event generator describes the gross features of the data but is found to fit less well than JETSET PS, even when systematic errors are taken into account. The HERWIG predictions

of the event shape distributions are somewhat too broad in the 2-jet peak region. In addition they are systematically low in the hard gluon region, i.e. the tails of S, T, P, M, O, y_3, and R_3 for high y_{cut} values. The discrepancy also shows up at large p_t^{in} (fig.18). While the deviations at low x_p are similar to those of JETSET, HERWIG generates too few particles at high x_p, $x_p > 0.4$. This problem was already noted in ref.[35]. On the other hand, the p_t^{out} distribution is better described than with JETSET PS.

In order to study the origin of the discrepancies, the HERWIG parton shower was combined with the JETSET string fragmentation program (the combination is called HERSET). After tuning of the parameters the following observations are made : the χ^2 contribution from the four bins in $0.4 < x_p < 0.8$ drops from 94 (HERWIG) to only 2 (HERSET). Thus, the high-x_p problem of HERWIG is clearly related to a weakness of the cluster hadronization scheme. However, the global χ^2 of HERSET, 960, is not much better than that of HERWIG, 1150. The lowness of the three-jet rate in HERWIG in the hard gluon region is also present for HERSET and has thus to be attributed to the HERWIG parton shower program.

Versions 4.3 and 5.0 yield about the same fit quality, although with different parameter values, see table 19d. The difference in Λ_{LLA} arises from the re-definition of this parameter in version 5.0. As for JETSET, the perturbative cut-off parameter M_g is close to 1 GeV. Given the best fit parameters of version 4.3, an average parton shower consists of 2.7 quarks (including antiquarks) and 3.1 gluons. The statistical correlation between the parameters M_g and M_{cl} is found to be strong (table 20c). Concerning heavy quark fragmentation, HERWIG predicts average scaled energies $< x_E >_{D*}= 0.47$ and $< x_E >_B= 0.63$ which are slightly lower than the experimental numbers.

5.2.5 JETSET 7.2 ME

As already mentioned in section 4.4, a reasonable overall description of event properties in terms of second order QCD requires a small value of the renormalization scale f. The $O(\alpha_s^2)$ model with f = 1 fails to explain quantities related to the momenta out of the event plane like p_t^{out}, A and m, as shown by the large χ^2 values in table 21. The fit assuming f = 1 results in $\Lambda_{eff} = 0.26$ GeV, $\sigma = 0.46$ GeV and B = 0.41 GeV^{-2}. With the optimal value f = 0.0014 corresponding to a mass $\mu = 3.4$ GeV, the agreement in the p_t^{out}, A and m distributions is about as good as with the LLA shower model. The description of the other shape variables, although markedly improved, is not as good as with the parton shower. Large contributions to χ^2 come from the peak regions of the S and T distributions and from the x_p distribution. The discrepancy is also clearly visible in the rapidity distributions, figs.15 and 16.

A smaller discrepancy can be seen in the far tails of the hard gluon region, for example in $S > 0.5$, $T < 0.8$, R_3 at large y_{cut} or in the 4-jet rate R_4, where the ME prediction is systematically high. As a consequence, Λ_{eff} depends on the region chosen for the fit. Whereas the global fit yields $\Lambda_{eff} = 0.14$ GeV , values between 0.10 and 0.14 GeV are obtained depending on which portion of the tails of the various shape variables are used to fit for Λ_{eff} . Furthermore, a separate study has shown that Λ_{eff} also depends on the value chosen for the cut-off parameter y_{min} (the fit gives $\Lambda_{eff} = 0.28$ GeV and f = 0.0016 for $y_{min} = 0.02$). The OPAL collaboration [36] has recently pointed to problems with the JETSET ME generator for small values of f arising from negative differential 3-jet cross sections in some regions of phase space. Thus, the value of Λ_{eff} given in table 19e should not be considered as a measurement of the fundamental parameter $\Lambda_{\overline{MS}}$, but merely as a parameter to be used in a specific model.

In an attempt [37] to match the ME model (with optimized scale) to the PS model it was found that the description of the rapidity distribution can be improved by raising $W_{min,0}$, the parameter used to stop the fragmentation chain, from the default value of 0.8 GeV to 1.9 GeV. This high

value however violates an important ingredient of the string model, namely that the mean rapidity distance between any two hadrons adjacent in rank should be approximately the same over the whole fragmentation chain in high energy $q\bar{q}$ systems. The value $W_{min,0} = 1.9$ GeV is therefore considered inappropriate, although the fit quality of the y- and x_p distributions improves. Even so, the description is still not as good as with the parton shower.

5.3 Comparison with previous results

A determination of the main parameters of JETSET 7.2 PS, ARIADNE 3.1 and HERWIG 3.4 from global event shapes has been performed by the OPAL collaboration [13]. Their values obtained for the QCD scale parameter Λ in the three models, $0.29^{+0.02}_{-0.01}$, 0.110 ± 0.007 and 0.20 ± 0.02 GeV respectively, are in good agreement with the results of the present paper. Due to some differences in the set-up of the generators the fragmentation parameters cannot be exactly compared. The OPAL collaboration used the Lund symmetric fragmentation function also for the heavy quarks and fixed the B-parameter to the TASSO value of 0.34 GeV^{-2} [30]. In case of HERWIG they used the decay tables of the JETSET program.

6 $E_{c.m.}$ - dependence

This section examines how well the QCD generators are able to explain the variation of event properties over the wide e^+e^- energy region from 14 to 91 GeV, using parameter values as determined in the present work at 91 GeV. Figures 20 to 24 show the average multiplicity of charged particles, the average sphericity, the average aplanarity, the average (1 – thrust) and the fraction of 3-jet events (defined by the JADE+E cluster algorithm with $y_{cut} = 0.08$) as measured by this experiment together with results obtained by other experiments at Z energy [13, 15, 16, 17, 38, 39] and at lower energies [26, 27, 40]. The ALEPH result for $< N_{ch} >$ is taken from [31]. The predictions of the JETSET and HERWIG parton shower models and of the JETSET $O(\alpha_s^2)$ matrix element model are shown as curves.

All quantities shown (except $< N_{ch} >$) exhibit a decrease with increasing $E_{c.m.}$. This is expected for two reasons : firstly, the jets of the dominant 2-jet structure become narrower and, secondly, the strong coupling α_s decreases with increasing energy. $< S >$ and $< 1 - T >$ decrease by 30 to 40 % between 35 and 91 GeV. In contrast, the 3-jet fraction R_3 decreases by only about 18 % in the same energy range. The quantity R_3 has been used previously [28, 29] to demonstrate the running of α_s since hadronization effects are small above ≈ 30 GeV.

A remarkably good description of the data over the full energy range is provided by the JETSET coherent PS + $O(\alpha_s)$ model. It predicts a 16 % decrease in R_3. The JETSET PS model with constant α_s shows essentially no variation of R_3 between 35 and 91 GeV, in disagreement with the data, see fig.24. The rise of R_3 below 30 GeV in this latter model is attributed to hadronization effects.

The curves from HERWIG PS show a slightly steeper $E_{c.m.}$- dependence than JETSET PS and are in less good agreement with the data. The predictions for R_3, although underestimated in absolute value, decrease by 17 % between 35 and 91 GeV. The rise of $< N_{ch} >$ with energy is well reproduced by both parton shower models.

The JETSET ME model with an optimized renormalization scale and with fixed parameters, is not expected to describe data over a wide energy range. This is due to the constant value employed for the dimensionless cut-off parameter y_{min}. Given the small y_{min} and f values, the 4-parton rate exceeds the 3-parton rate at PETRA/PEP energies, which signals the breakdown of fixed order perturbation theory and which produces too broad event shapes. This failure cannot be cured by merely adjusting fragmentation parameters at each energy.

7 Summary

Using 53000 selected hadronic annihilation events taken by the ALEPH detector at LEP at energies close to the Z peak, measurements are presented of several event shape and particle momentum distributions and of the n-jet production rates. Only charged particles are used in the analysis. The data distributions were corrected for detector effects and initial state photon radiation.

The predictions of the parton shower (PS) generators JETSET, ARIADNE and HERWIG as well as the $O(\alpha_s^2)$ matrix element (ME) option of JETSET are compared to these data. Selected parameters of these generators are determined by means of a global fit.

Taking statistical and systematic errors into account, JETSET coherent PS + $O(\alpha_s)$ and ARIADNE PS, both with string fragmentation, provide the best description of the data distributions. Even these models show small but significant discrepancies in the inclusive x_p and p_t^{out} distributions. Incoherent branching or constant α_s in the parton shower leads to worse descriptions of the data. In general, the HERWIG PS model fits less well than JETSET PS. Discrepancies are seen in the 2-jet peak and in the hard gluon and high-x regions. In all PS models, fitted values near 1 GeV are obtained for the cut-off mass (or p_t) parameters.

Due to the lack of higher orders, the JETSET ME generator, even with an optimized renormalization scale, cannot describe the data as well as JETSET PS. Although the rate of non-planar events is reproduced, deviations are seen in the 2-jet peak and in the momentum spectrum. In addition, a small discrepancy shows up in the hard gluon region such that the value for Λ_{eff} depends on the region chosen for the fit.

As expected, the JETSET ME model with fixed parameters does not describe data over a wide energy range. The parton shower models provide a good description of event shape data over the $E_{c.m.}$ range from 14 to 91 GeV, with JETSET being slightly better than HERWIG.

Acknowledgements

We would like to thank T.Sjöstrand and B.R.Webber for useful discussions. We thank our colleagues of the Accelerator divisions for the good performance of LEP. We are grateful to the engineering and technical personnel at all our collaborating institutions for their support in constructing and maintaining ALEPH. Those of us from non-member states wish to thank CERN for its hospitality.

Appendix: Definition of variables

1-3) Sphericity $S = 3(Q_1 + Q_2)/2$, aplanarity $A = 3/2Q_1$ and planarity $P = Q_2 - Q_1$ are computed from the eigenvalues $Q_1 < Q_2 < Q_3$ of the normalized 3x3 sphericity tensor $M_{\alpha\beta} = \sum_i p_{i\alpha} \cdot p_{i\beta} / \sum_i p_i^2$, where α, β denote the x,y,z momentum components of particle i. The unit eigenvector $\mathbf{n_3}$ is the sphericity axis and $\mathbf{n_1}$ and $\mathbf{n_2}$ span the event plane.

4) The quantity $C = 3(\lambda_1\lambda_2 + \lambda_1\lambda_3 + \lambda_2\lambda_3)$ is computed from the eigenvalues $\lambda_1, \lambda_2, \lambda_3$ of the linear momentum tensor $M'_{\alpha\beta} = \sum_i \frac{p_{i\alpha}p_{i\beta}}{|p_i|} / \sum_i |p_i|$.

5-8) The thrust value is defined as $T = \max(\sum_i |\mathbf{p_i} \cdot \mathbf{n}| / \sum_i |\mathbf{p_i}|)$ where $\mathbf{n}$ is the thrust axis. The same expression is used to compute the major value, M, but replacing the 3-dimensional momenta by the projections into a plane perpendicular to the thrust axis. The minor value, m, refers to an axis perpendicular to both the thrust and major axes.

9-11) Each event is divided into two hemispheres by a plane perpendicular to the thrust axis and the invariant masses are calculated in each hemisphere. The quantities M_h^2/s (M_l^2/s) are the

higher (lower) mass squared divided by the total energy squared. If only charged particles are used, $\sqrt{s}$ is replaced by the charged energy sum, E_{vis}.

12,13) The widely used cluster algorithm originally introduced by JADE [27] is applied in order to determine the jets in each event. At the start each particle is considered to be a cluster. The quantity $y_{ij} = 2E_iE_j(1-\cos\Theta_{ij})/E_{vis}^2$ ("JADE metric") is calculated for each pair and the pair with the smallest value is merged into one cluster. This procedure is iterated. The variable y_3 is defined as the smallest y_{ij} at the point when the algorithm arrives at three jets. The distribution of y_3 is often referred to as the differential 2-jet rate. Another way of analysing the data is to determine the number of jets corresponding to a pre-selected value of y_{cut}. The iterations are carried out until the smallest y_{ij} exceeds y_{cut}. The clusters remaining at this point are called jets. Different recombination schemes are proposed in the literature. In the JADE+E scheme, which is the original one, the clusters are merged simply by adding the 4-momenta, $p_{ij} = p_i + p_j$. The JADE+E0 prescription which has been used by ALEPH in a measurement of α_s [12], is slightly different : $E_{ij} = E_i + E_j$, $\mathbf{p_{ij}} = E_{ij}(\mathbf{p_i} + \mathbf{p_j})/|\mathbf{p_i} + \mathbf{p_j}|$.

14) The following single-particle variables are computed for charged particles only. The scaled momentum is defined as $x_p = 2|\mathbf{p}|/E_{c.m.}$.

15,16) The rapidity is $y = 1/2\ln((E+p_L)/(E-p_L))$, where p_L is the momentum component along either the sphericity or the thrust axis.

17) The transverse momentum component out of the event plane is defined as $p_t^{out} = |\mathbf{p}\cdot\mathbf{n_1}|$.

18) The transverse momentum component in the event plane is defined as $p_t^{in} = |\mathbf{p}\cdot\mathbf{n_2}|$.

Note : The variables 9-13) and 15,16) depend on the particle masses. For the experimental data the pion mass is assumed throughout. In the Monte Carlo calculations used to compute the corrections and the predictions, the "true" masses as given by the generators are inserted.

References

[1] T.Sjöstrand (conv.), *QCD Generators*, in : Proc. Workshop on Z Physics at LEP 1, eds. G.Altarelli, R.Kleiss and C.Verzegnassi, CERN Report 89-08 Vol 3.

[2] T.Sjöstrand, Comp. Phys. Commun. 39 (1986) 347;
T.Sjöstrand and M.Bengtsson, Comp. Phys. Commun. 43 (1987) 367;
M.Bengtsson and T.Sjöstrand, Phys. Lett. B185 (1987) 435;
JETSET version 7.2 Users Manual.

[3] G.Gustafson, U.Petterson, Nucl. Phys. B306 (1988) 746;
L.Lönnblad, preprint LU-TP 89-10.

[4] G.Marchesini and B.R.Webber, Nucl. Phys. B310 (1988) 461;
I.Knowles, Nucl. Phys. B310 (1988) 571;
G.Marchesini et al., Comp. Phys. Commun. 67 (1992) 465.

[5] ALEPH Collab., D.Decamp et al, Phys. Lett. B234 (1990) 209.

[6] ALEPH Collab., D.Decamp et al., Nucl. Instr. and Meth. A294 (1990) 121.

[7] W.B.Atwood et al., Nucl. Instr. and Meth. A306 (1991) 446.

[8] Z.Kunszt, P.Nason, G.Marchesini and B.R Webber, *QCD*, in : Proc. Workshop on Z Physics at LEP 1, eds. G.Altarelli, R.Kleiss and C.Verzegnassi,
CERN Report 89-08 Vol 1.

[9] T.Sjöstrand, Comp. Phys. Commun. 28 (1983) 229.

[10] JETSET version 6.3 PS parameters used for event simulation : Λ_{LLA} = 0.35 GeV, M_{min} = 1.46 GeV, σ = 0.34 GeV, A = 0.5, B = 1.00 GeV^{-2}.

[11] MARK II Collab., D.R.Wood et al., Phys. Rev. D37 (1988) 3091.

[12] ALEPH Collab., D.Decamp et al., Phys. Lett. B255 (1991) 623.

[13] OPAL Collab., M.Akrawy et al., Z. Phys. C47 (1990) 505.

[14] DELPHI Collab., P.Abreu et al., preprint CERN PPE/91-181.

[15] OPAL Collab., M.Akrawy et al., Z. Phys. C49 (1991) 375.

[16] DELPHI Collab., P.Abreu et al., Phys. Lett. B247 (1990) 167.

[17] L3 Collab., B.Adeva et al., Phys. Lett. B248 (1990) 464.

[18] G.Marchesini and B.R.Webber, Nucl. Phys. B238 (1984) 1.

[19] B.Anderson, G.Gustafson, G.Ingelman and T.Sjöstrand, Phys. Rep. 97 (1983) 31.

[20] C.Peterson et al., Phys. Rev. D27 (1983) 105.

[21] S.Bethke, Z. Phys. C29 (1985) 175.

[22] TASSO Collab., W.Braunschweig et al., Z. Phys. C44 (1989) 357.

[23] J.Chrin, Z. Phys. C36 (1987) 163.

[24] ALEPH Collab., D.Decamp et al., Phys. Lett. B266 (1991) 218.

[25] ALEPH Collab., D.Decamp et al., Phys. Lett. B244 (1990) 551.

[26] MARK II Collab., A.Petersen et al., Phys. Rev. D37 (1988) 1.

[27] JADE Collab., W.Bartel et al., Z. Phys. C33 (1986) 23;
JADE Collab., S.Bethke et al., Phys. Lett. B213 (1988) 235;
TASSO Collab., W.Braunschweig et al., Phys. Lett B214 (1988) 286.

[28] S.Bethke, Z. Phys. C43 (1989) 331.

[29] OPAL Collab., M.Akrawy et al., Phys. Lett. B235 (1990) 389.

[30] TASSO Collab., M.Althoff et al., Z. Phys. C26 (1984) 157;
TASSO Collab., W.Braunschweig et al., Z. Phys. C41 (1988) 359.

[31] ALEPH Collab., D.Decamp et al., Phys. Lett. B273 (1991) 181.

[32] ALEPH Collab., D.Decamp et al., Z. Phys. C53 (1992) 1.

[33] L3 Collab., B.Adeva et al., Phys. Lett. B257 (1991) 469.

[34] M.Bengtsson and T.Sjöstrand, Nucl. Phys. B289 (1987) 810.

[35] HRS Collab., M.Derrick et al., Phys. Lett. B164 (1985) 199.

[36] OPAL Collab., P.D.Acton et al., Phys. Lett. B276 (1992) 547.

[37] W.DeBoer, H.Fürstenau and J.Köhne, Z. Phys. C49 (1991) 141.

[38] DELPHI Collab., P.Abreu et al., Z. Phys. C50 (1991) 185.

[39] OPAL Collab., P.D.Acton et al., Z. Phys. C53 (1992) 539.

[40] TASSO Collab., W.Braunschweig et al., Z. Phys. C47 (1990) 187;
AMY Collab., I.H.Park et al., Phys. Rev. D41 (1990) 2675;
TASSO Collab., W.Braunschweig et al., Z. Phys. C45 (1989) 193;
JADE Collab., W.Bartel et al., Z. Phys. C20 (1983) 187;
HRS Collab., M.Derrick et al., Phys. Rev. D34 (1986) 3304;
AMY Collab., H.W.Zheng et al., Phys. Rev. D42 (1990) 737;
JADE Collab., S.Bethke et al., Phys. Lett. B213 (1988) 235;
MARK-2 Collab., S.Bethke et al., Z. Phys. C43 (1989) 325;
VENUS Collab., K.Abe et al., Phys. Lett. B240 (1990) 232;
AMY Collab., I.H.Park et al., Phys. Rev. Lett. 62 (1989) 1713.

Interval	corrected for charged only	corrected for charged+neutrals
0.000 - 0.005	12.60 ± 0.32 ± 0.40	9.90 ± 0.26 ± 0.79
0.005 - 0.010	24.22 ± 0.48 ± 0.39	24.37 ± 0.48 ± 1.62
0.010 - 0.015	19.94 ± 0.43 ± 0.41	20.31 ± 0.43 ± 1.49
0.015 - 0.020	16.65 ± 0.39 ± 0.23	17.72 ± 0.41 ± 0.39
0.020 - 0.025	13.45 ± 0.36 ± 0.26	14.35 ± 0.38 ± 0.46
0.025 - 0.030	11.62 ± 0.34 ± 0.24	12.14 ± 0.35 ± 0.53
0.030 - 0.035	8.89 ± 0.29 ± 0.17	9.32 ± 0.30 ± 0.30
0.035 - 0.040	7.33 ± 0.26 ± 0.20	7.31 ± 0.26 ± 0.22
0.040 - 0.050	5.87 ± 0.16 ± 0.15	5.81 ± 0.16 ± 0.22
0.050 - 0.060	4.63 ± 0.15 ± 0.10	4.64 ± 0.15 ± 0.24
0.060 - 0.080	3.145 ± 0.083 ± 0.062	3.201 ± 0.084 ± 0.089
0.080 - 0.100	2.218 ± 0.069 ± 0.035	2.236 ± 0.070 ± 0.082
0.100 - 0.120	1.656 ± 0.060 ± 0.058	1.618 ± 0.058 ± 0.059
0.120 - 0.160	1.180 ± 0.036 ± 0.031	1.177 ± 0.036 ± 0.047
0.160 - 0.200	0.817 ± 0.030 ± 0.016	0.840 ± 0.031 ± 0.023
0.200 - 0.250	0.592 ± 0.023 ± 0.020	0.582 ± 0.023 ± 0.019
0.250 - 0.300	0.390 ± 0.018 ± 0.013	0.371 ± 0.017 ± 0.013
0.300 - 0.350	0.283 ± 0.015 ± 0.013	0.283 ± 0.015 ± 0.014
0.350 - 0.400	0.218 ± 0.013 ± 0.012	0.213 ± 0.013 ± 0.012
0.400 - 0.500	0.159 ± 0.008 ± 0.006	0.150 ± 0.008 ± 0.010
0.500 - 0.600	0.074 ± 0.005 ± 0.004	0.073 ± 0.005 ± 0.013
0.600 - 0.700	0.041 ± 0.004 ± 0.005	0.037 ± 0.004 ± 0.011
$< S >$	0.0736 ± 0.0007 ± 0.0005	0.0727 ± 0.0007 ± 0.0016

Table 1 : Sphericity distribution. The statistical error is followed by the systematic error.

Interval	corrected for charged only	corrected for charged+neutrals
0.0000 - 0.0025	81.30 ± 1.17 ± 0.83	63.45 ± 0.94 ± 1.30
0.0025 - 0.0050	86.27 ± 1.26 ± 0.99	93.70 ± 1.36 ± 5.36
0.0050 - 0.0075	56.24 ± 1.01 ± 1.11	64.01 ± 1.13 ± 1.88
0.0075 - 0.0100	38.28 ± 0.84 ± 0.66	41.93 ± 0.91 ± 1.59
0.010 - 0.015	24.11 ± 0.47 ± 0.24	25.34 ± 0.50 ± 1.11
0.015 - 0.020	13.68 ± 0.36 ± 0.30	13.91 ± 0.36 ± 0.58
0.020 - 0.030	7.01 ± 0.18 ± 0.18	6.90 ± 0.18 ± 0.30
0.030 - 0.040	3.34 ± 0.12 ± 0.08	3.14 ± 0.12 ± 0.12
0.040 - 0.060	1.417 ± 0.055 ± 0.048	1.279 ± 0.050 ± 0.076
0.060 - 0.080	0.543 ± 0.033 ± 0.035	0.472 ± 0.029 ± 0.046
0.080 - 0.100	0.297 ± 0.027 ± 0.023	0.258 ± 0.023 ± 0.027
0.100 - 0.120	0.150 ± 0.018 ± 0.017	0.147 ± 0.018 ± 0.025
0.120 - 0.140	0.108 ± 0.017 ± 0.016	0.089 ± 0.015 ± 0.014
0.140 - 0.160	0.043 ± 0.009 ± 0.007	0.036 ± 0.008 ± 0.007
0.160 - 0.200	0.023 ± 0.005 ± 0.004	0.022 ± 0.004 ± 0.004
$< A >$	0.0119 ± 0.0001 ± 0.0001	0.0117 ± 0.0001 ± 0.0003

Table 2 : Aplanarity distribution.

Interval	corrected for charged only	corrected for charged+neutrals
0.000 - 0.005	66.89 ± 0.79 ± 0.28	68.62 ± 0.81 ± 2.20
0.005 - 0.010	32.99 ± 0.56 ± 0.30	32.72 ± 0.55 ± 1.56
0.010 - 0.015	18.66 ± 0.41 ± 0.52	18.07 ± 0.40 ± 0.71
0.015 - 0.020	11.83 ± 0.33 ± 0.19	11.45 ± 0.32 ± 0.61
0.020 - 0.025	8.83 ± 0.28 ± 0.13	8.45 ± 0.27 ± 0.43
0.025 - 0.030	6.23 ± 0.23 ± 0.10	6.35 ± 0.23 ± 0.31
0.030 - 0.035	5.36 ± 0.21 ± 0.16	5.33 ± 0.21 ± 0.19
0.035 - 0.040	4.62 ± 0.20 ± 0.20	4.53 ± 0.20 ± 0.26
0.040 - 0.050	3.42 ± 0.12 ± 0.12	3.55 ± 0.12 ± 0.18
0.050 - 0.060	2.84 ± 0.11 ± 0.09	2.79 ± 0.11 ± 0.13
0.060 - 0.080	1.926 ± 0.064 ± 0.065	1.896 ± 0.063 ± 0.068
0.080 - 0.100	1.385 ± 0.056 ± 0.048	1.420 ± 0.057 ± 0.047
0.100 - 0.120	1.000 ± 0.046 ± 0.026	1.034 ± 0.048 ± 0.045
0.120 - 0.160	0.660 ± 0.026 ± 0.024	0.656 ± 0.026 ± 0.030
0.160 - 0.200	0.432 ± 0.021 ± 0.019	0.412 ± 0.021 ± 0.019
0.200 - 0.250	0.271 ± 0.015 ± 0.010	0.269 ± 0.015 ± 0.022
0.250 - 0.300	0.194 ± 0.013 ± 0.009	0.176 ± 0.012 ± 0.019
0.300 - 0.350	0.090 ± 0.008 ± 0.008	0.096 ± 0.008 ± 0.028
0.350 - 0.400	0.054 ± 0.006 ± 0.007	0.052 ± 0.006 ± 0.017
0.400 - 0.500	0.013 ± 0.002 ± 0.001	0.011 ± 0.002 ± 0.007
$< P >$	0.0337 ± 0.0004 ± 0.0003	0.0333 ± 0.0004 ± 0.0014

Table 3 : Planarity distribution.

Interval	corrected for charged only	corrected for charged+neutrals
0.000 - 0.040	0.44 ± 0.02 ± 0.07	0.12 ± 0.01 ± 0.09
0.040 - 0.080	2.57 ± 0.05 ± 0.15	1.90 ± 0.04 ± 0.38
0.080 - 0.120	3.76 ± 0.07 ± 0.13	4.22 ± 0.07 ± 0.44
0.120 - 0.160	3.34 ± 0.06 ± 0.16	3.70 ± 0.07 ± 0.36
0.160 - 0.200	2.54 ± 0.05 ± 0.09	2.62 ± 0.06 ± 0.29
0.200 - 0.240	2.042 ± 0.049 ± 0.067	2.125 ± 0.051 ± 0.076
0.240 - 0.280	1.604 ± 0.043 ± 0.043	1.683 ± 0.045 ± 0.085
0.280 - 0.320	1.391 ± 0.041 ± 0.034	1.368 ± 0.040 ± 0.088
0.320 - 0.360	1.142 ± 0.037 ± 0.041	1.141 ± 0.037 ± 0.073
0.360 - 0.400	0.922 ± 0.032 ± 0.037	0.955 ± 0.033 ± 0.043
0.400 - 0.440	0.858 ± 0.031 ± 0.033	0.824 ± 0.030 ± 0.042
0.440 - 0.480	0.711 ± 0.029 ± 0.030	0.725 ± 0.029 ± 0.030
0.480 - 0.520	0.658 ± 0.028 ± 0.028	0.668 ± 0.028 ± 0.028
0.520 - 0.560	0.566 ± 0.026 ± 0.016	0.583 ± 0.027 ± 0.031
0.560 - 0.600	0.534 ± 0.026 ± 0.034	0.505 ± 0.024 ± 0.041
0.600 - 0.640	0.451 ± 0.023 ± 0.022	0.457 ± 0.023 ± 0.022
0.640 - 0.680	0.348 ± 0.019 ± 0.020	0.361 ± 0.019 ± 0.019
0.680 - 0.720	0.358 ± 0.020 ± 0.024	0.367 ± 0.020 ± 0.034
0.720 - 0.760	0.271 ± 0.016 ± 0.016	0.271 ± 0.016 ± 0.018
0.760 - 0.800	0.260 ± 0.017 ± 0.018	0.251 ± 0.016 ± 0.056
0.800 - 0.840	0.140 ± 0.012 ± 0.014	0.127 ± 0.011 ± 0.022
0.840 - 0.880	0.065 ± 0.008 ± 0.010	0.064 ± 0.008 ± 0.012
0.880 - 0.920	0.021 ± 0.004 ± 0.007	0.017 ± 0.003 ± 0.006
$< C >$	0.2587 ± 0.0013 ± 0.0018	0.2617 ± 0.0013 ± 0.0034

Table 4 : C-parameter distribution.

Interval	corrected for charged only	corrected for charged+neutrals
0.600 - 0.650	0.021 ± 0.005 ± 0.006	0.026 ± 0.006 ± 0.010
0.650 - 0.700	0.112 ± 0.009 ± 0.015	0.099 ± 0.008 ± 0.027
0.700 - 0.750	0.308 ± 0.016 ± 0.023	0.291 ± 0.016 ± 0.044
0.750 - 0.800	0.527 ± 0.021 ± 0.016	0.542 ± 0.021 ± 0.016
0.800 - 0.820	0.864 ± 0.045 ± 0.030	0.873 ± 0.045 ± 0.039
0.820 - 0.840	1.070 ± 0.049 ± 0.057	1.088 ± 0.050 ± 0.057
0.840 - 0.860	1.413 ± 0.058 ± 0.052	1.444 ± 0.060 ± 0.058
0.860 - 0.880	1.948 ± 0.069 ± 0.090	1.929 ± 0.069 ± 0.090
0.880 - 0.900	2.463 ± 0.076 ± 0.101	2.423 ± 0.075 ± 0.163
0.900 - 0.920	3.36 ± 0.09 ± 0.11	3.42 ± 0.09 ± 0.12
0.920 - 0.940	5.06 ± 0.11 ± 0.08	5.05 ± 0.11 ± 0.31
0.940 - 0.950	6.93 ± 0.18 ± 0.24	7.21 ± 0.19 ± 0.18
0.950 - 0.960	9.30 ± 0.21 ± 0.37	9.73 ± 0.22 ± 0.87
0.960 - 0.965	11.23 ± 0.33 ± 0.39	11.75 ± 0.34 ± 1.48
0.965 - 0.970	12.70 ± 0.34 ± 0.51	14.10 ± 0.38 ± 1.67
0.970 - 0.975	15.18 ± 0.38 ± 0.56	17.18 ± 0.43 ± 0.98
0.975 - 0.980	16.78 ± 0.39 ± 0.66	19.49 ± 0.45 ± 2.15
0.980 - 0.985	16.80 ± 0.38 ± 0.85	17.57 ± 0.40 ± 3.28
0.985 - 0.990	12.86 ± 0.31 ± 0.85	9.37 ± 0.24 ± 2.08
0.990 - 0.995	6.55 ± 0.21 ± 0.82	2.55 ± 0.10 ± 1.42
0.995 - 1.000	1.15 ± 0.07 ± 0.29	0.17 ± 0.02 ± 0.19
$< 1 - T >$	0.0654 ± 0.0004 ± 0.0006	0.0662 ± 0.0004 ± 0.0011

Table 5 : Thrust distribution.

Interval	corrected for charged only	corrected for charged+neutrals
0.020 - 0.040	0.31 ± 0.02 ± 0.05	0.10 ± 0.01 ± 0.05
0.040 - 0.050	1.34 ± 0.07 ± 0.09	0.90 ± 0.05 ± 0.24
0.050 - 0.060	2.90 ± 0.11 ± 0.22	2.63 ± 0.10 ± 0.47
0.060 - 0.070	4.36 ± 0.14 ± 0.16	4.74 ± 0.15 ± 0.26
0.070 - 0.080	5.51 ± 0.16 ± 0.10	5.88 ± 0.17 ± 0.63
0.080 - 0.100	6.13 ± 0.12 ± 0.12	6.57 ± 0.13 ± 0.51
0.100 - 0.120	5.95 ± 0.12 ± 0.16	6.31 ± 0.13 ± 0.23
0.120 - 0.140	4.77 ± 0.10 ± 0.08	4.91 ± 0.11 ± 0.14
0.140 - 0.160	4.04 ± 0.10 ± 0.10	4.01 ± 0.10 ± 0.14
0.160 - 0.200	2.910 ± 0.057 ± 0.044	2.918 ± 0.057 ± 0.115
0.200 - 0.240	2.147 ± 0.049 ± 0.038	2.069 ± 0.048 ± 0.053
0.240 - 0.280	1.586 ± 0.042 ± 0.042	1.608 ± 0.043 ± 0.047
0.280 - 0.320	1.190 ± 0.036 ± 0.022	1.167 ± 0.036 ± 0.027
0.320 - 0.360	0.917 ± 0.032 ± 0.038	0.889 ± 0.031 ± 0.049
0.360 - 0.400	0.712 ± 0.029 ± 0.032	0.701 ± 0.028 ± 0.033
0.400 - 0.440	0.490 ± 0.022 ± 0.015	0.481 ± 0.022 ± 0.014
0.440 - 0.480	0.352 ± 0.018 ± 0.012	0.336 ± 0.018 ± 0.017
0.480 - 0.520	0.248 ± 0.015 ± 0.007	0.228 ± 0.014 ± 0.041
0.520 - 0.560	0.179 ± 0.013 ± 0.023	0.137 ± 0.010 ± 0.053
0.560 - 0.600	0.104 ± 0.010 ± 0.014	0.063 ± 0.006 ± 0.024
0.600 - 0.640	0.042 ± 0.006 ± 0.009	0.014 ± 0.002 ± 0.006
$< M >$	0.1784 ± 0.0008 ± 0.0007	0.1750 ± 0.0007 ± 0.0021

Table 6 : Major distribution.

Interval	corrected for charged only	corrected for charged+neutrals
0.000 - 0.020	0.216 ± 0.018 ± 0.055	0.024 ± 0.004 ± 0.030
0.020 - 0.040	3.29 ± 0.08 ± 0.19	1.62 ± 0.04 ± 0.42
0.040 - 0.050	8.24 ± 0.19 ± 0.15	6.68 ± 0.15 ± 0.55
0.050 - 0.060	10.66 ± 0.22 ± 0.15	10.48 ± 0.21 ± 0.41
0.060 - 0.070	11.35 ± 0.23 ± 0.25	12.42 ± 0.25 ± 1.03
0.070 - 0.080	10.83 ± 0.22 ± 0.21	12.21 ± 0.25 ± 0.79
0.080 - 0.100	8.80 ± 0.14 ± 0.11	10.05 ± 0.16 ± 0.28
0.100 - 0.120	6.20 ± 0.12 ± 0.10	6.73 ± 0.13 ± 0.40
0.120 - 0.140	4.18 ± 0.10 ± 0.08	4.33 ± 0.11 ± 0.17
0.140 - 0.160	2.554 ± 0.078 ± 0.057	2.531 ± 0.078 ± 0.089
0.160 - 0.200	1.287 ± 0.039 ± 0.030	1.215 ± 0.037 ± 0.046
0.200 - 0.240	0.523 ± 0.025 ± 0.021	0.479 ± 0.023 ± 0.038
0.240 - 0.280	0.196 ± 0.014 ± 0.012	0.202 ± 0.015 ± 0.026
0.280 - 0.320	0.095 ± 0.010 ± 0.011	0.084 ± 0.009 ± 0.011
0.320 - 0.360	0.029 ± 0.005 ± 0.006	0.029 ± 0.005 ± 0.006
0.360 - 0.400	0.010 ± 0.003 ± 0.004	0.013 ± 0.004 ± 0.005
$< m >$	0.0922 ± 0.0003 ± 0.0003	0.0945 ± 0.0003 ± 0.0006

Table 7 : Minor distribution.

Interval	corrected for charged only	corrected for charged+neutrals
0.000 - 0.020	7.63 ± 0.14 ± 0.13	9.21 ± 0.16 ± 0.41
0.020 - 0.040	10.96 ± 0.16 ± 0.12	11.62 ± 0.17 ± 0.26
0.040 - 0.050	8.65 ± 0.20 ± 0.15	8.14 ± 0.19 ± 0.37
0.050 - 0.060	6.92 ± 0.18 ± 0.11	6.49 ± 0.17 ± 0.53
0.060 - 0.070	5.66 ± 0.16 ± 0.20	5.34 ± 0.15 ± 0.33
0.070 - 0.080	4.81 ± 0.15 ± 0.10	4.28 ± 0.13 ± 0.33
0.080 - 0.100	3.75 ± 0.09 ± 0.08	3.55 ± 0.09 ± 0.24
0.100 - 0.120	2.878 ± 0.080 ± 0.066	2.760 ± 0.077 ± 0.102
0.120 - 0.140	2.219 ± 0.070 ± 0.079	2.140 ± 0.068 ± 0.111
0.140 - 0.160	1.764 ± 0.061 ± 0.059	1.622 ± 0.057 ± 0.062
0.160 - 0.200	1.311 ± 0.038 ± 0.040	1.273 ± 0.037 ± 0.043
0.200 - 0.240	0.866 ± 0.030 ± 0.050	0.844 ± 0.029 ± 0.050
0.240 - 0.280	0.648 ± 0.027 ± 0.034	0.608 ± 0.025 ± 0.033
0.280 - 0.320	0.441 ± 0.021 ± 0.014	0.407 ± 0.020 ± 0.019
0.320 - 0.360	0.253 ± 0.015 ± 0.018	0.245 ± 0.014 ± 0.033
0.360 - 0.400	0.193 ± 0.014 ± 0.010	0.151 ± 0.011 ± 0.040
0.400 - 0.440	0.109 ± 0.010 ± 0.008	0.069 ± 0.006 ± 0.035
0.440 - 0.480	0.060 ± 0.007 ± 0.010	0.034 ± 0.004 ± 0.023
0.480 - 0.520	0.030 ± 0.005 ± 0.007	0.009 ± 0.002 ± 0.005
$< O >$	0.0861 ± 0.0006 ± 0.0005	0.0806 ± 0.0006 ± 0.0022

Table 8 : Oblateness distribution.

Interval	corrected for charged only	corrected for charged+neutrals
0.000 - 0.005	1.13 ± 0.06 ± 0.41	0.17 ± 0.02 ± 0.29
0.005 - 0.010	8.32 ± 0.21 ± 1.43	4.34 ± 0.13 ± 2.34
0.010 - 0.015	16.70 ± 0.34 ± 2.15	17.70 ± 0.36 ± 4.92
0.015 - 0.020	20.60 ± 0.43 ± 1.79	25.54 ± 0.52 ± 3.79
0.020 - 0.025	19.30 ± 0.44 ± 1.67	22.74 ± 0.51 ± 2.30
0.025 - 0.030	16.20 ± 0.40 ± 0.79	17.36 ± 0.43 ± 3.17
0.030 - 0.035	14.10 ± 0.39 ± 0.86	14.23 ± 0.39 ± 2.23
0.035 - 0.040	11.78 ± 0.36 ± 0.65	11.54 ± 0.35 ± 1.08
0.040 - 0.050	8.94 ± 0.21 ± 0.27	8.61 ± 0.21 ± 0.47
0.050 - 0.060	6.79 ± 0.19 ± 0.41	6.57 ± 0.18 ± 0.38
0.060 - 0.080	4.75 ± 0.11 ± 0.22	4.37 ± 0.10 ± 0.31
0.080 - 0.100	3.03 ± 0.09 ± 0.17	2.92 ± 0.08 ± 0.15
0.100 - 0.120	2.106 ± 0.072 ± 0.085	2.034 ± 0.070 ± 0.105
0.120 - 0.140	1.423 ± 0.059 ± 0.063	1.373 ± 0.057 ± 0.068
0.140 - 0.160	1.079 ± 0.052 ± 0.056	1.103 ± 0.053 ± 0.062
0.160 - 0.180	0.741 ± 0.042 ± 0.043	0.723 ± 0.041 ± 0.044
0.180 - 0.200	0.614 ± 0.040 ± 0.042	0.608 ± 0.040 ± 0.041
0.200 - 0.250	0.341 ± 0.018 ± 0.013	0.316 ± 0.017 ± 0.043
0.250 - 0.300	0.139 ± 0.011 ± 0.012	0.109 ± 0.009 ± 0.055
0.300 - 0.350	0.054 ± 0.007 ± 0.008	0.017 ± 0.003 ± 0.012
0.350 - 0.400	0.0144 ± 0.0029 ± 0.0021	0.0005 ± 0.0003 ± 0.0003
$< M_h^2/s >$	0.0550 ± 0.0004 ± 0.0006	0.0528 ± 0.0003 ± 0.0018

Table 9 : Heavy jet mass distribution.

Interval	corrected for charged only	corrected for charged+neutrals
0.000 - 0.005	32.27 ± 0.43 ± 3.36	9.19 ± 0.17 ± 4.28
0.005 - 0.010	48.29 ± 0.64 ± 3.51	42.28 ± 0.57 ± 8.59
0.010 - 0.015	37.73 ± 0.63 ± 2.92	48.69 ± 0.80 ± 7.03
0.015 - 0.020	25.79 ± 0.56 ± 1.79	34.47 ± 0.73 ± 4.01
0.020 - 0.025	16.94 ± 0.47 ± 0.84	21.05 ± 0.57 ± 0.75
0.025 - 0.030	11.25 ± 0.38 ± 0.42	13.09 ± 0.44 ± 0.53
0.030 - 0.035	7.62 ± 0.31 ± 0.49	8.74 ± 0.35 ± 0.83
0.035 - 0.040	4.78 ± 0.23 ± 0.48	5.61 ± 0.27 ± 0.82
0.040 - 0.045	3.78 ± 0.22 ± 0.53	4.18 ± 0.24 ± 0.82
0.045 - 0.050	2.63 ± 0.17 ± 0.30	3.06 ± 0.20 ± 0.43
0.050 - 0.060	2.06 ± 0.12 ± 0.20	2.17 ± 0.12 ± 0.27
0.060 - 0.070	1.21 ± 0.09 ± 0.11	1.35 ± 0.10 ± 0.15
0.070 - 0.080	0.603 ± 0.058 ± 0.069	0.726 ± 0.069 ± 0.076
0.080 - 0.090	0.373 ± 0.045 ± 0.039	0.422 ± 0.051 ± 0.055
0.090 - 0.100	0.181 ± 0.029 ± 0.039	0.205 ± 0.033 ± 0.040
0.100 - 0.120	0.101 ± 0.017 ± 0.027	0.104 ± 0.017 ± 0.027
$< M_l^2/s >$	0.0169 ± 0.0001 ± 0.0003	0.0193 ± 0.0001 ± 0.0008

Table 10: Light jet mass distribution.

Interval	corrected for charged only	corrected for charged+neutrals
0.000 - 0.005	31.65 ± 0.49 ± 0.49	38.51 ± 0.59 ± 1.16
0.005 - 0.010	27.88 ± 0.49 ± 1.01	32.05 ± 0.55 ± 1.38
0.010 - 0.015	21.86 ± 0.45 ± 0.40	23.84 ± 0.48 ± 1.00
0.015 - 0.020	17.59 ± 0.41 ± 0.49	16.95 ± 0.39 ± 1.09
0.020 - 0.025	14.00 ± 0.37 ± 0.55	12.82 ± 0.34 ± 1.05
0.025 - 0.030	11.58 ± 0.34 ± 0.21	10.21 ± 0.31 ± 0.56
0.030 - 0.035	8.90 ± 0.29 ± 0.22	7.77 ± 0.26 ± 0.43
0.035 - 0.040	7.42 ± 0.27 ± 0.30	6.46 ± 0.24 ± 0.56
0.040 - 0.050	5.94 ± 0.17 ± 0.16	5.12 ± 0.15 ± 0.55
0.050 - 0.060	4.05 ± 0.14 ± 0.25	3.63 ± 0.12 ± 0.38
0.060 - 0.080	3.04 ± 0.09 ± 0.13	2.70 ± 0.08 ± 0.21
0.080 - 0.100	1.87 ± 0.07 ± 0.06	1.68 ± 0.06 ± 0.12
0.100 - 0.120	1.286 ± 0.054 ± 0.052	1.209 ± 0.051 ± 0.059
0.120 - 0.140	1.008 ± 0.051 ± 0.052	0.874 ± 0.044 ± 0.059
0.140 - 0.160	0.712 ± 0.041 ± 0.048	0.665 ± 0.039 ± 0.057
0.160 - 0.180	0.483 ± 0.033 ± 0.037	0.473 ± 0.032 ± 0.046
0.180 - 0.200	0.418 ± 0.033 ± 0.031	0.358 ± 0.029 ± 0.048
0.200 - 0.250	0.224 ± 0.014 ± 0.012	0.173 ± 0.011 ± 0.045
0.250 - 0.300	0.102 ± 0.009 ± 0.010	0.066 ± 0.006 ± 0.041
0.300 - 0.350	0.039 ± 0.005 ± 0.006	0.006 ± 0.001 ± 0.005
0.350 - 0.400	0.0119 ± 0.0026 ± 0.0026	0.0003 ± 0.0002 ± 0.0001
$< M_d^2/s >$	0.0383 ± 0.0003 ± 0.0006	0.0337 ± 0.0003 ± 0.0021

Table 11 : Jet mass difference distribution.

Interval	corrected for charged only	corrected for charged+neutrals
0.000 - 0.005	25.94 ± 0.44 ± 0.81	26.01 ± 0.44 ± 2.42
0.005 - 0.010	26.56 ± 0.47 ± 0.48	25.32 ± 0.45 ± 1.45
0.010 - 0.015	21.02 ± 0.44 ± 0.49	20.21 ± 0.43 ± 0.57
0.015 - 0.020	16.73 ± 0.40 ± 0.97	16.20 ± 0.39 ± 1.07
0.020 - 0.025	12.50 ± 0.34 ± 0.46	12.29 ± 0.33 ± 0.58
0.025 - 0.030	10.43 ± 0.31 ± 0.35	10.33 ± 0.31 ± 0.31
0.030 - 0.035	9.08 ± 0.30 ± 0.42	9.10 ± 0.30 ± 0.53
0.035 - 0.040	7.57 ± 0.27 ± 0.42	7.60 ± 0.27 ± 0.46
0.040 - 0.050	6.00 ± 0.17 ± 0.25	6.02 ± 0.17 ± 0.30
0.050 - 0.060	4.67 ± 0.15 ± 0.14	4.78 ± 0.15 ± 0.17
0.060 - 0.080	3.54 ± 0.09 ± 0.10	3.53 ± 0.09 ± 0.14
0.080 - 0.100	2.407 ± 0.075 ± 0.076	2.469 ± 0.077 ± 0.091
0.100 - 0.120	1.608 ± 0.060 ± 0.070	1.656 ± 0.062 ± 0.086
0.120 - 0.140	1.369 ± 0.059 ± 0.066	1.479 ± 0.063 ± 0.095
0.140 - 0.160	0.985 ± 0.050 ± 0.055	1.021 ± 0.052 ± 0.081
0.160 - 0.180	0.706 ± 0.041 ± 0.047	0.789 ± 0.045 ± 0.061
0.180 - 0.200	0.476 ± 0.032 ± 0.033	0.544 ± 0.036 ± 0.047
0.200 - 0.250	0.318 ± 0.017 ± 0.020	0.350 ± 0.019 ± 0.023
0.250 - 0.300	0.120 ± 0.011 ± 0.015	0.148 ± 0.013 ± 0.045
0.300 - 0.350	0.017 ± 0.005 ± 0.009	0.039 ± 0.010 ± 0.023
$< y_3 >$	0.0439 ± 0.0004 ± 0.0006	0.0460 ± 0.0004 ± 0.0006

Table 12 : Differential two-jet distribution, y_3.

y_{cut}	R_2	R_3	R_4	R_5
0.005	13.49 ± 0.48	42.61 ± 0.48	30.95 ± 0.59	10.70 ± 0.34
0.010	27.22 ± 0.64	50.45 ± 0.62	19.39 ± 0.43	2.86 ± 0.18
0.015	37.77 ± 0.72	49.28 ± 0.65	12.02 ± 0.37	0.88 ± 0.09
0.020	45.89 ± 0.73	45.74 ± 0.61	8.02 ± 0.33	0.26 ± 0.06
0.030	57.51 ± 0.74	38.52 ± 0.62	3.77 ± 0.24	
0.040	65.49 ± 0.58	32.51 ± 0.57	1.82 ± 0.16	
0.050	71.29 ± 0.52	27.66 ± 0.50	0.89 ± 0.10	
0.060	75.86 ± 0.49	23.54 ± 0.51	0.43 ± 0.06	
0.070	79.69 ± 0.41	19.87 ± 0.44	0.22 ± 0.05	
0.080	82.92 ± 0.40	16.73 ± 0.42	0.11 ± 0.03	
0.100	87.46 ± 0.33	12.29 ± 0.34		
0.120	90.59 ± 0.28	9.18 ± 0.30		
0.140	93.24 ± 0.27	6.50 ± 0.25		
0.160	95.13 ± 0.27	4.58 ± 0.21		
0.180	96.48 ± 0.24	3.20 ± 0.17		
0.200	97.34 ± 0.23	2.28 ± 0.15		

Table 13a : The n-jet production rates (in percent) corrected for charged particles only. The jets are defined by the JADE+E algorithm for various values of the resolution parameter y_{cut}. The errors contain statistical and systematic contributions added in quadrature.

y_{cut}	R_2	R_3	R_4	R_5
0.005	13.76 ± 1.36	44.81 ± 0.85	30.37 ± 1.11	9.35 ± 0.47
0.010	26.81 ± 1.60	51.69 ± 1.86	18.83 ± 1.38	2.60 ± 0.84
0.015	37.05 ± 1.50	50.16 ± 1.73	11.92 ± 0.95	0.85 ± 0.43
0.020	44.98 ± 1.31	46.52 ± 1.48	8.16 ± 0.71	0.27 ± 0.19
0.030	56.51 ± 1.09	39.32 ± 1.04	4.00 ± 0.33	
0.040	64.31 ± 0.84	33.59 ± 0.87	1.94 ± 0.19	
0.050	70.05 ± 0.66	28.86 ± 0.74	0.98 ± 0.11	
0.060	74.67 ± 0.56	24.72 ± 0.67	0.49 ± 0.08	
0.070	78.58 ± 0.48	21.02 ± 0.54	0.26 ± 0.05	
0.080	81.77 ± 0.41	17.93 ± 0.47	0.14 ± 0.04	
0.100	86.47 ± 0.38	13.38 ± 0.38		
0.120	89.69 ± 0.40	10.25 ± 0.32		
0.140	92.65 ± 0.47	7.28 ± 0.29		
0.160	94.67 ± 0.57	5.24 ± 0.31		
0.180	96.22 ± 0.59	3.72 ± 0.29		
0.200	97.28 ± 0.63	2.68 ± 0.33		

Table 13b : The n-jet production rates (in percent) corrected for charged and neutral particles. The jets are defined by the JADE+E algorithm for various values of the resolution parameter y_{cut}. The errors contain statistical and systematic contributions added in quadrature.

Interval	corrected for charged only
0.005 - 0.010	514.9 ± 2.5 ± 11.6
0.010 - 0.015	451.3 ± 2.1 ± 6.8
0.015 - 0.020	355.9 ± 1.8 ± 4.2
0.020 - 0.030	262.0 ± 1.1 ± 2.8
0.030 - 0.040	184.31 ± 0.93 ± 1.44
0.040 - 0.050	136.70 ± 0.80 ± 0.88
0.050 - 0.060	103.00 ± 0.69 ± 0.58
0.060 - 0.070	83.32 ± 0.63 ± 0.38
0.070 - 0.080	67.67 ± 0.56 ± 0.55
0.080 - 0.090	56.11 ± 0.51 ± 0.30
0.090 - 0.100	47.01 ± 0.47 ± 0.24
0.100 - 0.120	37.04 ± 0.30 ± 0.24
0.120 - 0.140	27.90 ± 0.26 ± 0.10
0.140 - 0.160	21.33 ± 0.23 ± 0.08
0.160 - 0.180	16.81 ± 0.20 ± 0.10
0.180 - 0.200	13.71 ± 0.19 ± 0.13
0.200 - 0.250	8.928 ± 0.092 ± 0.123
0.250 - 0.300	5.427 ± 0.072 ± 0.078
0.300 - 0.400	2.880 ± 0.037 ± 0.039
0.400 - 0.500	1.245 ± 0.024 ± 0.018
0.500 - 0.600	0.534 ± 0.016 ± 0.012
0.600 - 0.700	0.230 ± 0.011 ± 0.004
0.700 - 0.800	0.090 ± 0.006 ± 0.002

Table 14 : Scaled momentum, x_p, distribution.

Interval	corrected for charged only	corrected for charged+neutrals
0.000 - 0.250	5.785 ± 0.042 ± 0.116	5.908 ± 0.042 ± 0.124
0.250 - 0.500	6.342 ± 0.042 ± 0.060	6.368 ± 0.042 ± 0.059
0.500 - 0.750	6.577 ± 0.041 ± 0.106	6.585 ± 0.041 ± 0.091
0.750 - 1.000	6.704 ± 0.039 ± 0.100	6.707 ± 0.039 ± 0.088
1.000 - 1.250	6.645 ± 0.037 ± 0.135	6.653 ± 0.037 ± 0.134
1.250 - 1.500	6.636 ± 0.036 ± 0.087	6.608 ± 0.036 ± 0.099
1.500 - 1.750	6.582 ± 0.035 ± 0.078	6.550 ± 0.035 ± 0.087
1.750 - 2.000	6.482 ± 0.035 ± 0.073	6.403 ± 0.035 ± 0.098
2.000 - 2.250	6.093 ± 0.034 ± 0.065	6.050 ± 0.033 ± 0.063
2.250 - 2.500	5.772 ± 0.033 ± 0.043	5.689 ± 0.032 ± 0.052
2.500 - 2.750	5.104 ± 0.031 ± 0.042	5.035 ± 0.031 ± 0.058
2.750 - 3.000	4.306 ± 0.028 ± 0.047	4.279 ± 0.028 ± 0.028
3.000 - 3.250	3.456 ± 0.025 ± 0.061	3.455 ± 0.025 ± 0.065
3.250 - 3.500	2.575 ± 0.022 ± 0.057	2.602 ± 0.022 ± 0.059
3.500 - 3.750	1.802 ± 0.018 ± 0.054	1.823 ± 0.018 ± 0.071
3.750 - 4.000	1.148 ± 0.014 ± 0.039	1.191 ± 0.015 ± 0.050
4.000 - 4.250	0.685 ± 0.011 ± 0.031	0.720 ± 0.011 ± 0.031
4.250 - 4.500	0.371 ± 0.008 ± 0.015	0.400 ± 0.008 ± 0.020
4.500 - 5.000	0.148 ± 0.003 ± 0.004	0.162 ± 0.004 ± 0.005
5.000 - 5.500	0.0269 ± 0.0013 ± 0.0008	0.0302 ± 0.0014 ± 0.0009
5.500 - 6.000	0.0046 ± 0.0005 ± 0.0006	0.0049 ± 0.0006 ± 0.0008

Table 15 : Distribution of rapidity, y_T, with respect to the thrust axis.

Interval	corrected for charged only	corrected for charged+neutrals
0.000 - 0.250	6.459 ± 0.042 ± 0.055	6.462 ± 0.042 ± 0.059
0.250 - 0.500	6.499 ± 0.042 ± 0.087	6.496 ± 0.042 ± 0.094
0.500 - 0.750	6.546 ± 0.041 ± 0.107	6.542 ± 0.041 ± 0.115
0.750 - 1.000	6.580 ± 0.039 ± 0.089	6.583 ± 0.039 ± 0.084
1.000 - 1.250	6.432 ± 0.037 ± 0.104	6.449 ± 0.037 ± 0.102
1.250 - 1.500	6.467 ± 0.036 ± 0.090	6.496 ± 0.036 ± 0.094
1.500 - 1.750	6.446 ± 0.035 ± 0.081	6.454 ± 0.035 ± 0.076
1.750 - 2.000	6.305 ± 0.034 ± 0.073	6.321 ± 0.034 ± 0.066
2.000 - 2.250	6.017 ± 0.034 ± 0.056	6.080 ± 0.034 ± 0.065
2.250 - 2.500	5.602 ± 0.032 ± 0.048	5.682 ± 0.033 ± 0.057
2.500 - 2.750	4.931 ± 0.030 ± 0.050	5.026 ± 0.031 ± 0.045
2.750 - 3.000	4.193 ± 0.028 ± 0.038	4.247 ± 0.028 ± 0.062
3.000 - 3.250	3.304 ± 0.025 ± 0.052	3.350 ± 0.025 ± 0.042
3.250 - 3.500	2.530 ± 0.022 ± 0.043	2.529 ± 0.022 ± 0.057
3.500 - 3.750	1.844 ± 0.018 ± 0.048	1.800 ± 0.018 ± 0.058
3.750 - 4.000	1.249 ± 0.015 ± 0.037	1.187 ± 0.014 ± 0.040
4.000 - 4.250	0.814 ± 0.012 ± 0.039	0.750 ± 0.011 ± 0.032
4.250 - 4.500	0.505 ± 0.009 ± 0.024	0.448 ± 0.008 ± 0.021
4.500 - 5.000	0.243 ± 0.004 ± 0.012	0.190 ± 0.003 ± 0.013
5.000 - 5.500	0.0744 ± 0.0021 ± 0.0033	0.0494 ± 0.0015 ± 0.0020
5.500 - 6.000	0.0202 ± 0.0011 ± 0.0008	0.0107 ± 0.0006 ± 0.0011

Table 16 : Distribution of rapidity, y_S, with respect to the sphericity axis.

Interval (GeV)	corrected for charged only	corrected for charged+neutrals
0.000 - 0.050	72.35 ± 0.28 ± 1.03	70.33 ± 0.27 ± 1.24
0.050 - 0.100	64.63 ± 0.26 ± 0.78	62.74 ± 0.26 ± 0.70
0.100 - 0.150	55.67 ± 0.24 ± 0.58	54.34 ± 0.24 ± 0.48
0.150 - 0.200	46.50 ± 0.22 ± 0.38	45.70 ± 0.21 ± 0.47
0.200 - 0.250	38.09 ± 0.19 ± 0.19	37.84 ± 0.19 ± 0.25
0.250 - 0.300	30.56 ± 0.17 ± 0.22	30.37 ± 0.17 ± 0.25
0.300 - 0.350	23.64 ± 0.15 ± 0.19	23.90 ± 0.15 ± 0.19
0.350 - 0.400	18.53 ± 0.13 ± 0.07	18.89 ± 0.14 ± 0.14
0.400 - 0.450	14.65 ± 0.12 ± 0.08	15.15 ± 0.12 ± 0.08
0.450 - 0.500	11.06 ± 0.10 ± 0.09	11.55 ± 0.11 ± 0.13
0.500 - 0.600	7.655 ± 0.060 ± 0.057	8.194 ± 0.064 ± 0.062
0.600 - 0.700	4.740 ± 0.048 ± 0.046	5.209 ± 0.052 ± 0.053
0.700 - 0.800	2.892 ± 0.038 ± 0.023	3.278 ± 0.042 ± 0.043
0.800 - 1.000	1.528 ± 0.020 ± 0.014	1.759 ± 0.022 ± 0.031
1.000 - 1.200	0.658 ± 0.013 ± 0.010	0.800 ± 0.015 ± 0.015
1.200 - 1.400	0.301 ± 0.009 ± 0.006	0.383 ± 0.011 ± 0.016
1.400 - 1.600	0.164 ± 0.007 ± 0.004	0.213 ± 0.008 ± 0.011
1.600 - 1.800	0.089 ± 0.005 ± 0.003	0.121 ± 0.007 ± 0.004
1.800 - 2.000	0.046 ± 0.003 ± 0.004	0.064 ± 0.005 ± 0.004
2.000 - 2.500	0.0237 ± 0.0018 ± 0.0011	0.0352 ± 0.0025 ± 0.0024
2.500 - 3.000	0.0060 ± 0.0008 ± 0.0008	0.0085 ± 0.0011 ± 0.0016
3.000 - 3.500	0.0021 ± 0.0005 ± 0.0003	0.0035 ± 0.0007 ± 0.0006
$< p_t^{out} >$	0.2302 ± 0.0016 ± 0.0010	0.2413 ± 0.0017 ± 0.0016

Table 17 : Transverse momentum, p_t^{out}, distribution.

Interval (GeV)	corrected for charged only	corrected for charged+neutrals
0.000 - 0.050	51.84 ± 0.25 ± 1.37	52.01 ± 0.25 ± 1.31
0.050 - 0.100	46.41 ± 0.23 ± 0.57	46.54 ± 0.23 ± 0.48
0.100 - 0.150	41.25 ± 0.21 ± 0.48	41.34 ± 0.21 ± 0.40
0.150 - 0.200	35.64 ± 0.19 ± 0.35	35.61 ± 0.19 ± 0.34
0.200 - 0.250	30.29 ± 0.18 ± 0.26	30.17 ± 0.17 ± 0.33
0.250 - 0.300	25.85 ± 0.16 ± 0.20	25.62 ± 0.16 ± 0.21
0.300 - 0.350	22.12 ± 0.15 ± 0.15	22.09 ± 0.15 ± 0.15
0.350 - 0.400	18.73 ± 0.13 ± 0.15	18.61 ± 0.13 ± 0.14
0.400 - 0.450	16.07 ± 0.12 ± 0.12	15.96 ± 0.12 ± 0.12
0.450 - 0.500	13.57 ± 0.11 ± 0.12	13.40 ± 0.11 ± 0.17
0.500 - 0.600	11.106 ± 0.072 ± 0.059	10.964 ± 0.071 ± 0.086
0.600 - 0.700	8.560 ± 0.064 ± 0.059	8.431 ± 0.063 ± 0.056
0.700 - 0.800	6.623 ± 0.056 ± 0.050	6.530 ± 0.055 ± 0.058
0.800 - 1.000	4.639 ± 0.033 ± 0.023	4.624 ± 0.033 ± 0.036
1.000 - 1.200	3.019 ± 0.026 ± 0.023	3.006 ± 0.026 ± 0.032
1.200 - 1.400	2.061 ± 0.022 ± 0.017	2.086 ± 0.022 ± 0.022
1.400 - 1.600	1.479 ± 0.019 ± 0.016	1.516 ± 0.019 ± 0.027
1.600 - 1.800	1.082 ± 0.016 ± 0.010	1.081 ± 0.016 ± 0.015
1.800 - 2.000	0.795 ± 0.013 ± 0.008	0.830 ± 0.014 ± 0.017
2.000 - 2.500	0.501 ± 0.007 ± 0.007	0.521 ± 0.007 ± 0.007
2.500 - 3.000	0.279 ± 0.005 ± 0.003	0.294 ± 0.005 ± 0.004
3.000 - 3.500	0.157 ± 0.004 ± 0.004	0.166 ± 0.004 ± 0.005
3.500 - 4.000	0.090 ± 0.003 ± 0.002	0.100 ± 0.003 ± 0.004
4.000 - 5.000	0.0495 ± 0.0015 ± 0.0010	0.0559 ± 0.0017 ± 0.0015
5.000 - 6.000	0.0198 ± 0.0010 ± 0.0004	0.0238 ± 0.0012 ± 0.0006
6.000 - 7.000	0.0075 ± 0.0006 ± 0.0003	0.0099 ± 0.0007 ± 0.0004
7.000 - 8.000	0.0036 ± 0.0004 ± 0.0002	0.0050 ± 0.0005 ± 0.0003
8.000 - 10.000	0.0010 ± 0.0001 ± 0.0001	0.0016 ± 0.0002 ± 0.0001
$< p_t^{in} >$	0.4514 ± 0.0042 ± 0.0029	0.4587 ± 0.0043 ± 0.0028

Table 18 : Transverse momentum, p_t^{in}, distribution.

Parameter	Name	Default	Fit range	Best fit ± stat.± syst.error
Λ_{LLA} (GeV)	PARJ(81)	0.40	0.30 ± 0.10	$0.318 \pm 0.006 \pm 0.024$
M_{min} (GeV)	PARJ(82)	1.00	1.40 ± 0.50	$1.43 \pm 0.08 \pm 0.14$
σ (GeV)	PARJ(21)	0.35	0.36 ± 0.08	$0.360 \pm 0.003 \pm 0.011$
B (GeV^{-2})	PARJ(42)	0.90	0.90 ± 0.25	$0.92 \pm 0.03 \pm 0.09$
A	PARJ(41)	0.50		0.50 (fixed)

Table 19a : Parameters for JETSET 7.2 coherent PS + O(α_s)

Parameter	Without O(α_s)	Incoherent	Constant α_s
Λ_{LLA} (GeV)	$0.189 \pm 0.003 \pm 0.012$	$0.38 \pm 0.01 \pm 0.04$	$\alpha_s = 0.215 \pm 0.001 \pm 0.005$
M_{min} (GeV)	$1.18 \pm 0.04 \pm 0.23$	$1.59 \pm 0.05 \pm 0.16$	$1.07 \pm 0.05 \pm 0.10$
σ (GeV)	$0.392 \pm 0.002 \pm 0.007$	$0.414 \pm 0.003 \pm 0.012$	$0.421 \pm 0.002 \pm 0.008$
B (GeV^{-2})	$0.63 \pm 0.01 \pm 0.03$	$1.23 \pm 0.06 \pm 0.25$	$0.410 \pm 0.006 \pm 0.021$
A	0.50 (fixed)	0.50 (fixed)	0.50 (fixed)

Table 19b : Fitted parameters for three variants of JETSET 7.2 PS. The first error is statistical, the second systematic.

Parameter	Name	Default	Fit range	Best fit ± stat.± syst.error
Λ_{QCD} (GeV)	VAR(1)	0.25	0.20 ± 0.10	$0.212 \pm 0.003 \pm 0.019$
p_t^{min} (GeV)	VAR(3)	0.50	0.70 ± 0.40	$0.90 \pm 0.05 \pm 0.19$
σ (GeV)	PARJ(21)	0.35	0.36 ± 0.10	$0.364 \pm 0.003 \pm 0.005$
B (GeV^{-2})	PARJ(42)	0.75	0.75 ± 0.25	$0.76 \pm 0.02 \pm 0.05$
A	PARJ(41)	0.50		0.50 (fixed)

Table 19c : Parameters for ARIADNE 3.1 (with JETSET 7.2 for fragmentation).

Parameter	Name	Default	Fit range	Best fit ± stat. ± syst. error
Λ_{LLA} (GeV)	QCDLAM	0.11	0.10 ± 0.05	$0.099 \pm 0.001 \pm 0.008$
M_g (GeV)	RMASS(13)	0.65	0.85 ± 0.25	$0.83 \pm 0.01 \pm 0.07$
M_{cl} (GeV)	CLMAX	3.0	3.7 ± 1.0	$3.78 \pm 0.03 \pm 0.30$
Additional	VQCUT	0.0		0.0 (fixed)
virtual mass	VGCUT	0.0		0.0 (fixed)
cuts				
Λ_{LLA} (GeV)	QCDLAM	0.20	0.15 ± 0.05	$0.179 \pm 0.002 \pm 0.011$
M_g (GeV)	RMASS(13)	0.75	1.00 ± 0.20	$0.91 \pm 0.01 \pm 0.05$
M_{cl} (GeV)	CLMAX	3.5	3.8 ± 1.0	$3.67 \pm 0.03 \pm 0.25$
Additional	VQCUT	0.48		0.48 (fixed)
virtual mass	VGCUT	0.06		0.0 (fixed)
cuts				

Table 19d : Parameters for HERWIG PS 4.3 (upper part) and 5.0 (lower part)

Parameter	Name	Default	Fit range	Best fit ± stat. ± syst. error
Λ_{eff} (GeV)	PARJ(122)	0.10	0.15 ± 0.10	$0.140 \pm 0.002 \pm 0.008$
$f = (\mu/E_{cm})^2$	PARJ(129)	.002	$.0015 \pm .0007$	$.00136 \pm .00003 \pm .00025$
σ (GeV)	PARJ(21)	0.40	0.45 ± 0.08	$0.440 \pm 0.002 \pm 0.006$
B (GeV^{-2})	PARJ(42)	0.70	0.50 ± 0.15	$0.496 \pm 0.004 \pm 0.014$
A	PARJ(41)	1.0		1.0 (fixed)

Table 19e : Parameters for JETSET 7.2 ME, with optimized scale.

	Λ_{LLA}	M_{min}	σ
M_{min}	–0.16		
σ	–0.84	0.30	
B	0.82	–0.65	–0.86

Table 20a : Correlation coefficients for JETSET 7.2 coh. PS + O(α_s)

	Λ_{QCD}	p_t^{min}	σ
p_t^{min}	0.0		
σ	–0.52	0.68	
B	0.45	–0.86	–0.90

Table 20b : Correlation coefficients for ARIADNE 3.1

	Λ_{LLA}	M_g
M_g	–0.31	
M_{cl}	–0.39	0.84

Table 20c : Correlation coefficients for HERWIG 5.0 PS

	Λ_{eff}	f	σ
f	0.64		
σ	–0.70	–0.38	
B	0.81	0.40	–0.79

Table 20d : Correlation coefficients for JETSET 7.2 ME, optimized scale

Distribution	x_p	p_t^{out}	p_t^{in}	S	A	T	m	Sum
No.of bins	23	22	28	22	15	21	16	147
QCD Model								
JETSET coh PS + O(α_s)	124	185	109	34	13	23	19	507
JETSET coh PS, no O(α_s)	131	227	124	58	13	82	18	653
JETSET incoh PS + O(α_s)	233	276	355	85	48	233	154	1385
JETSET coh PS, const α_s	266	248	128	89	14	104	20	865
ARIADNE 3.1 PS	153	136	112	39	6	50	21	517
HERWIG 4.3 PS	246	94	231	129	77	241	130	1149
HERWIG 5.0 PS	227	114	296	135	71	208	84	1135
JETSET ME f=1	638	1530	400	473	850	1840	1150	6890
JETSET ME opt scale	658	167	148	138	27	344	36	1517

Table 21 : The χ^2 values for the fits of the QCD models to the corrected data distributions, based on statistical errors only.

	JETSET coh.PS	JETSET ME opt.	HERWIG 4.3
JETSET coh.PS	507	1517	1149
JETSET ME opt.	564	1486	1232
HERWIG 4.3	684	1730	1040

Table 22 : The total χ^2 values of the QCD models fitted (given in the top line) versus the QCD models used for correcting the data (given in the left hand column).

Figure Captions

Fig.1: (a) The sphericity distribution computed from the charged particles. The error bars on the data are the combined statistical and systematic errors. The predictions of the tuned QCD models JETSET 7.2 coherent parton shower (PS) + $O(\alpha_s)$, HERWIG 4.3 and JETSET 7.2 matrix elements (ME) with optimized scale are shown as curves.
(b) The difference between the distributions of the QCD models and the data in units of the data error.

Fig.2: The aplanarity distribution. The data points and curves are as described for fig.1.

Fig.3: The planarity distribution. The data points and curves are as described for fig.1.

Fig.4: The C-parameter distribution. The data points and curves are as described for fig.1.

Fig.5: The thrust distribution. The data points and curves are as described for fig.1.

Fig.6: The major distribution. The data points and curves are as described for fig.1.

Fig.7: The minor distribution. The data points and curves are as described for fig.1.

Fig.8: The oblateness distribution. The data points and curves are as described for fig.1.

Fig.9: The heavy jet mass distribution. The data points and curves are as described for fig.1.

Fig.10: The light jet mass distribution. The data points and curves are as described for fig.1.

Fig.11: The jet mass difference distribution. The data points and curves are as described for fig.1.

Fig.12: The differential 2-jet distribution. The data points and curves are as described for fig.1.

Fig.13: The n-jet production rates computed from the charged particles using the JADE+E cluster algorithm, as a function of the jet resolution parameter y_{cut}. The data points and curves are as described for fig.1.

Fig.14: The scaled momentum distribution of charged particles. The data points and curves are as described for fig.1.

Fig.15: The distribution of rapidity of charged particles with respect to the thrust axis. The data points and curves are as described for fig.1.

Fig.16: The distribution of rapidity of charged particles with respect to the sphericity axis. The data points and curves are as described for fig.1.

Fig.17: The distribution of transverse momentum of charged particles out of the event plane. The data points and curves are as described for fig.1.

Fig.18: The distribution of transverse momentum of charged particles in the event plane. The data points and curves are as described for fig.1.

Fig.19: The correction factors C_i computed from the full detector simulation for the distributions (a) x_p, (b) p_t^{out}, (c) thrust and (d) minor are shown as dots. The error bars are the Monte Carlo statistical errors. The curves are computed from a simplified detector simulation using the generators JETSET 7.2 PS (solid), HERWIG 4.3 (dashed) and JETSET 7.2 ME (dotted).

Fig.20: The energy dependence of the mean multiplicity of charged particles measured in e^+e^- annihilation in comparison to the QCD model predictions.

Fig.21: The energy dependence of the mean sphericity measured in e^+e^- annihilation in comparison to the QCD model predictions.

Fig.22: The energy dependence of the mean aplanarity measured in e^+e^- annihilation in comparison to the QCD model predictions.

Fig.23: The energy dependence of the mean (1 – thrust) measured in e^+e^- annihilation in comparison to the QCD model predictions.

Fig.24: The energy dependence of the 3-jet rate for $y_{cut} = 0.08$ measured in e^+e^- annihilation in comparison to the QCD model predictions.

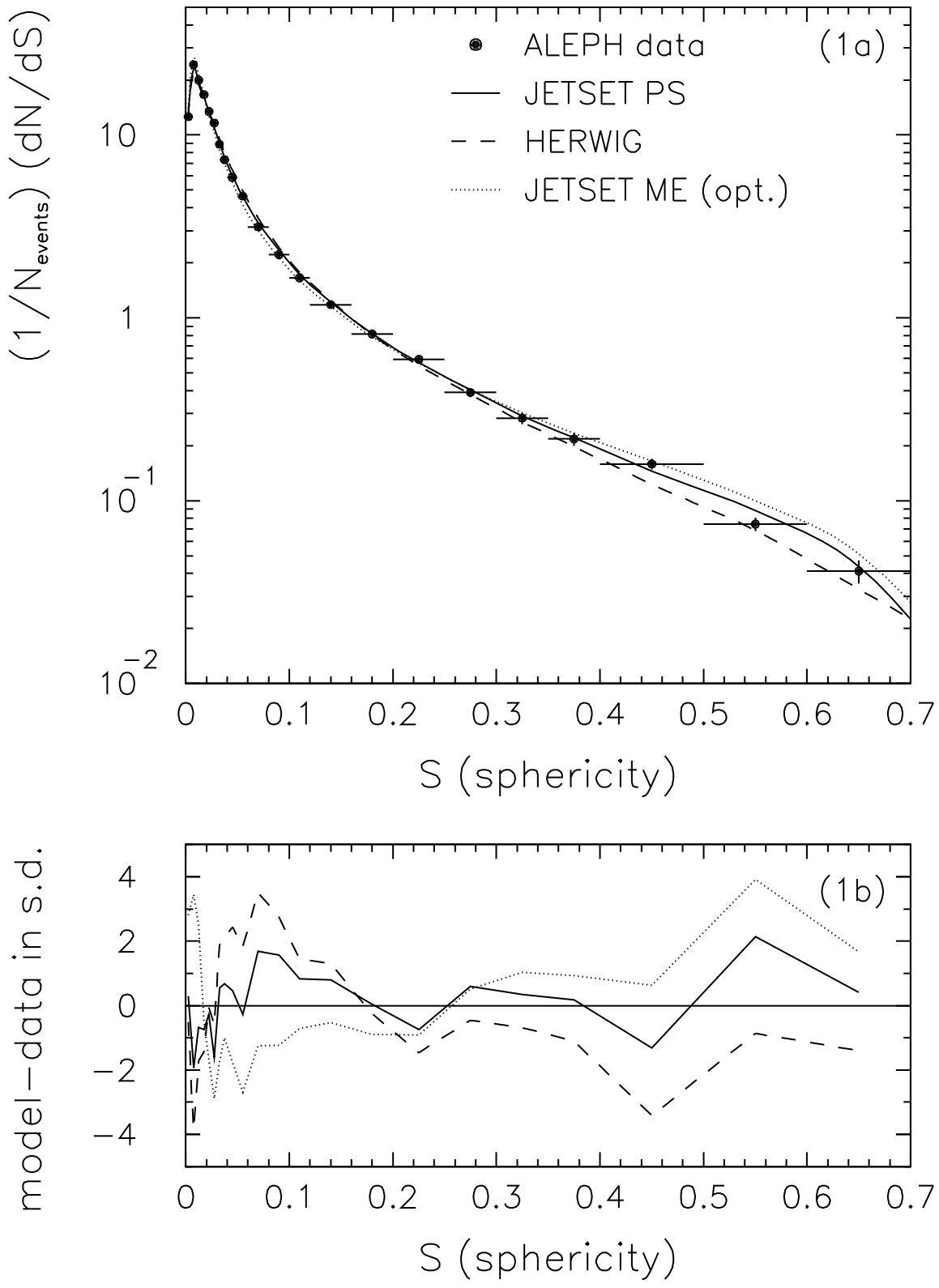
ALEPH data
JETSET PS
HERWIG
JETSET ME (opt.)
(1a)
$(1/N_{events})\ (dN/dS)$
10
1
10^{-1}
10^{-2}
0
0.1
0.2
0.3
0.4
0.5
0.6
0.7
S (sphericity)
(1b)
model − data in s.d.
4
2
0
−2
−4
0
0.1
0.2
0.3
0.4
0.5
0.6
0.7
S (sphericity)

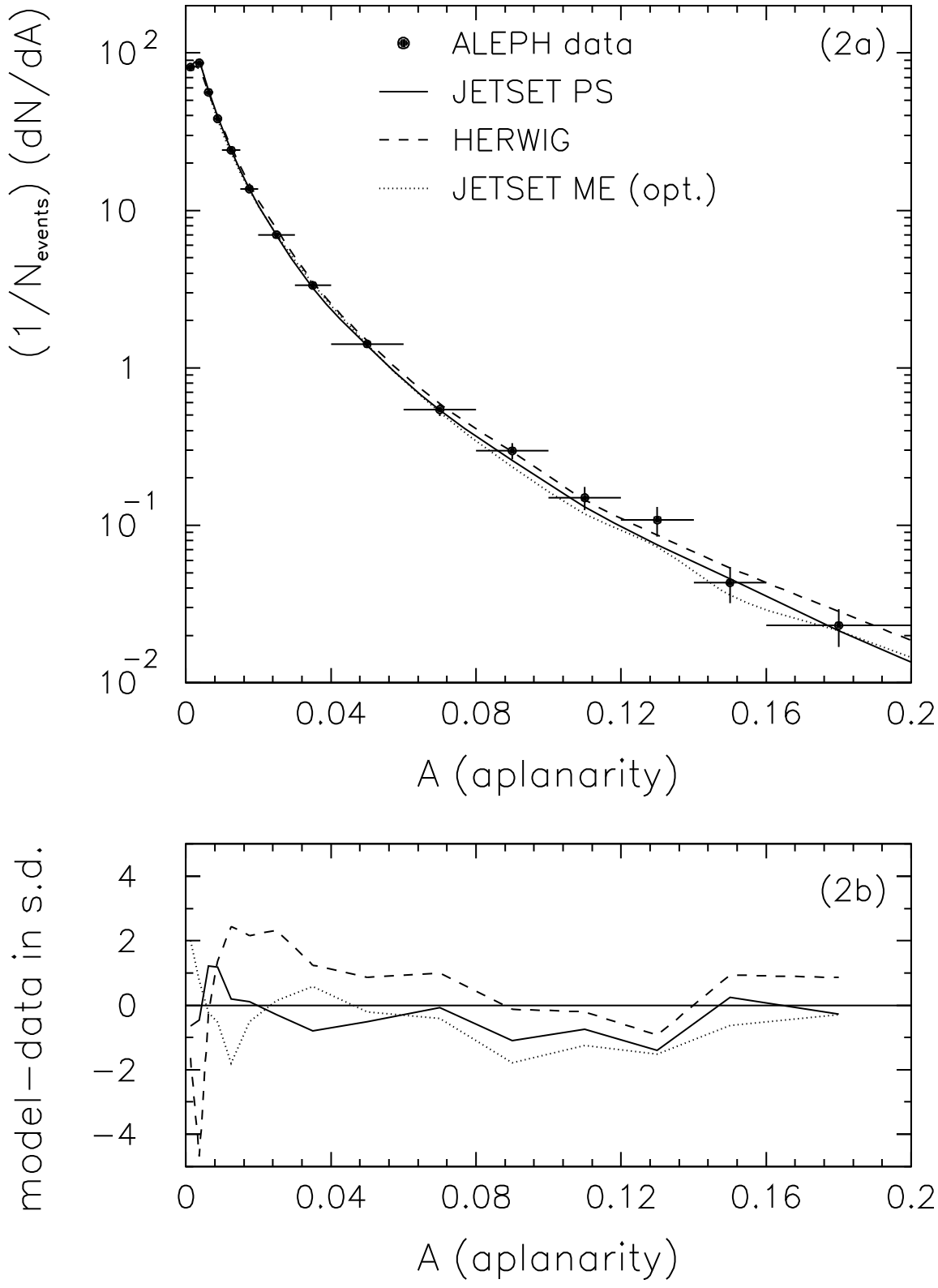
ALEPH data
JETSET PS
HERWIG
JETSET ME (opt.)
(2a)
$(1/N_{events})\ (dN/dA)$
10^2
10
1
10^{-1}
10^{-2}
0
0.04
0.08
0.12
0.16
0.2
A (aplanarity)
(2b)
model − data in s.d.
4
2
0
−2
−4
0
0.04
0.08
0.12
0.16
0.2
A (aplanarity)

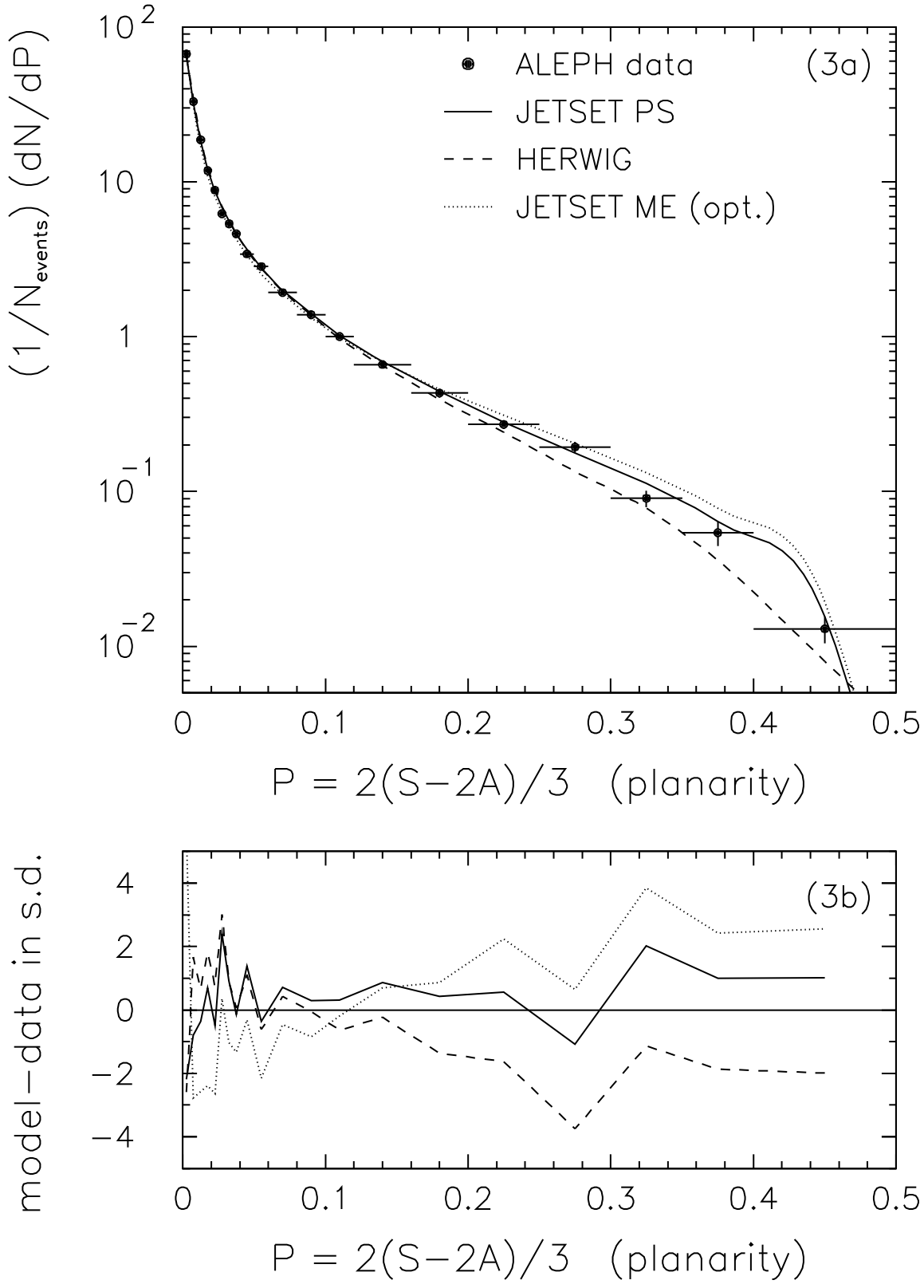
ALEPH data
JETSET PS
HERWIG
JETSET ME (opt.)
(3a)
$(1/N_{events})\ (dN/dP)$
10^2
10
1
10^{-1}
10^{-2}
0
0.1
0.2
0.3
0.4
0.5
P = 2(S−2A)/3 (planarity)
(3b)
model−data in s.d.
4
2
0
−2
−4
0
0.1
0.2
0.3
0.4
0.5
P = 2(S−2A)/3 (planarity)

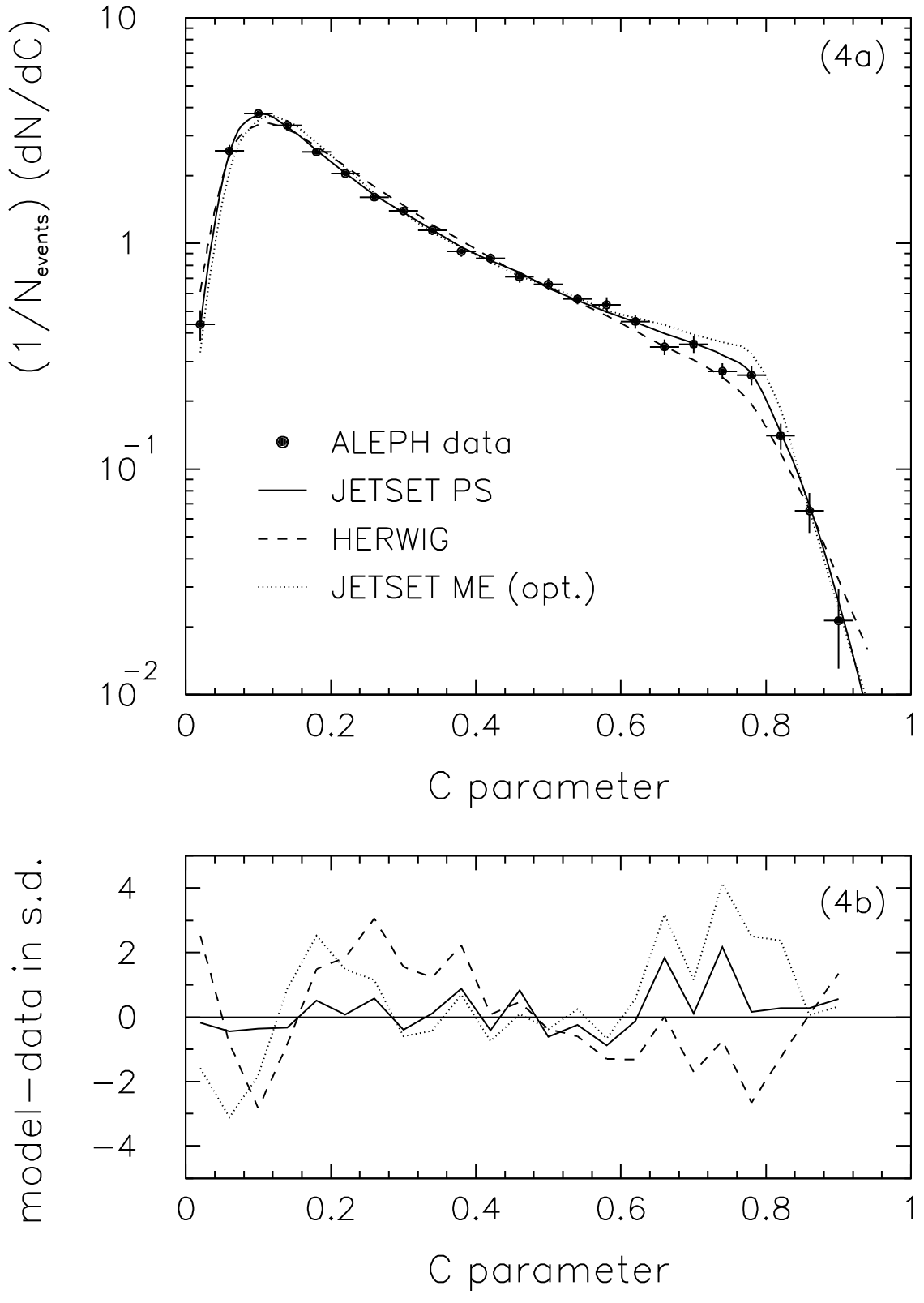
(4a)
$(1/N_{events})\ (dN/dC)$
10
1
10^{-1}
10^{-2}
ALEPH data
JETSET PS
HERWIG
JETSET ME (opt.)
0
0.2
0.4
0.6
0.8
1
C parameter
(4b)
model − data in s.d.
4
2
0
−2
−4
0
0.2
0.4
0.6
0.8
1
C parameter

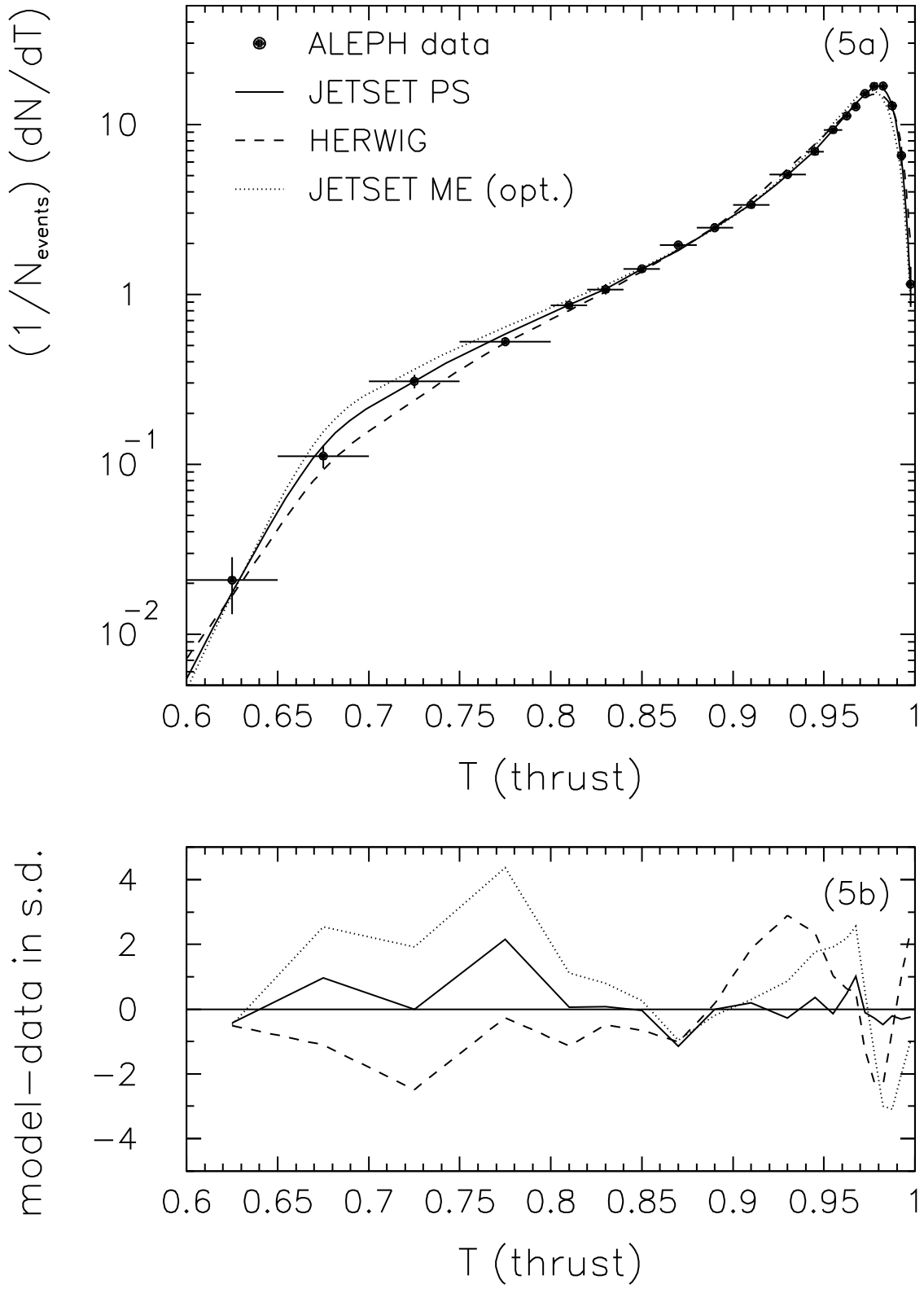
ALEPH data
JETSET PS
HERWIG
JETSET ME (opt.)
(5a)
$(1/N_{events})\ (dN/dT)$
10
1
10^{-1}
10^{-2}
0.6
0.65
0.7
0.75
0.8
0.85
0.9
0.95
1
T (thrust)
(5b)
model − data in s.d.
4
2
0
−2
−4
0.6
0.65
0.7
0.75
0.8
0.85
0.9
0.95
1
T (thrust)

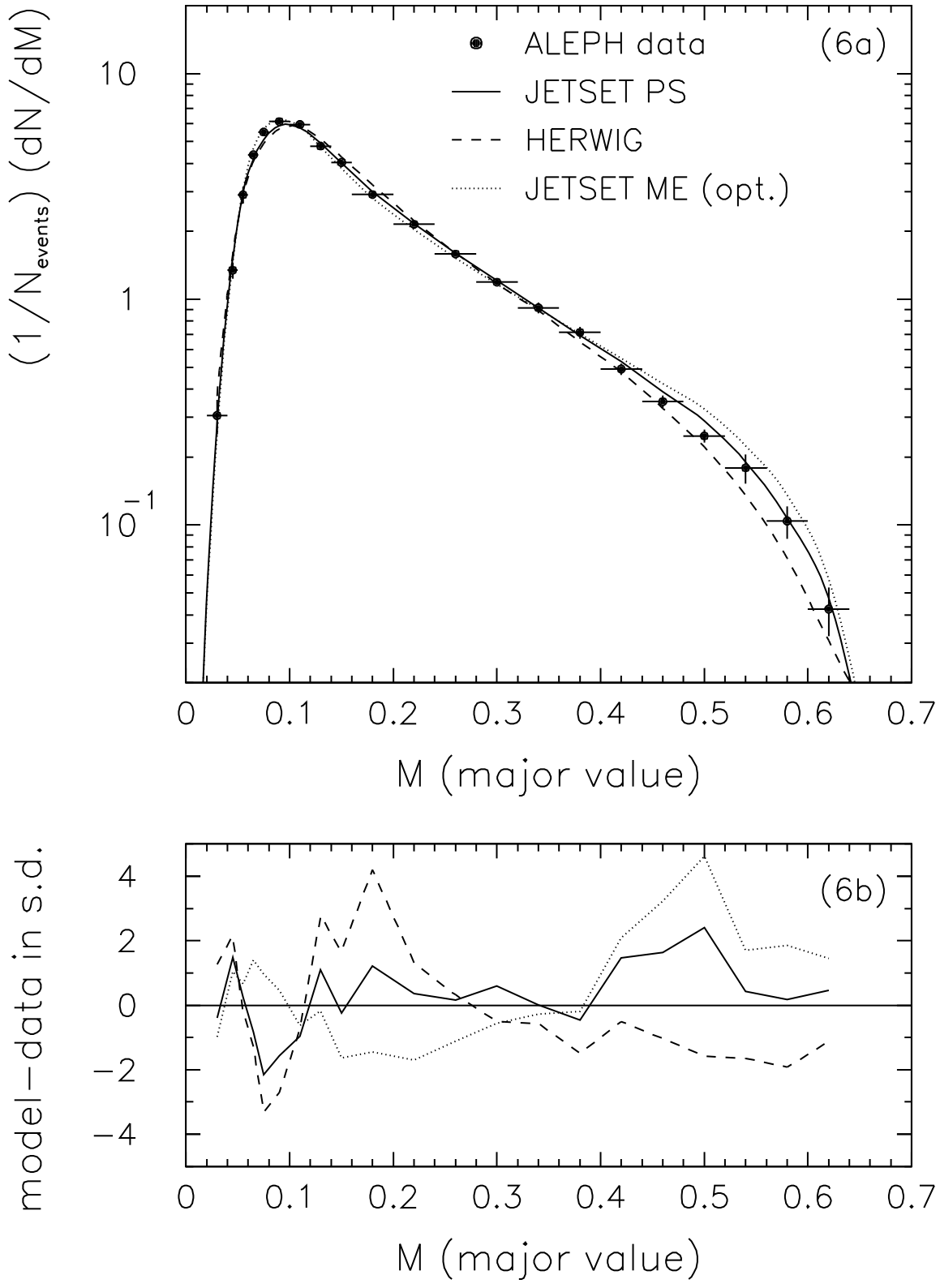
ALEPH data
(6a)
JETSET PS
HERWIG
JETSET ME (opt.)
(1/N_events) (dN/dM)
10
1
10^-1
0
0.1
0.2
0.3
0.4
0.5
0.6
0.7
M (major value)
model−data in s.d.
(6b)
4
2
0
−2
−4
0
0.1
0.2
0.3
0.4
0.5
0.6
0.7
M (major value)

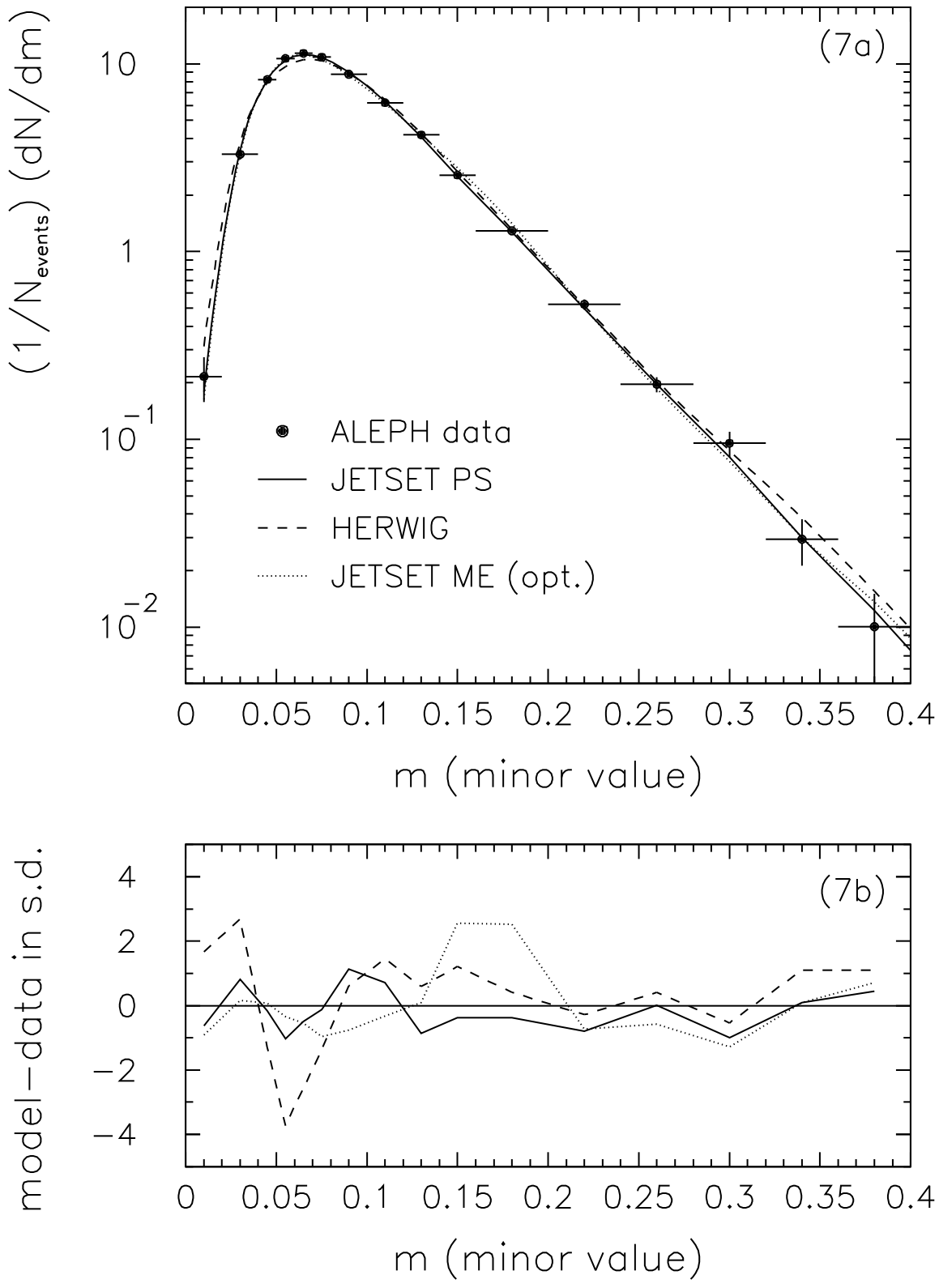
(7a)
$(1/N_{events})$ (dN/dm)
10
1
10^{-1}
10^{-2}
ALEPH data
JETSET PS
HERWIG
JETSET ME (opt.)
0
0.05
0.1
0.15
0.2
0.25
0.3
0.35
0.4
m (minor value)
(7b)
model−data in s.d.
4
2
0
−2
−4
0
0.05
0.1
0.15
0.2
0.25
0.3
0.35
0.4
m (minor value)

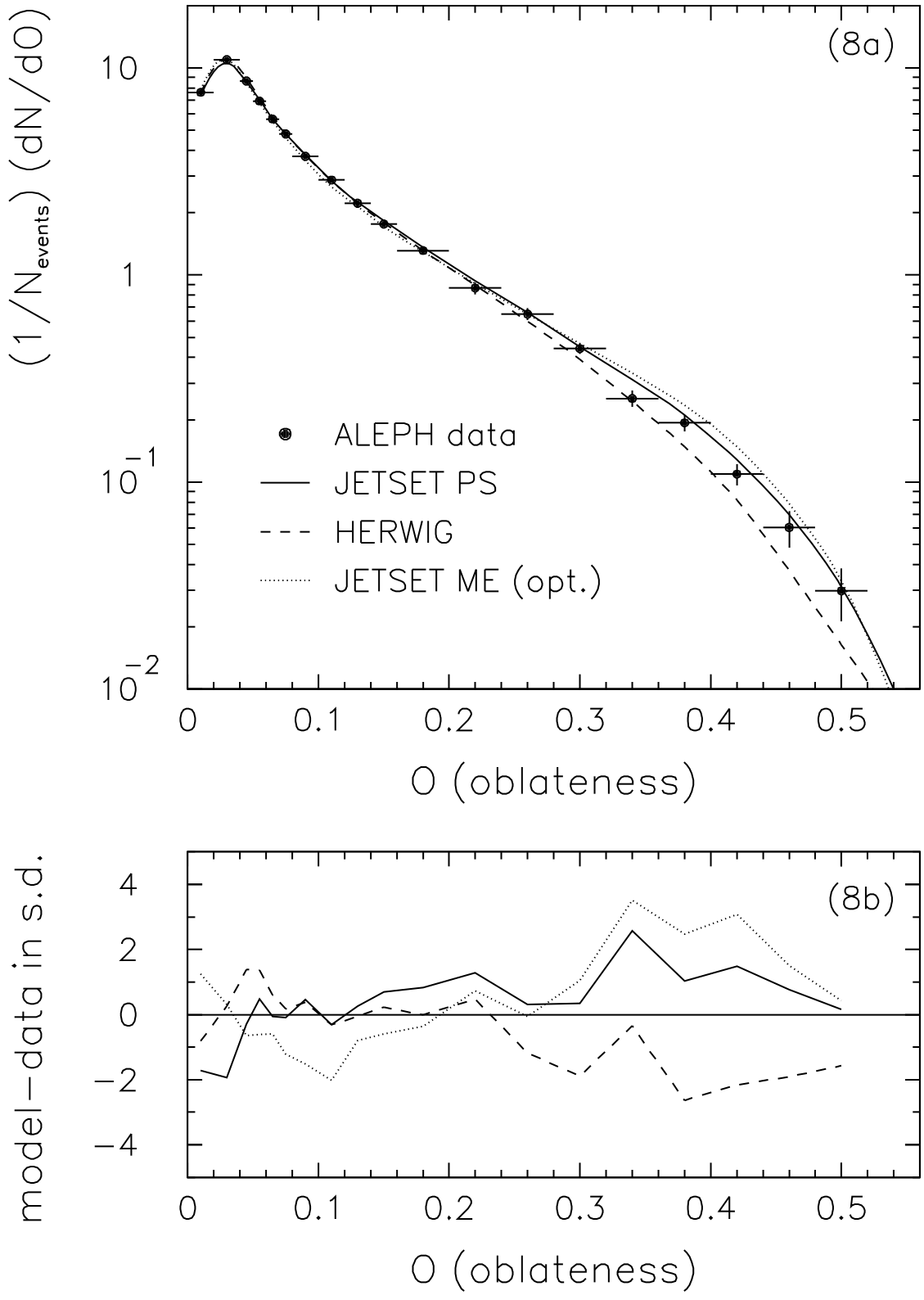
(8a)
$(1/N_{events})\ (dN/dO)$
10
1
10^{-1}
10^{-2}
ALEPH data
JETSET PS
HERWIG
JETSET ME (opt.)
0
0.1
0.2
0.3
0.4
0.5
O (oblateness)
(8b)
model−data in s.d.
4
2
0
−2
−4
0
0.1
0.2
0.3
0.4
0.5
O (oblateness)

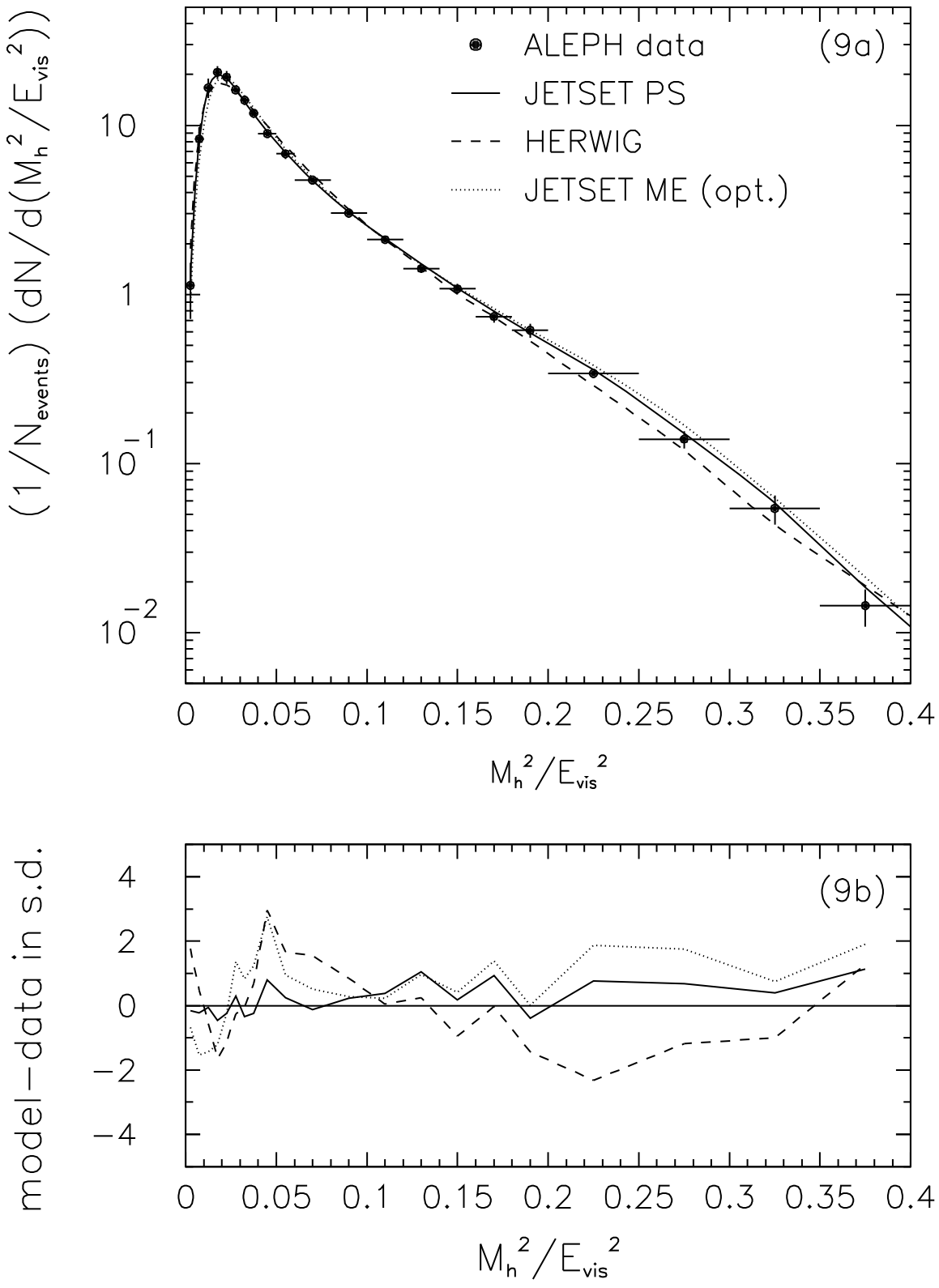
ALEPH data
(9a)
JETSET PS
HERWIG
JETSET ME (opt.)
$(1/N_{events})\ (dN/d(M_h^2/E_{vis}^2))$
M_h^2/E_{vis}^2
model−data in s.d.
(9b)
M_h^2/E_{vis}^2

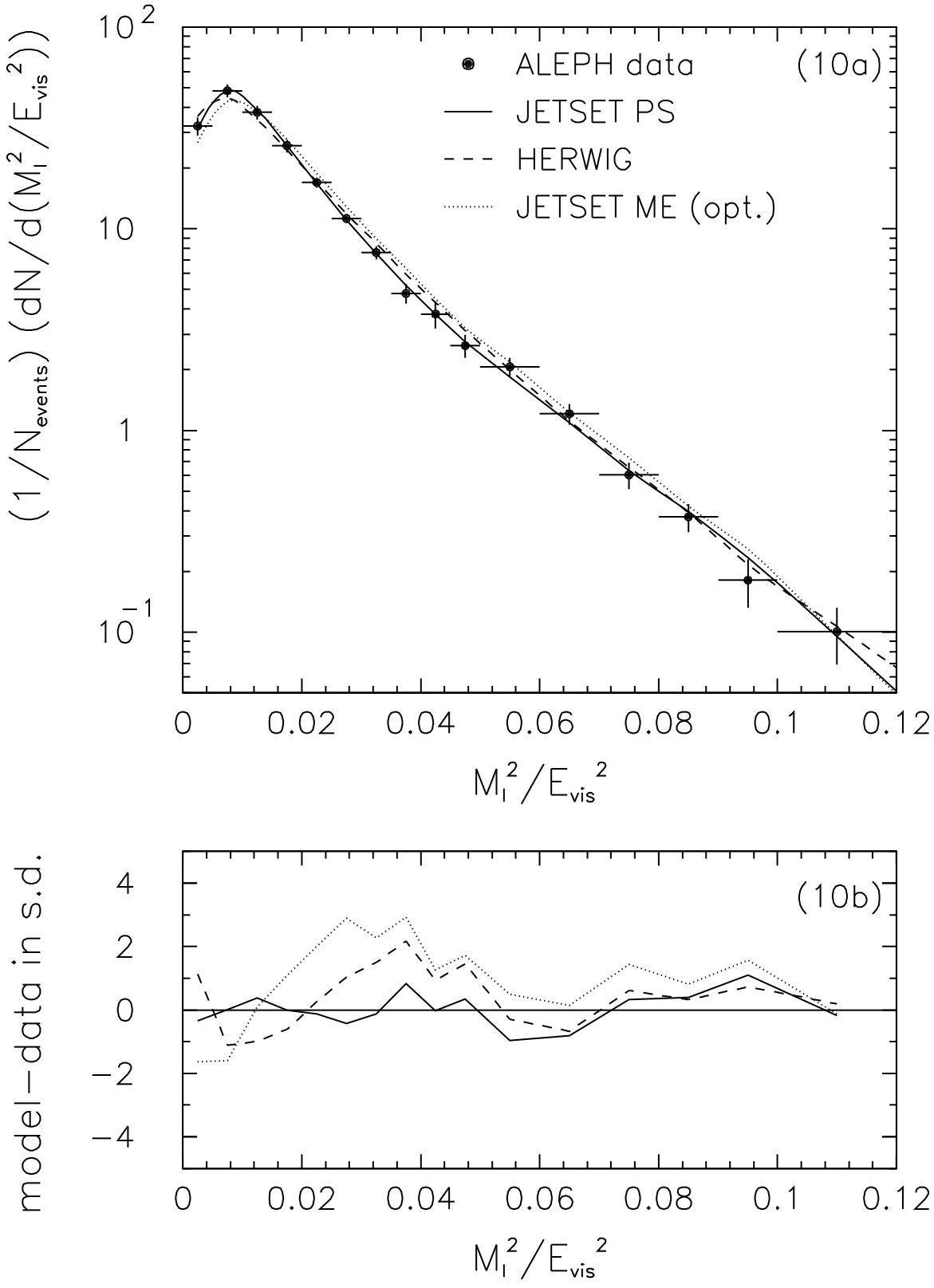
ALEPH data
JETSET PS
HERWIG
JETSET ME (opt.)
(10a)
$(1/N_{events})\ (dN/d(M_l^2/E_{vis}^2))$
M_l^2/E_{vis}^2
(10b)
model−data in s.d.
M_l^2/E_{vis}^2

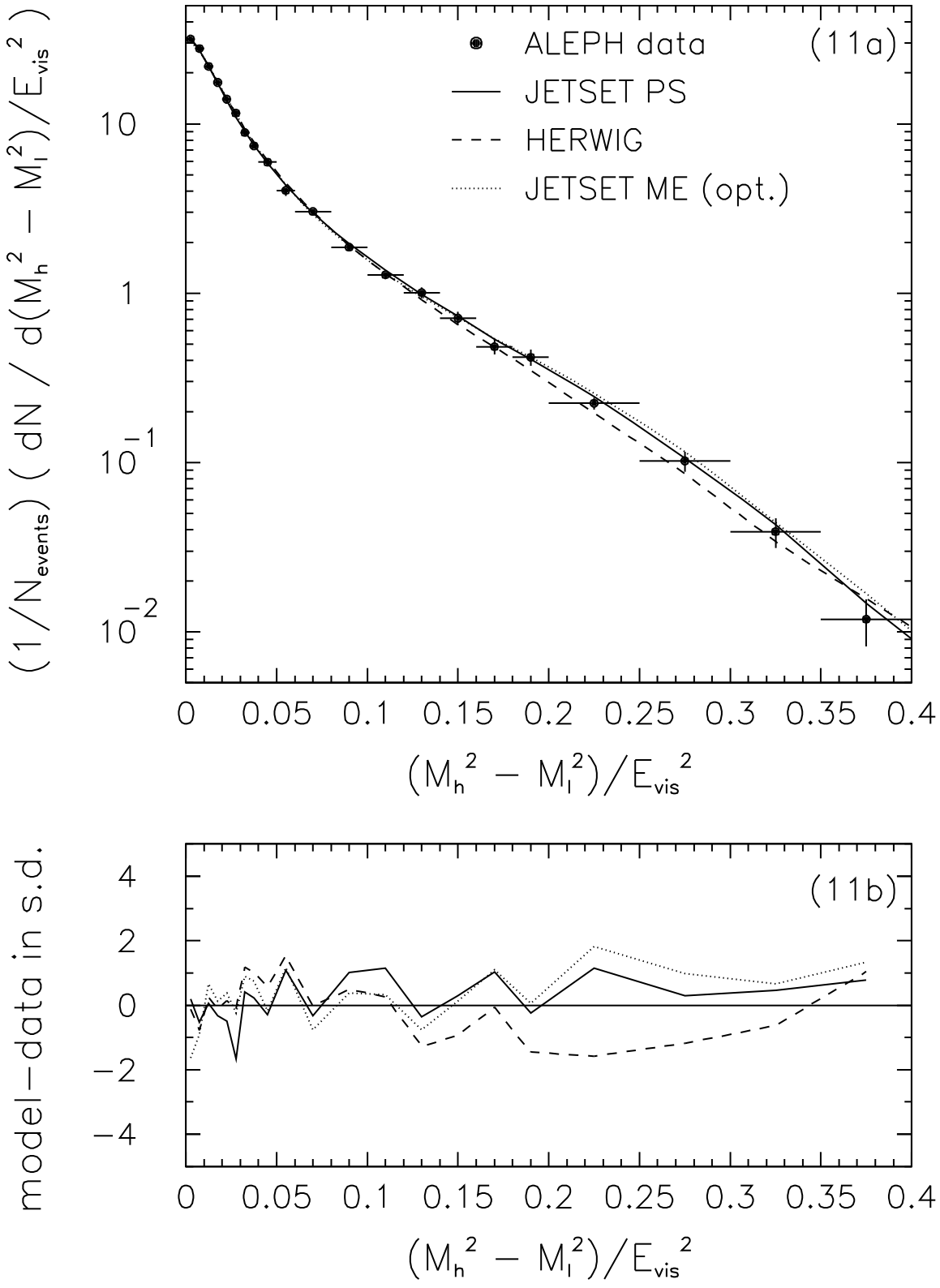
ALEPH data
JETSET PS
HERWIG
JETSET ME (opt.)
(11a)
$(1/N_{events})\ (\ dN\ /\ d(M_h^2 - M_l^2)/E_{vis}^2\ )$
10
1
10^{-1}
10^{-2}
0
0.05
0.1
0.15
0.2
0.25
0.3
0.35
0.4
$(M_h^2 - M_l^2)/E_{vis}^2$
(11b)
model−data in s.d.
4
2
0
−2
−4
0
0.05
0.1
0.15
0.2
0.25
0.3
0.35
0.4
$(M_h^2 - M_l^2)/E_{vis}^2$

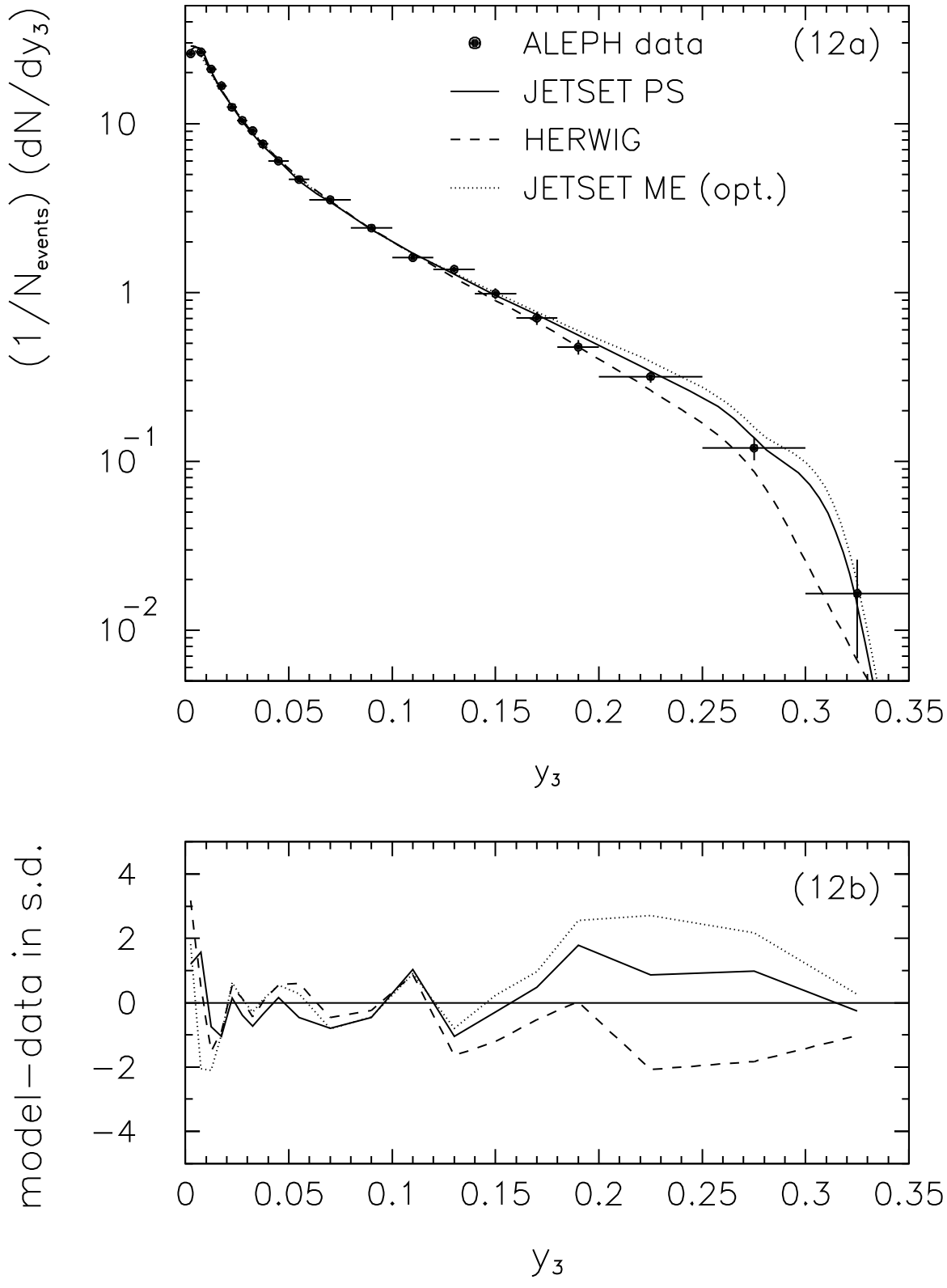
ALEPH data
(12a)
JETSET PS
HERWIG
JETSET ME (opt.)
$(1/N_{events})\ (dN/dy_3)$
10
1
10^{-1}
10^{-2}
0
0.05
0.1
0.15
0.2
0.25
0.3
0.35
y_3
model−data in s.d.
(12b)
4
2
0
−2
−4
0
0.05
0.1
0.15
0.2
0.25
0.3
0.35
y_3

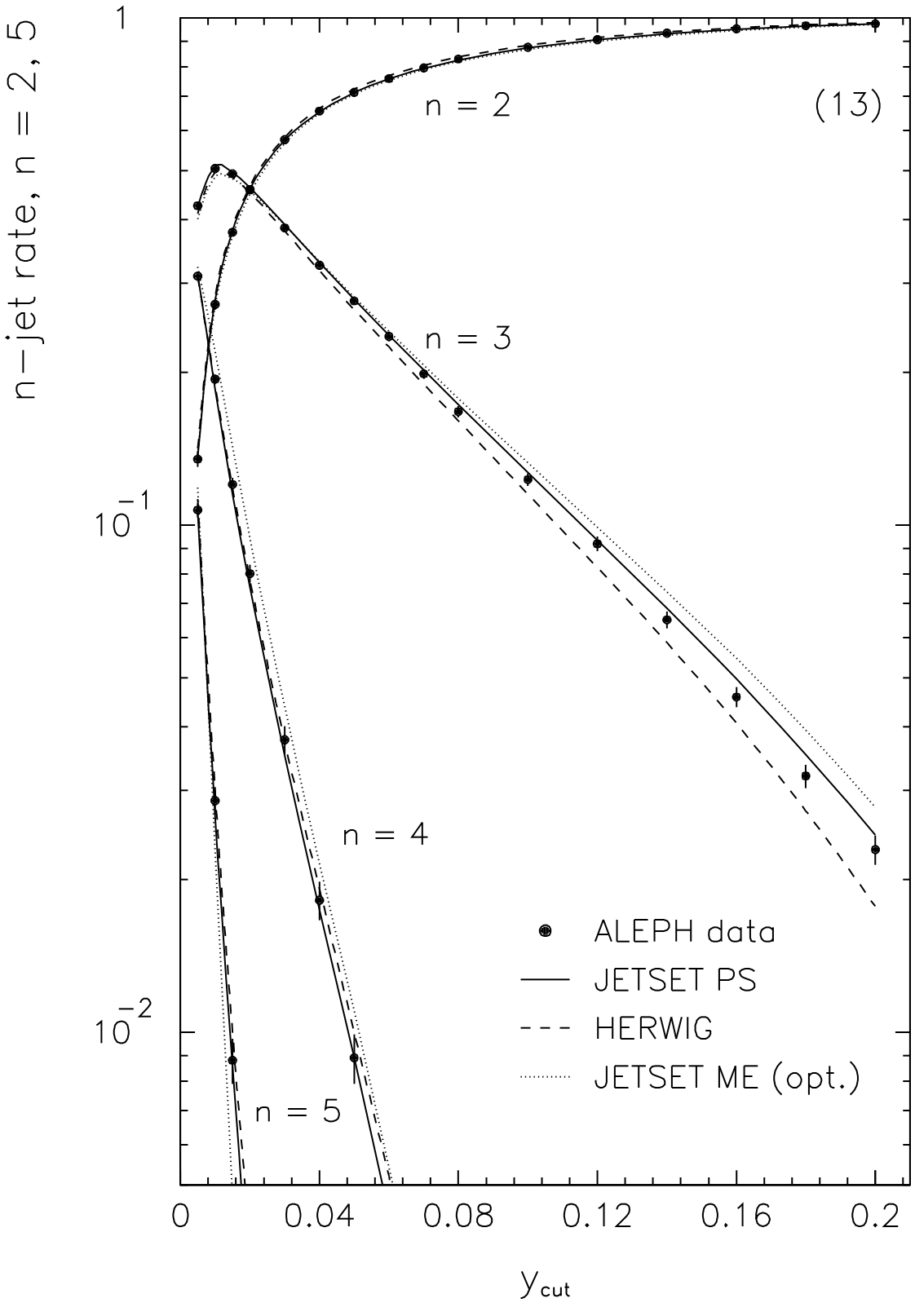
n−jet rate, n = 2, 5
1
10^{-1}
10^{-2}
n = 2
(13)
n = 3
n = 4
n = 5
ALEPH data
JETSET PS
HERWIG
JETSET ME (opt.)
0
0.04
0.08
0.12
0.16
0.2
y_{cut}

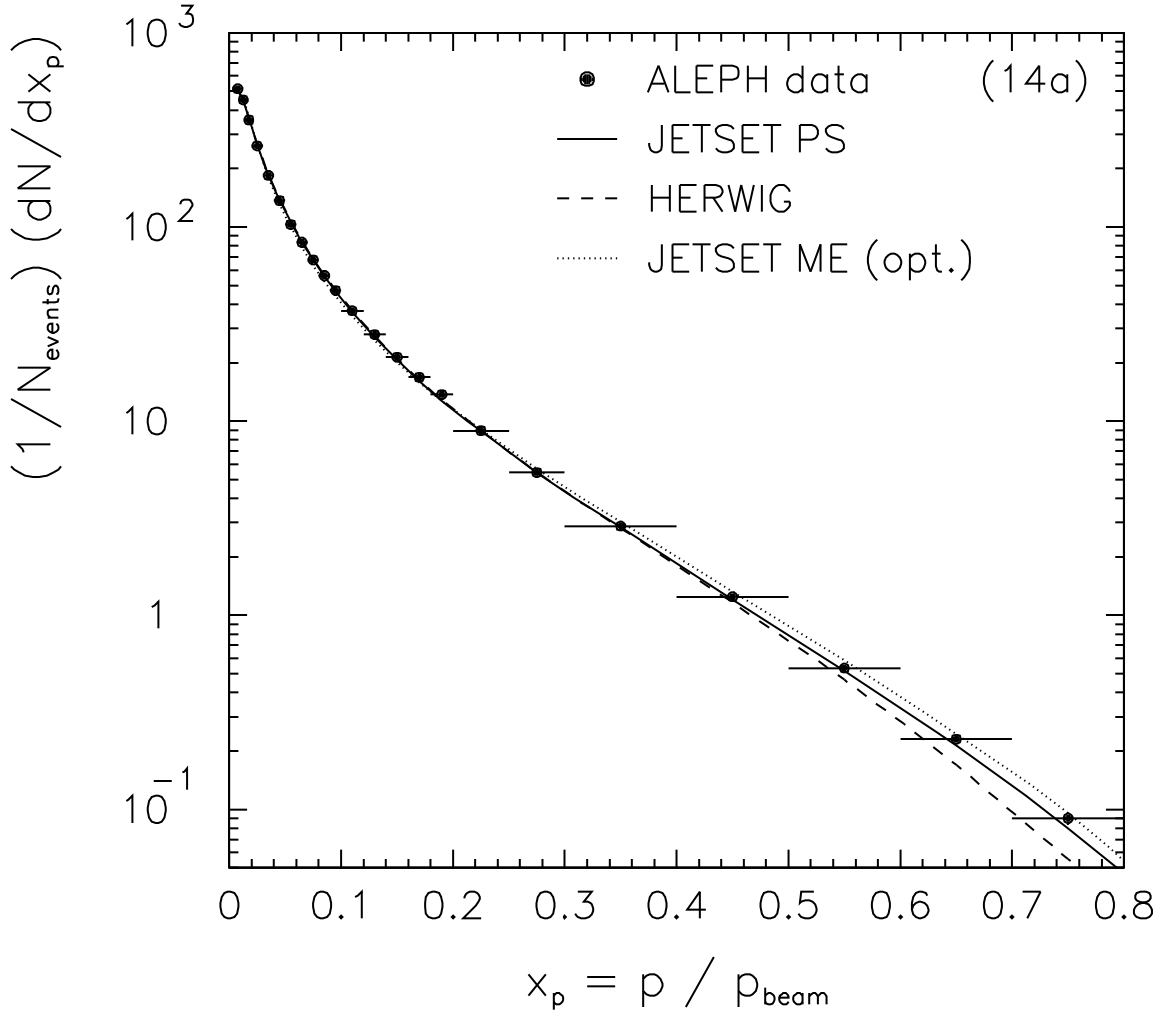
ALEPH data
(14a)
JETSET PS
HERWIG
JETSET ME (opt.)
$(1/N_{events})\ (dN/dx_p)$
10^3
10^2
10
1
10^{-1}
0
0.1
0.2
0.3
0.4
0.5
0.6
0.7
0.8
$x_p = p / p_{beam}$

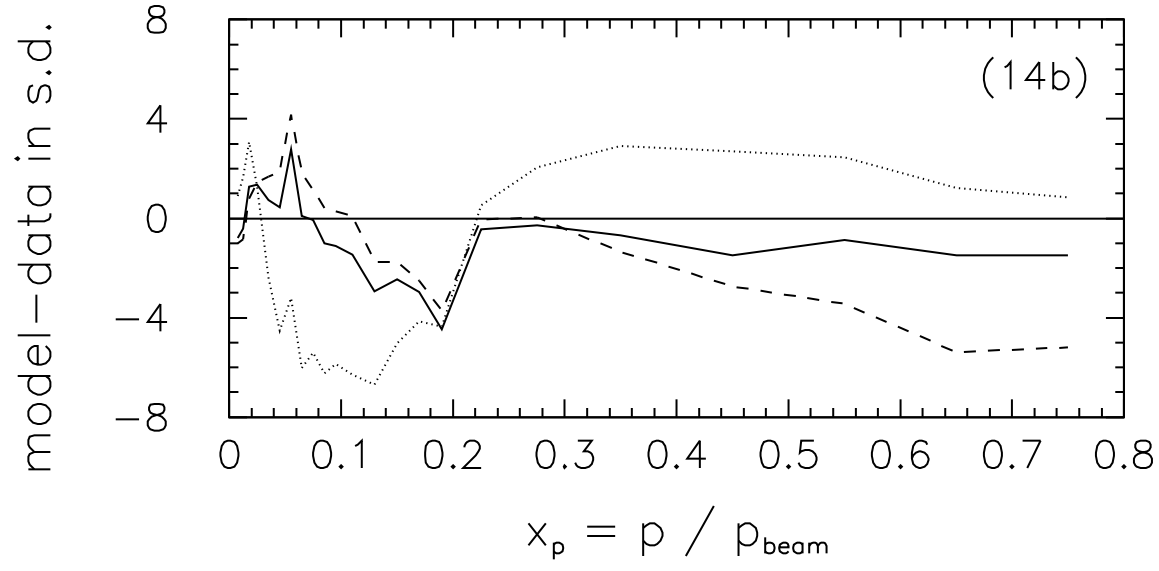
(14b)
model − data in s.d.
8
4
0
−4
−8
0
0.1
0.2
0.3
0.4
0.5
0.6
0.7
0.8
$x_p = p / p_{beam}$

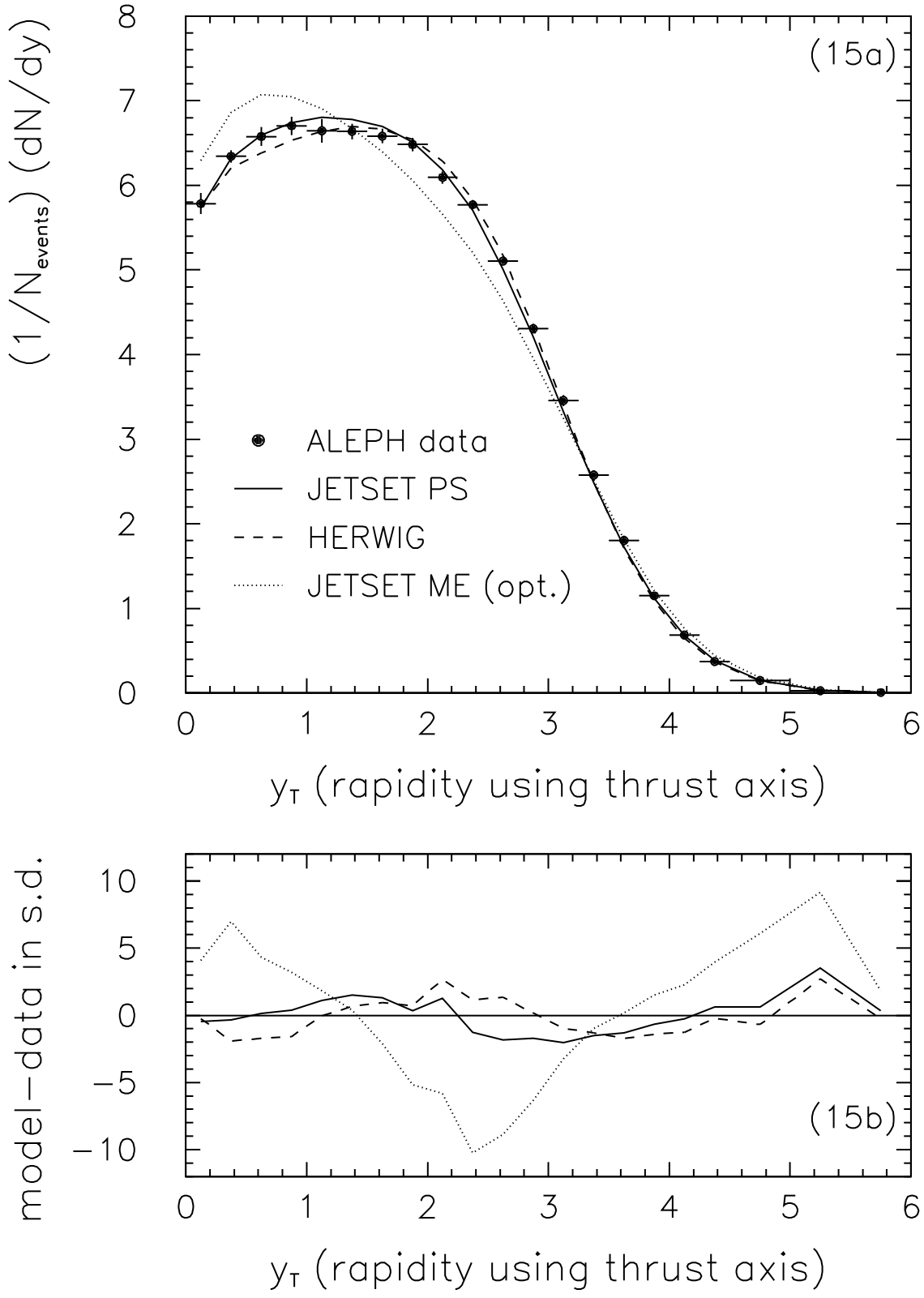
(15a)
$(1/N_{events})\ (dN/dy)$
ALEPH data
JETSET PS
HERWIG
JETSET ME (opt.)
y_T (rapidity using thrust axis)
model − data in s.d.
(15b)
y_T (rapidity using thrust axis)

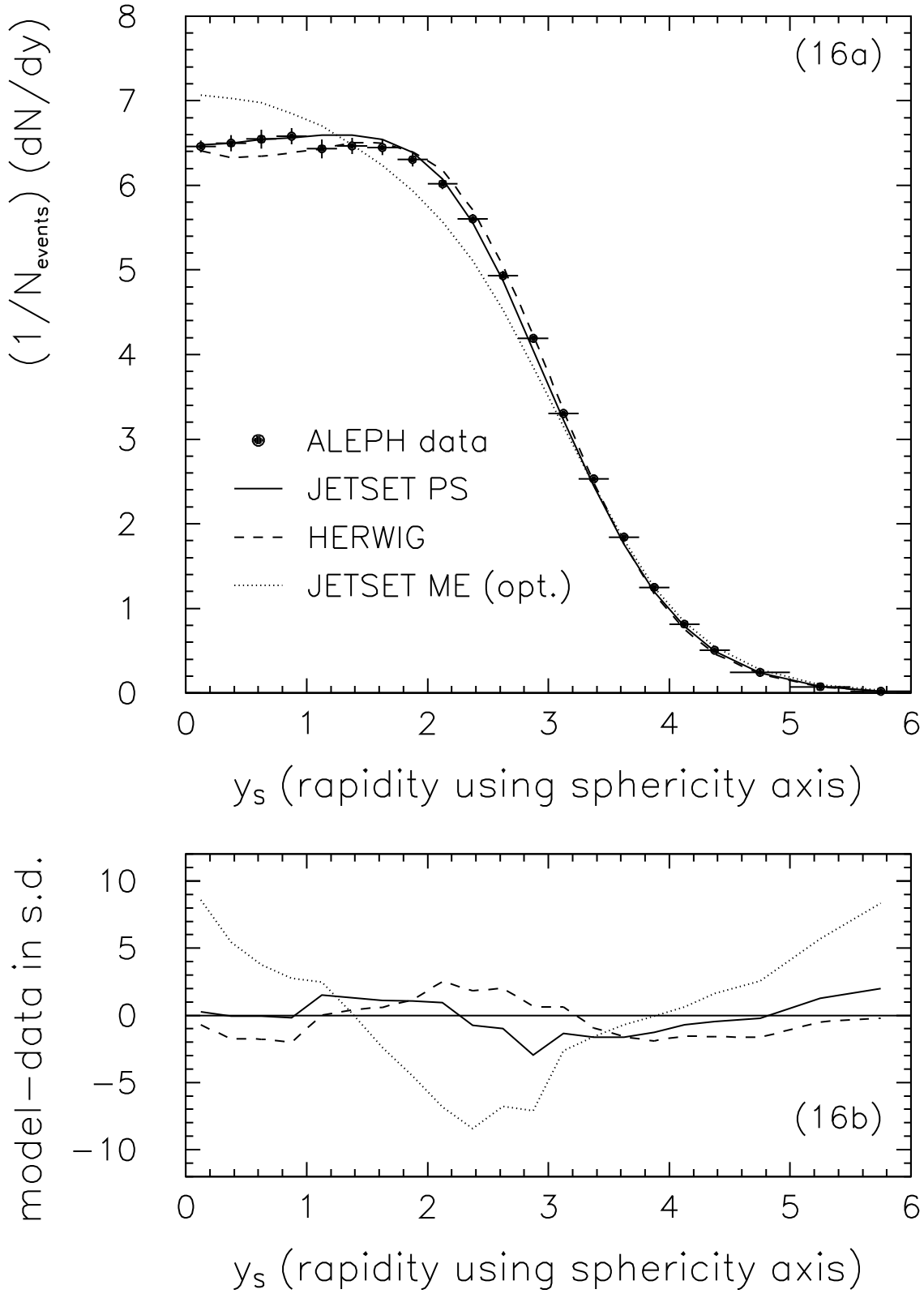
(16a)
$(1/N_{events})\ (dN/dy)$
ALEPH data
JETSET PS
HERWIG
JETSET ME (opt.)
y_s (rapidity using sphericity axis)
model − data in s.d.
(16b)
y_s (rapidity using sphericity axis)

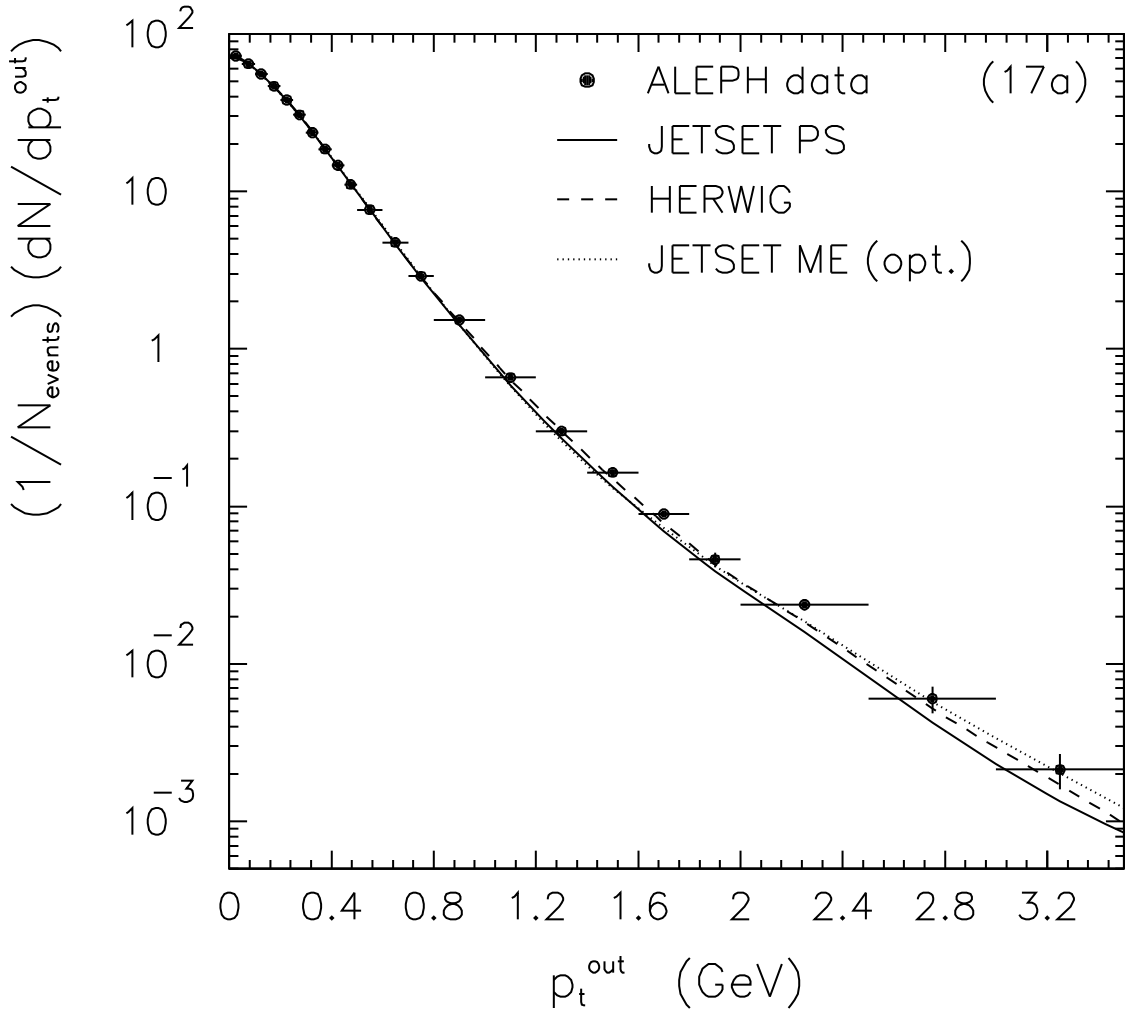
ALEPH data
(17a)
JETSET PS
HERWIG
JETSET ME (opt.)
$(1/N_{events})\ (dN/dp_t^{out})$
10^2
10
1
10^{-1}
10^{-2}
10^{-3}
0
0.4
0.8
1.2
1.6
2
2.4
2.8
3.2
p_t^{out} (GeV)

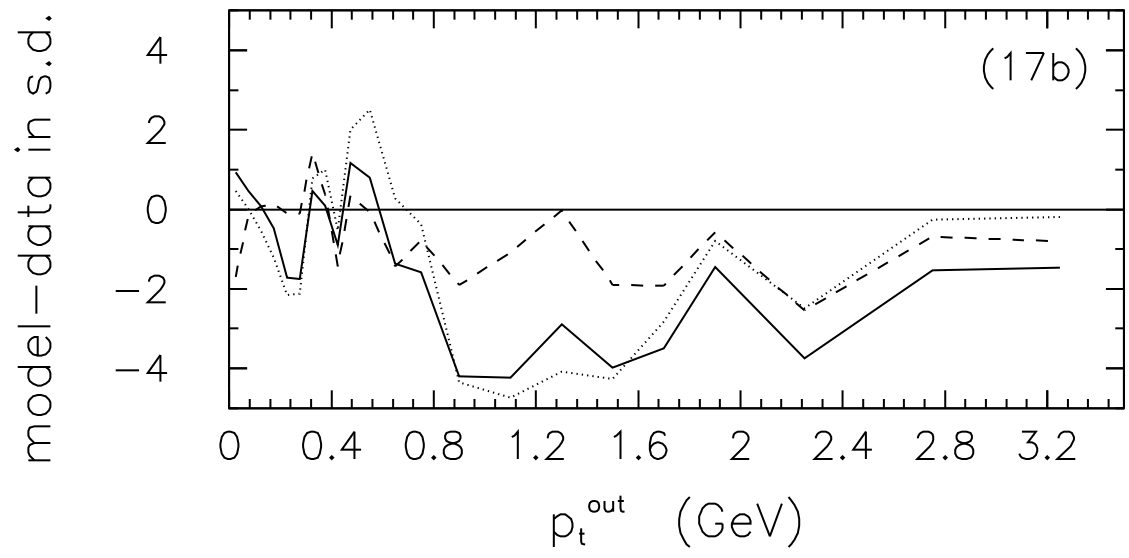
(17b)
model−data in s.d.
4
2
0
−2
−4
0
0.4
0.8
1.2
1.6
2
2.4
2.8
3.2
p_t^{out} (GeV)

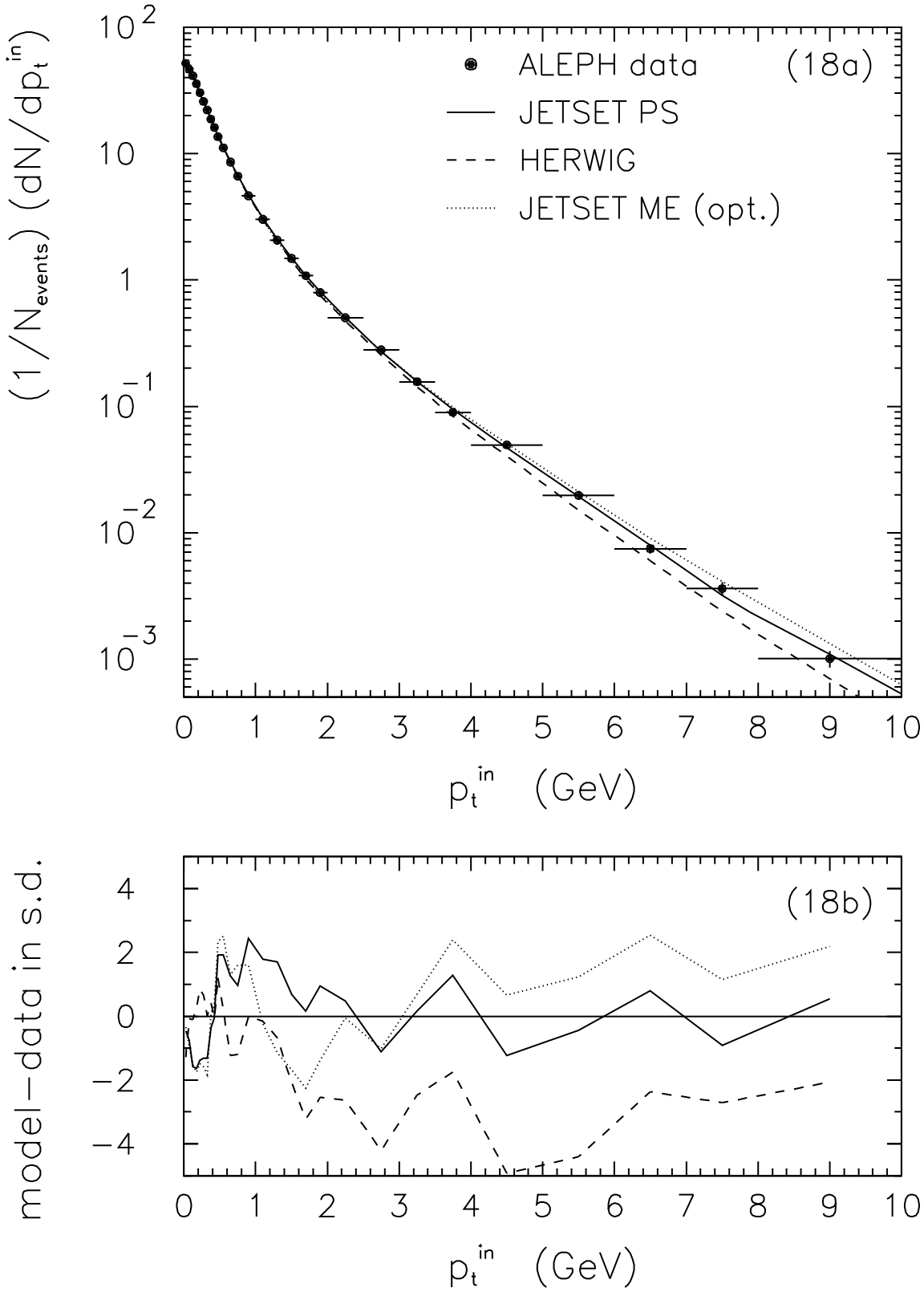
ALEPH data
(18a)
JETSET PS
HERWIG
JETSET ME (opt.)
$(1/N_{events})\ (dN/dp_t^{in})$
p_t^{in} (GeV)
model − data in s.d.
(18b)
p_t^{in} (GeV)

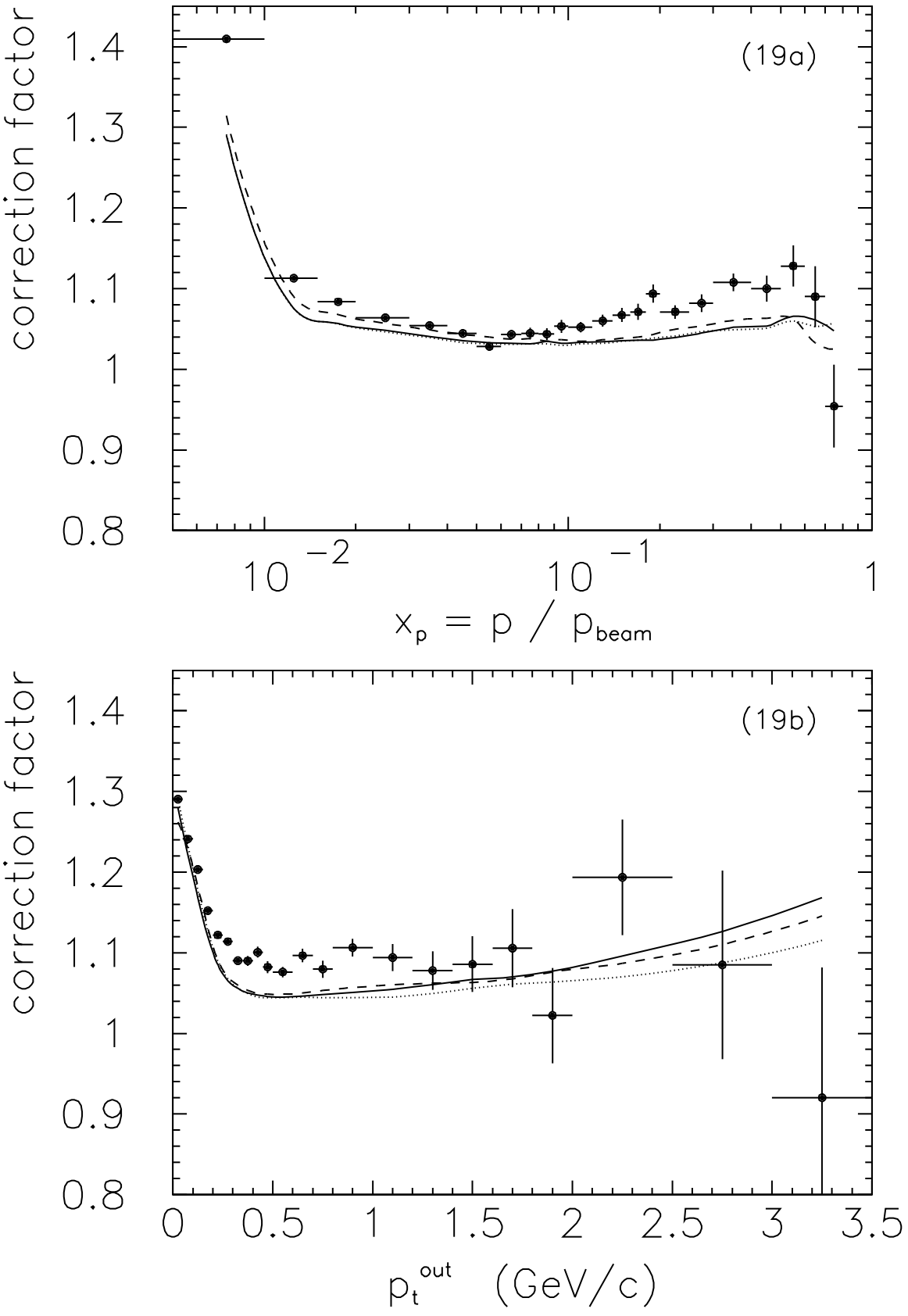
correction factor
1.4
1.3
1.2
1.1
1
0.9
0.8
(19a)
10^{-2}
10^{-1}
1
$x_p = p / p_{beam}$
correction factor
1.4
1.3
1.2
1.1
1
0.9
0.8
(19b)
0
0.5
1
1.5
2
2.5
3
3.5
p_t^{out} (GeV/c)

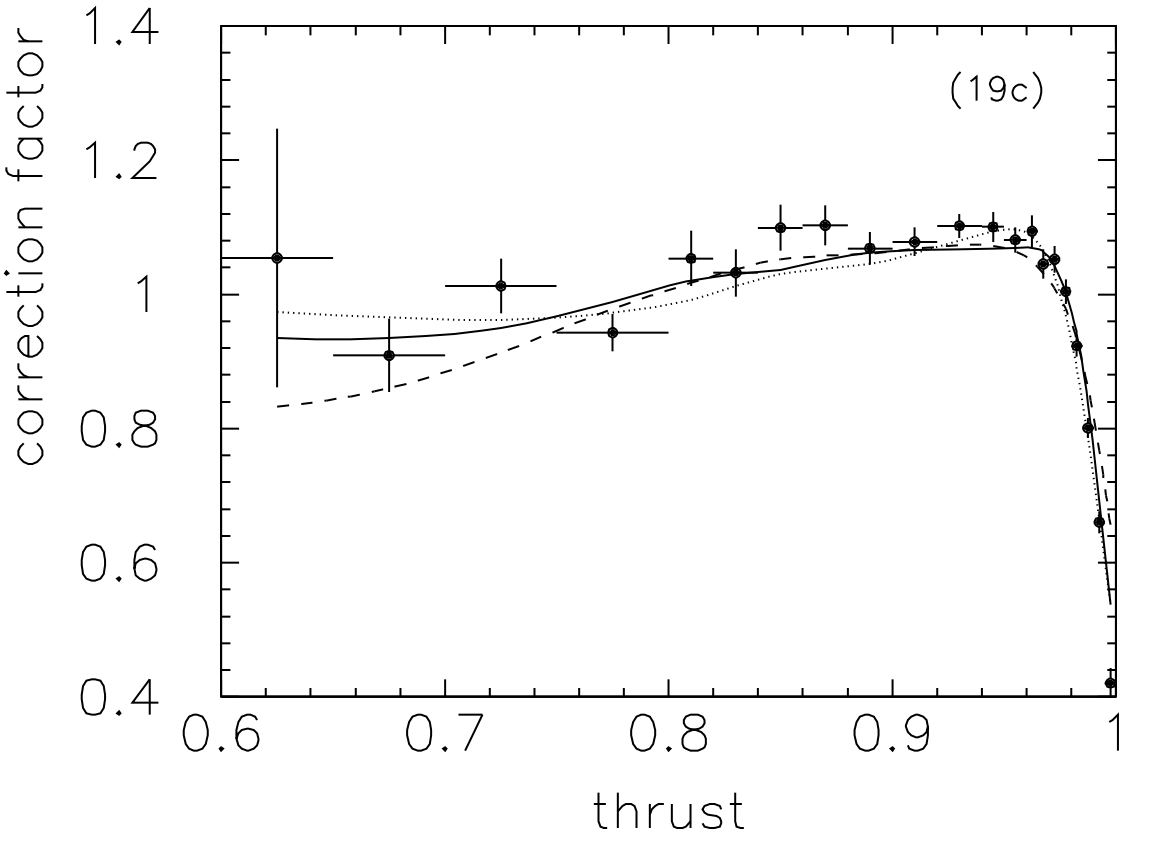
(19c)
correction factor
1.4
1.2
1
0.8
0.6
0.4
0.6
0.7
0.8
0.9
1
thrust

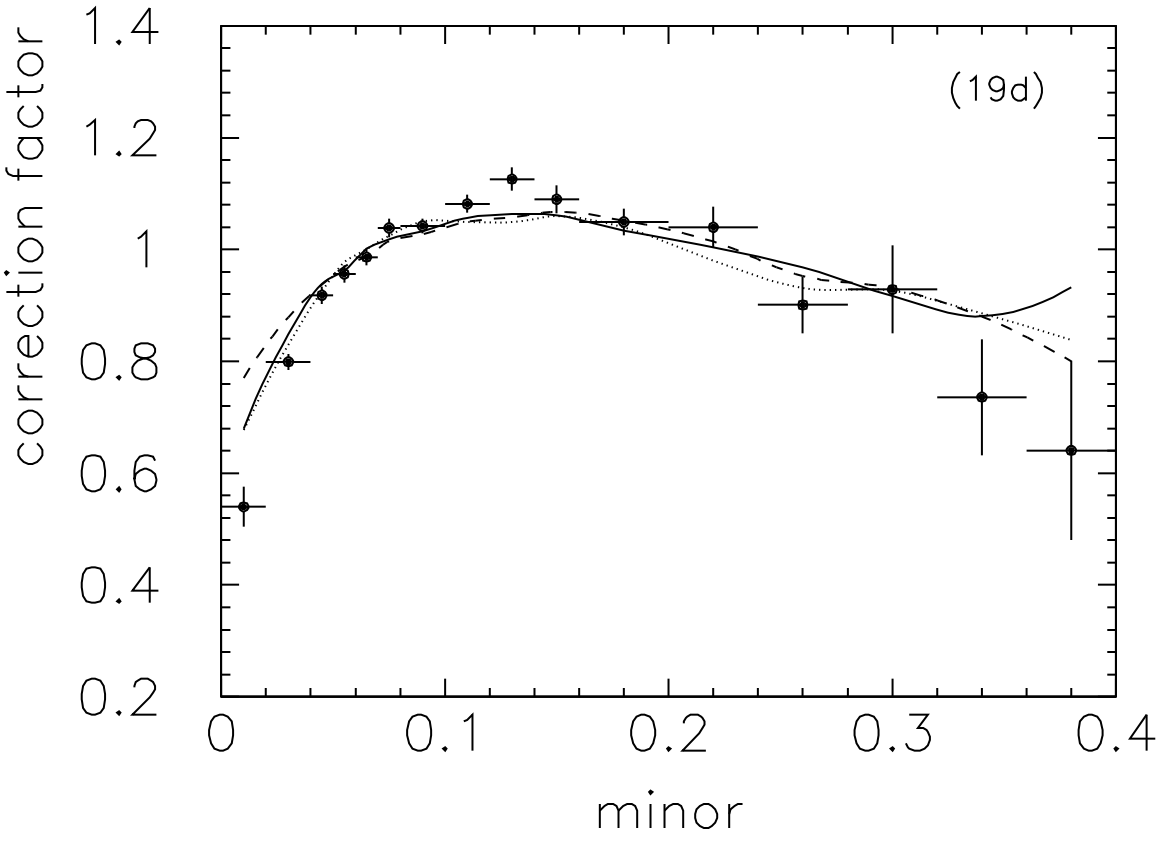
(19d)
correction factor
1.4
1.2
1
0.8
0.6
0.4
0.2
0
0.1
0.2
0.3
0.4
minor

Figure 20

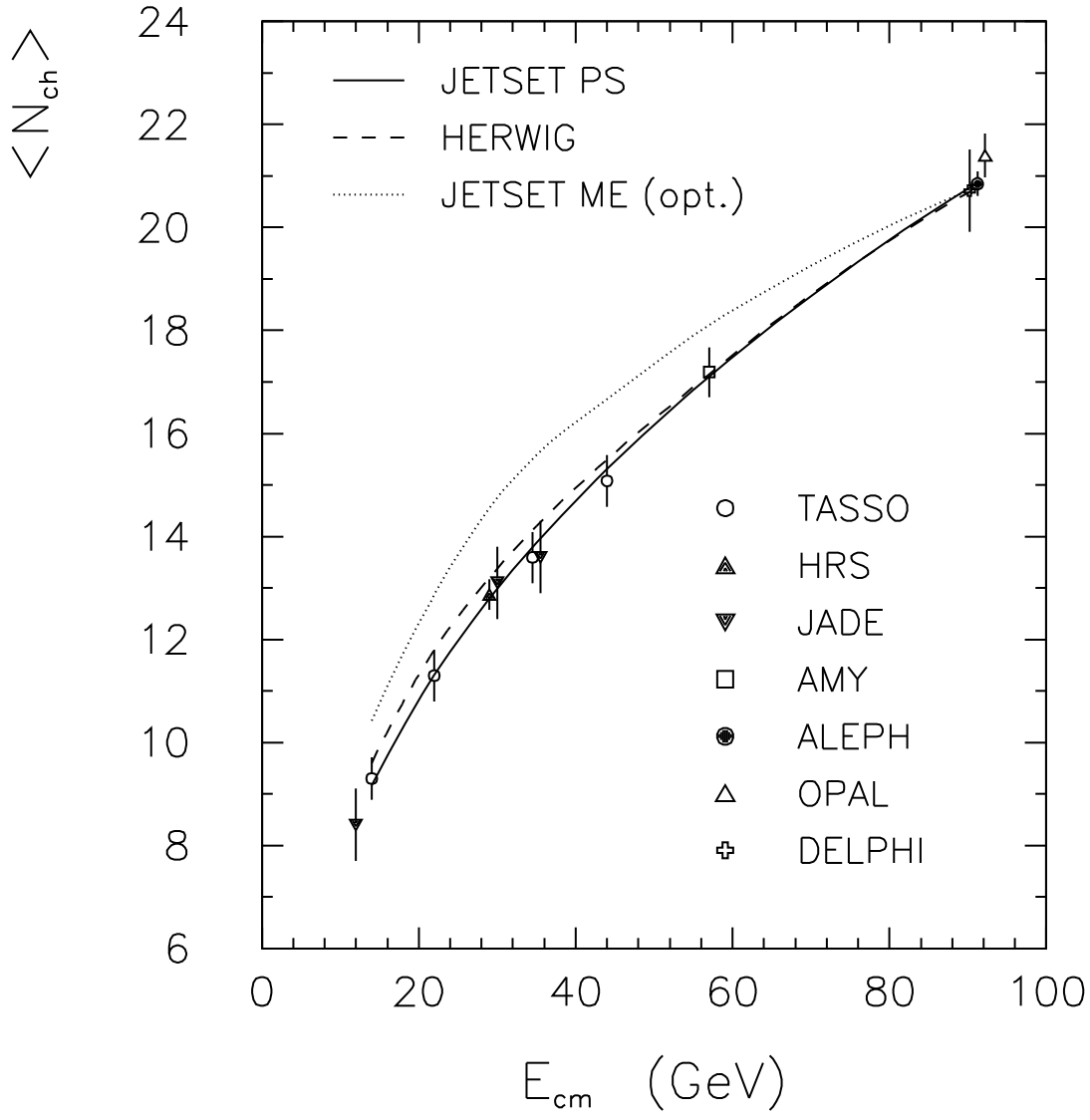
$\langle N_{ch} \rangle$
24
22
20
18
16
14
12
10
8
6
0
20
40
60
80
100
E_{cm} (GeV)
JETSET PS
HERWIG
JETSET ME (opt.)
TASSO
HRS
JADE
AMY
ALEPH
OPAL
DELPHI

Figure 21

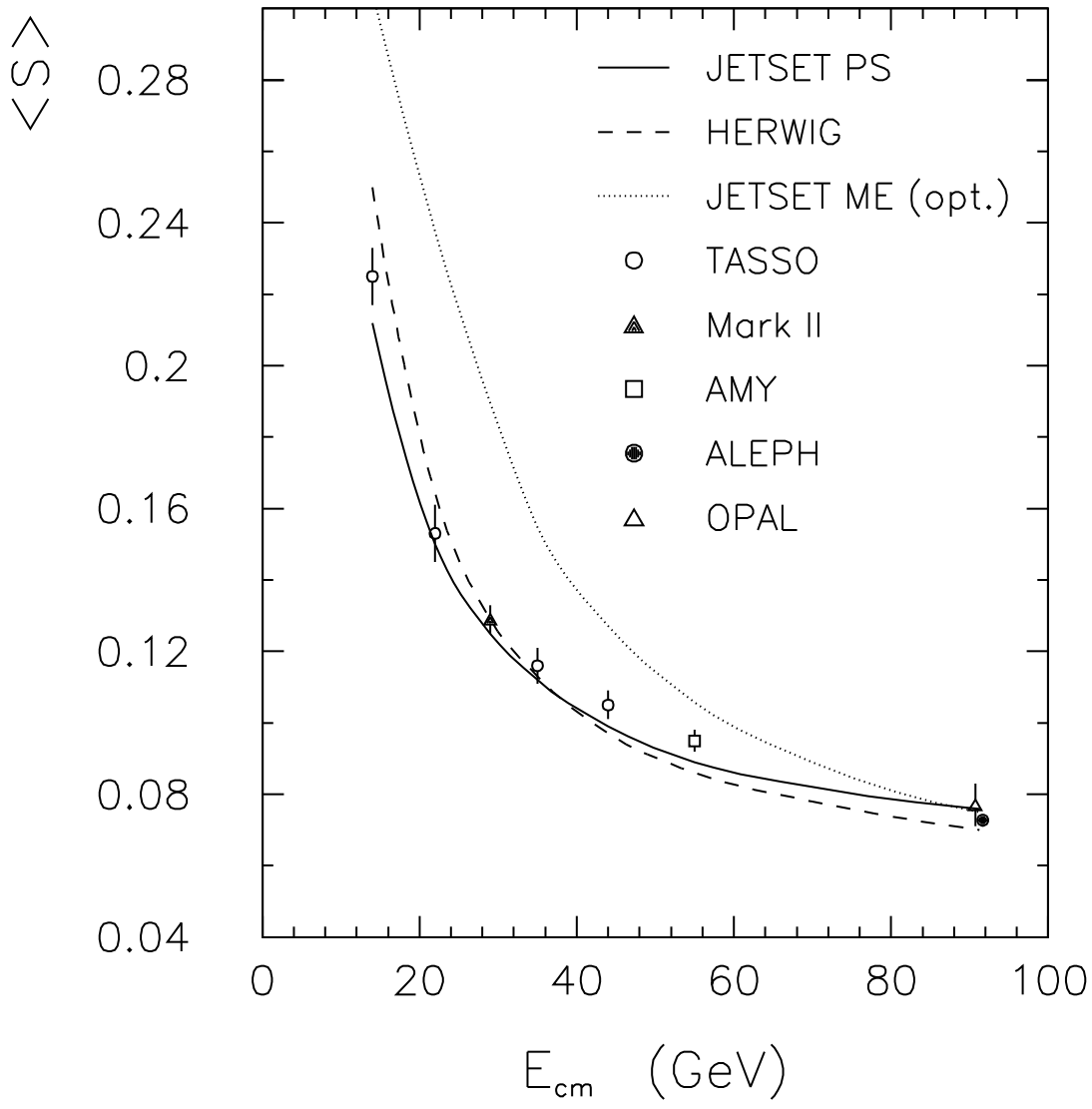
⟨S⟩
0.28
0.24
0.2
0.16
0.12
0.08
0.04
0
20
40
60
80
100
E_{cm} (GeV)
JETSET PS
HERWIG
JETSET ME (opt.)
TASSO
Mark II
AMY
ALEPH
OPAL

Figure 22

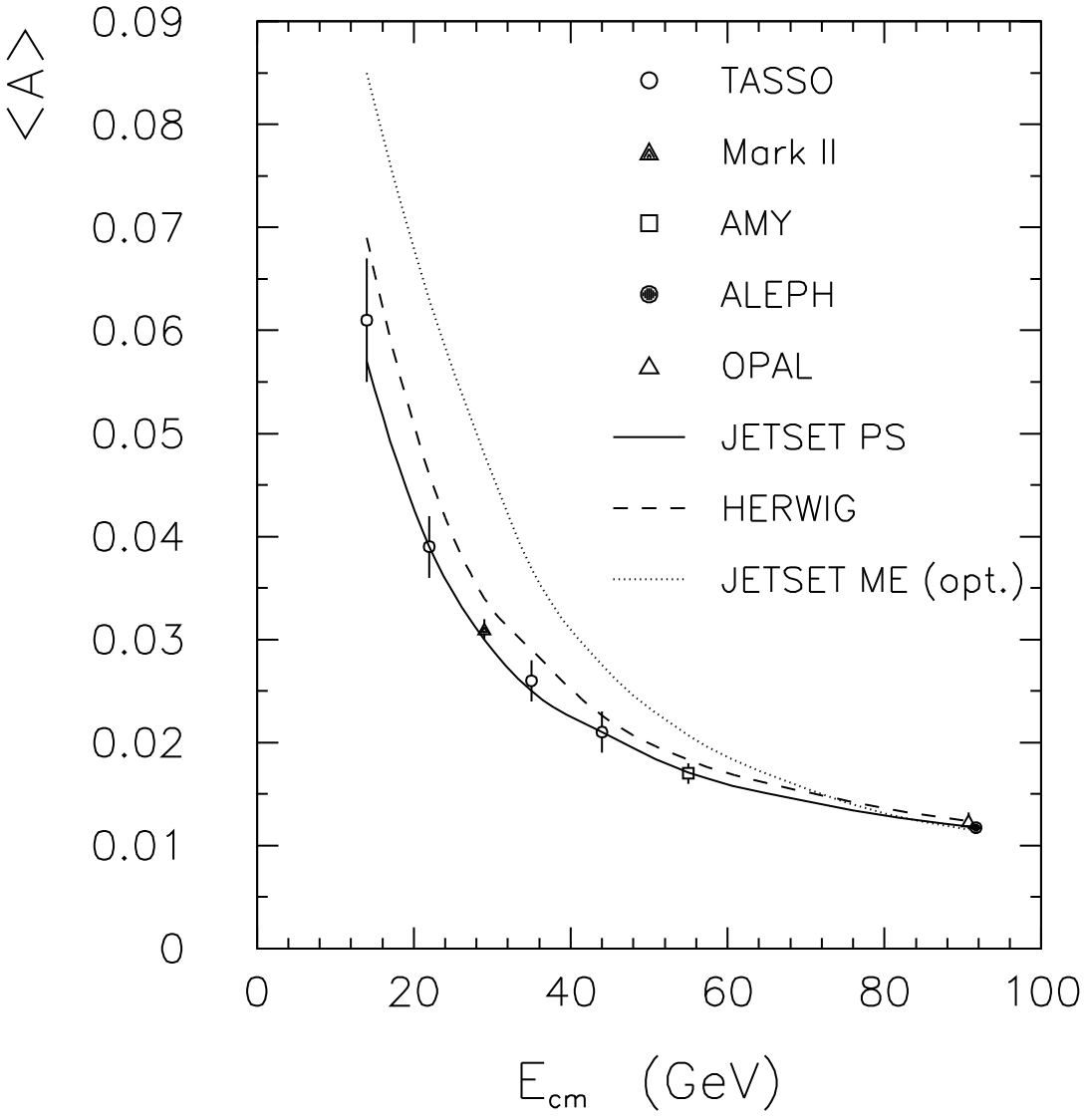
0.09
0.08
0.07
0.06
0.05
0.04
0.03
0.02
0.01
0
<A>
0
20
40
60
80
100
E_{cm} (GeV)
TASSO
Mark II
AMY
ALEPH
OPAL
JETSET PS
HERWIG
JETSET ME (opt.)

Figure 23

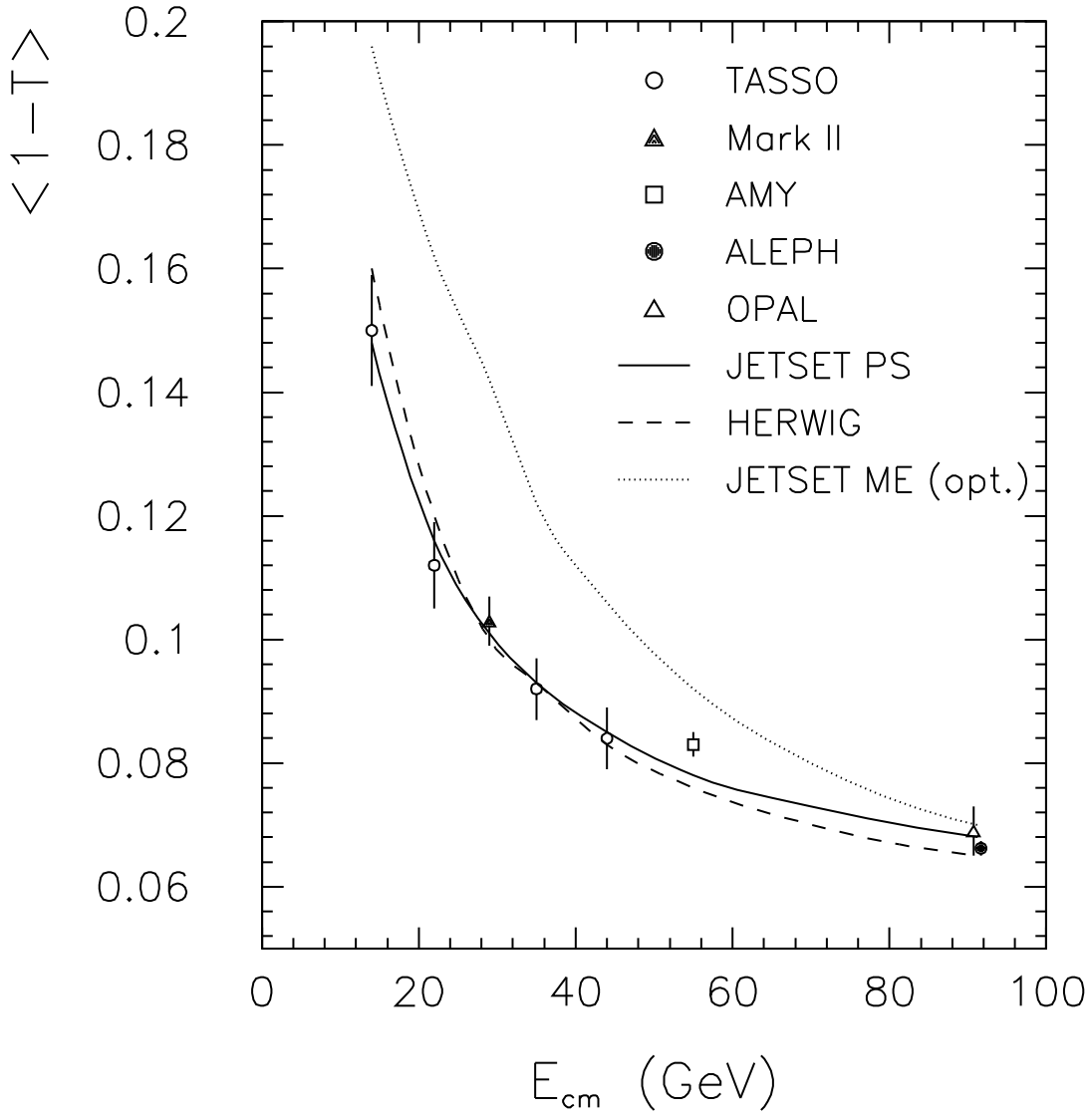
0.2
0.18
0.16
0.14
0.12
0.1
0.08
0.06
< 1 − T >
TASSO
Mark II
AMY
ALEPH
OPAL
JETSET PS
HERWIG
JETSET ME (opt.)
0
20
40
60
80
100
E_cm (GeV)

Figure 24

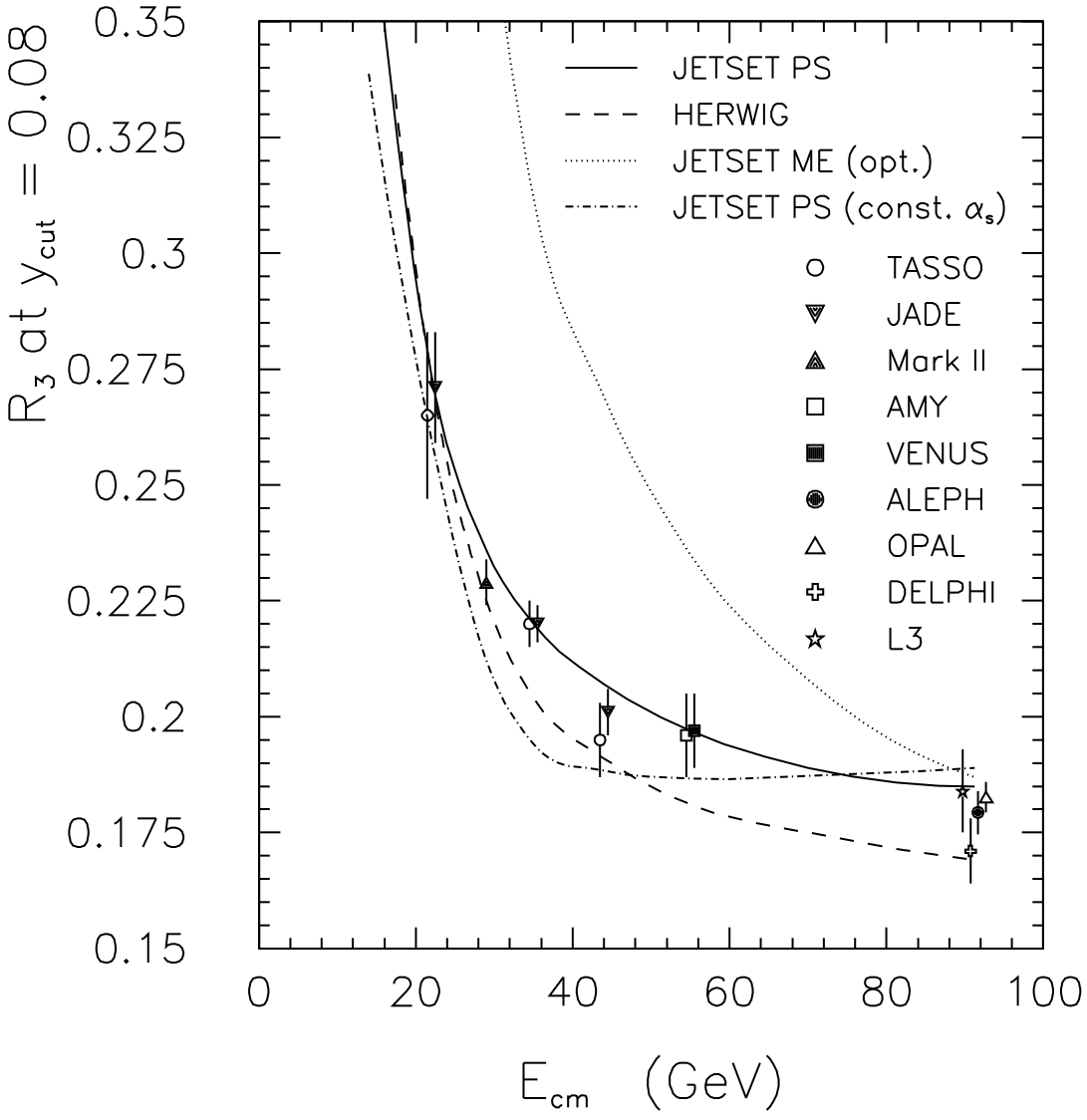
R_3 at y_{cut} = 0.08
0.35
0.325
0.3
0.275
0.25
0.225
0.2
0.175
0.15
0
20
40
60
80
100
E_{cm} (GeV)
JETSET PS
HERWIG
JETSET ME (opt.)
JETSET PS (const. α_s)
TASSO
JADE
Mark II
AMY
VENUS
ALEPH
OPAL
DELPHI
L3